DEVELOPMENT OF NOVEL EDIBLE LUMINESCENT NANOPARTICLE

SENSORS

by

SANAZ JALALIAN

A dissertation submitted to the

Graduate School-New Brunswick

Rutgers, The State University of New Jersey

In partial fulfillment of the requirements

For the degree of

Doctor of Philosophy

Graduate Program in Food Science

Written under the direction of

Dr. Richard D. Ludescher

And approved by

_____

_____

_____

_____

New Brunswick, New Jersey

JANUARY, 2015

ABSTRACT OF THE DISSERTATION

Development of Novel Edible Luminescent Nanoparticle Sensors

By SANAZ JALALIAN

Dissertation Director: Dr. Richard D. Ludescher

This project has developed a novel class of edible hydrocolloid food nanosensors which are doped with luminescent chromophores and investigated whether they can be used to provide information about the local food matrix - temperature, oxygen concentration, and the presence of food-borne pathogens. The luminescence properties of the probes such as phosphorescence and fluorescence provide the sensor sensitivity to the food properties. Hydrocolloid nanoparticles were made from gelatin and starch with diameters ranging from 50 to ~200 nm and labeled with food grade luminescent probes. The chromophore was covalently and non-covalently attached to the nanoparticle and the photophysical properties of the probe in the food system were studied. Temperature sensors were developed by using the phosphorescence sensitivity of a chromophore to temperature. Experiments with two different probes, namely erythrosine B labeled gelatin nanoparticles and phloxine B labeled gelatin nanoparticles have demonstrated that both probes can be effectively used as temperature sensors in liquid and solid food. The Van't Hoff plots of $\ln(I_{DF}/I_P)$ versus $1/T$ vary monotonically over a relatively wide temperature range and thus provide a basis for estimating temperature from measurements of

phosphorescence and delayed fluorescence. The tests indicated that the presence of some ingredients such as tannin and anthocyanins in the composition of the food may prohibit the use of gelatin nanoparticle probes due to precipitation of gelatin nanoparticles. The luminescence quenching of the probe by oxygen was used to develop a nanoparticle sensor for oxygen. The results of experiments on liquid and solid food samples indicate that erythrosine B labeled gelatin nanoparticles can be used as a probe to detect the presence or absence of oxygen in some liquid foods. Precise control of oxygen concentration in solutions will pose a challenge as has been observed in this study. The probe did not work as an appropriate oxygen sensor in the case of solid food samples with low relative humidity. The use of gelatin nanoparticles as a sensor to detect the presence of food-borne pathogens requires a measurable change in the spectrum of fluorescence resonance energy transfer between two chromophores which was not observed in the tests.

ACKNOWLEDGMENT

I would like to express my sincere gratitude to Dr. Richard D. Ludescher for his unfailing and valuable support and supervision over the years. He has been a tremendous mentor. I would like to thank him for allowing me to grow as a research scientist. His advice on both my research and my career has been priceless. I also deeply appreciate the guidance provided by my dissertation committee members: Dr. Paul Takhistov, Dr. Qingrong Huang, and Dr. Peter Kahn.

Special thanks are given to the members of Dr. Ludescher's research laboratory for their valuable assistance during this work.

Lastly, my heartfelt thanks go to my family, especially my husband Saeid, who always believed in me. Their encouragement has always helped me through times of difficulty.

Table of Contents

LIST OF FIGURES

LIST OF TABLES

1   INTRODUCTION

1.1   Summary

The food industry has always faced the complex challenge of controlling the quality and safety of food during the food production cycle. A recent advancement is the use of sensors, which are designed to monitor certain characteristics of the food that are indicative of food quality and safety. In addition to being accurate, food sensors should be inexpensive, easy to use, and safe.

This project has developed a novel class of edible hydrocolloid food nanosensors which are doped with luminescent chromophores and investigated whether they can be used to provide information about the local food matrix such as temperature, oxygen concentration, and the presence of food-borne pathogens. This will also establish the potential of an entirely novel class of nanoscopic sensory devices for the food industry. The luminescence properties of the probes such as phosphorescence and fluorescence provide the sensor sensitivity to the food properties. Hydrocolloid nanoparticles were made from gelatin and starch with diameters ranging from 50 to ~200 nm and labeled with food grade luminescent probes.

These luminescent food grade nanoparticles exhibit many advantages due to their small size such as being tasteless, dispersible, luminescent, high signal, site-specific, etc. In this project we have covalently and non-covalently attached the chromophore to the nanoparticle and studied the photophysical properties of the probe in the food system. By

applying the phosphorescence sensitivity of the erythrosin B to temperature, we have developed a sensor for temperature. The luminescence quenching of the probe by oxygen allows us to develop a nanoparticle sensor for oxygen. For developing a sensor to detect food-borne pathogens, we have used the phenomenon of resonance energy transfer between two chromophores, which act as donor and acceptor.

1.2   Hydrocolloid Nanoparticles

Food hydrocolloid nanoparticles can be made from gelatin, starch, chitosan and alginate with diameters ranging from ~50 to ~200 nm. Hydrocolloids are mostly used as drug carrier systems (Weber et al., 2000) and other possible pharmaceutical and biomedical vehicles. Gelatin nanoparticles have been massively studied. These nanoparticles have been used for drug delivery systems such as cell uptake (Azarmi et al., 2006), polymeric micelles as vehicles for drug delivery (Kataoka et al., 1993) and solid lipid nanoparticles for controlled drug delivery (Muller et al., 2000). Several researchers have investigated the use of gelatin as biomaterial to synthesize drug delivery systems such as doxorubicin-loaded gelatin nanoparticles for involvement of the drug in cross-linking with glutaraldehyde (Leo et al, 1997), encapsulating the protein synthesis inhibitor cycloheximide for possible therapeutic applications (Verma et al., 2005) and formulating paclitaxel in nanoparticles which alters its disposition into tissues (Yeh et al., 2005).

Hydrocolloid nanoparticles, have been loaded with fluorescent dyes such as fluorescein isothiocyanate which covalently label at surface amino groups (Oppenheim & Stewart,

1979). Non-covalent attachment of the fluorescent dyes Texas red and fluorescein amine to gelatin nanoparticles has also been achieved (Coester et al., 2000). Other examples include fluorescein labeled dextran which is encapsulated in gelatin nanoparticles for intracellular DNA delivery in response to glutathione (Kommareddy & Amiji, 2005) and retinoic acid labeled gelatin as an anticancer drug carrier (Kim & Byun, 1999).

Dziechciarek et al. (1998) studied the development of starch-based nanoparticles and their structural, colloidal and rheological properties. Xiao et al. (2006) have shown that the folate-conjugated starch nanoparticle system is a potentially useful system for the targeted delivery of anticancer drug doxorubicin. Zhai et al. (2007) studied the synthesis and characterization of polyoxometalate loaded starch nanocomplex and its antitumoral activity. Effective insulin delivery using starch nanoparticles as a potential trans-nasal mucoadhesive carrier has been shown by Jain et al. (2008). Starch granules have been non-covalently labeled with a wide range of fluorescent dyes such as congo red (Alder et al., 1995), eosin Y (Seguchi, 1986), and acridine orange (Badenhuizen, 1965; Alder et al., 1995). Alginate and chitosan have their role in biomedical, pharmaceutical and food science fields such as characterization and *in vitro* testing of alginate nanoparticles, embedded with magnetite, which respond to externally applied magnetic fields for targeted drug delivery (Ciofani et al., 2008); alginate nanoparticles for increasing and sustaining the delivery of the drug inside the cell (Chavanpatil et al., 2007); and sponge-like alginate nanoparticles for delivery of antisense oligonucleotides (Aynie et al., 1999). Some other studies have investigated preparation and characterization of antibacterial properties of chitosan nanoparticle loaded with copper ions against E. coli K88 (Wen-Li

et al., 2008), stability of chitosan nanoparticles loaded with L-ascorbic acid during heat treatment in aqueous solution and the antioxidant effect of ascorbic acid that is continuously released from chitosan nanoparticles in food processing (Jang and Lee, 2008) and *in vitro* effects of chitosan nanoparticles on proliferation of human gastric carcinoma cell line MGC803 cells (Qi et al., 2005).

1.3   Luminescent Nanoparticles and Their Advantages

In the past decade, the synthesis of nano-scale luminescent particles has been developed rapidly (Kamat, 2002; Daniel and Astruc, 2004; Rosi and Mirkin, 2005). Luminescent nanoparticles can be either intrinsic which contain luminescent material such as nanocrystalline semiconductors (Murphy, 2002), individual organic chromophores such as new nanometer-sized fluorescent particles (1-pyrenemethylamine nanoparticles) (Wang et al., 2005), and individual carbon nanotubes (Baron et al., 2005a, b) or extrinsic which are labeled with luminescent chromophores such as an aromatic ruthenium complex (He et al., 2002), gelatin labeled with the organic chromophores Texas red or fluorescein amine (Coester et al., 2000), and zirconia doped with lanthanides (Ye et al., 2005).

The luminescent nanoparticles developed in this project were labeled with organic chromophores. Due to their small size, nanoparticles are tasteless, odorless and will not alter food texture. These small particles do not cream or settle and they are easily dispersed in solution or on food surfaces because their small size makes them susceptible

to Brownian motion which keeps them in solution. They can be easily dispersed in emulsions, liquids, sprayed on surfaces of foods or packaging materials, or mixed into food or food ingredients. Chromophores which are attached to nanoparticles are more stable against chemical and photochemical degradation and have longer shelf lives (Wang, et al., 2005). Each labeled nanoparticle will provide a luminescence signal and provide the information about the local food matrix. Nanoparticles with a diameter between 70-130 nm have high surface/volume ratio; therefore, for some hydrocolloid nanoparticles such as gelatin nanoparticles, more surface amino groups will be accessible to be labeled by fluorescent dyes, like fluorescein isothiocyanate or Tetramethylrhodamine isothiocyanate which are amine reactive dyes due to having ITC groups in their molecular structure. The small size of nanoparticles leads them to rapid equilibrium with local food properties or local analyte concentration. Since nanoparticles are in close contact with food matrix they can provide accurate information about the local matrix properties. Luminescent nanoparticles are versatile yet selective and can provide a wide range of frameworks to attain diverse analytical sensing functions. Luminescent nanoparticles can provide specific signals which include intensity ratios, luminescent lifetimes, or energy transfer intensities, and once calibrated, can offer explicit analytical indicators. The luminescence signal is easily detectable with inexpensive hand-held instruments such as those sold by Ocean Optics (www.oceanoptics.com).

1.4   Gelatin Nanoparticles

Among colloidal systems those based on protein are very promising, since they are biodegradable and only weakly antigenic (Azarmi et al., 2006). Gelatin is one of the most versatile, naturally occurring biopolymers widely used in cosmetics, pharmaceutical formulations, as well as in many different types of food products. Gelatin is obtained by acid or base hydrolysis of collagen (Kommareddy and Amiji, 2007). The properties of gelatin depend on the gelatin manufacturing method (acidic or basic), its origin (bovine or pig), the molecular weight, type and the number of amino acids (Coester et al., 2000).

Gelatin nanoparticles are easy to prepare, and their size distribution can be measured easily. Due to having defined primary structures protein-based nanoparticles offer potential for surface modification, covalent and non-covalent attachment.

Gelatin nanoparticles are extensively used as vehicles for drug delivery (Kaul and Amiji, 2004); gene delivery (Kommareddy and Tiwari 2005; Zwoirok, et al., 2005); and protein/peptide delivery (Li et al., 1998). Gelatin has a number of advantages as a nanoparticle material: it is a natural macromolecule that is extensively available; it is nearly tasteless, colorless, and inexpensive; it shows low antigenicity (Schwik and Heide, 1969); and many studies exist that address its use in parenteral formulation (Haessig and Stapfil, 1969). Gelatin nanoparticles can be prepared by coacervation-phase separation technique (Oppenheim and Stewart, 1979), based on the simple water-in-oil emulsion (Cascone et al., 2002; Gupta et al., 2004), or two-step desolvation method (Coester et al., 2000). The molecular weight heterogeneity present in a solution of gelatin is clearly

responsible for the observed variation in the experimental conditions required for gelatin nanoparticle formation (Farrugia & Groves, 1999). It has been shown that the phase behavior of gelatin is very complex and influenced by the temperature of the medium. This affects the initial heterogeneity of the molecular-weight-distribution of the gelatin sample and might explain the observed sensitivity to the experimental conditions in the production of gelatin nanoparticles by addition of solvents (Elysee-Collen & Lencki, 1996).

This project adopted the modified two-step desolvation to make gelatin nanoparticles (Azarmi et al., 2006). The size of nanoparticles produced by the two-step desolvation technique varies from 20 nm to 150 nm, depending on many factors, such as temperature, pH, gelatin type, agitation speed, crosslink level, and desolvating agent (Jahanshahi et al., 2008; Azarmi et al., 2006). Advantages of making nanoparticles by two-step desolvation is to produce nanoparticles which are more stable, as their tendency for aggregation is small, and one can easily attach chromophores to the particles by either covalent or non-covalent bonding (Coester et al., 2000).

1.5   Luminescent Probes

1.5.1   Erythrosin-B

Erythrosin-B ($C_{20}H_6I_4Na_2O_5$), FD&C Red #3, is an E-type luminescent chromophore and a water-soluble dye which shows delayed fluorescence, because the first exited singlet state (S_1) and triplet state (T_1) are close in energy (Parker, 1968). Erythrosin-B shows

98% of conversion of excited molecules to the triplet state and has triplet high quantum yield. It is considered as an ideal probe for phosphorescence studies (Garland and Moore, 1979). The phosphorescence of erythrosin-B is due to the xanthene ring with four iodine atoms. When erythrosin-B is thermally activated it goes through reverse intersystem crossing from triplet state to singlet state and generates delayed fluorescence. The correlation between delayed fluorescence (I_{DF}) to phosphorescence (I_P) ratio of erythrosin-B and temperature (T) has been investigated in this study to explore its possible use as a temperature sensor.

This probe is chemically stable and its phosphorescence is sensitive to oxygen. The phosphorescence emission of erythrosin-B is in the red or near infrared, where biological molecules absorb very little (Vanderkooi et al., 1987), and its lifetime in aqueous solution at room temperature is long, ~0.2 ms (Duchowicz et al., 1998) which increases to ~0.6 ms in an immobile glassy matrix (Simon-Lukasik & Ludescher, 2004). Erythrosin-B has long wavelength absorption ($\lambda_{max} \approx 520$) nm and a large stokes shift for phosphorescence ($\lambda_{max} \approx 680$ nm). It has shown sensitivity to oxygen in food polymers such as BSA (Nack & Ludescher, 2006), B-lactoglobulin (Sundaresan & Ludescher, 2008), and gelatin (Simon-Lukasik & Ludescher, 2004; Lukasik & Ludescher, 2006). Figure 1-1 shows erythrosin-B's molecular structure.

1.5.2 Phloxine B

Phloxine B (2′,4′,5′,7′-tetrabromo-4,5,6,7-tetrachloro-fluorescein) D&C Red No. 28 is a red dye found in drugs, cosmetics and foods (Inbaraj et al, 2005). The phosphorescence of ploxine B is due to the xanthene ring with four bromine atoms (Figure 1-2). When ploxine B is thermally activated it goes through reverse intersystem crossing from the triplet state to singlet state and generates delayed fluorescence. Phloxine B has the maximum phosphorescence emission is at about 710 nm, absorption at about 500 nm and shows delayed fluorescence at about 570 nm. Acid dyes are water-soluble dyes employed mostly in the form of sodium salts of the sulfonic or carboxylic acids. They are anionic and attach strongly and directly to cationic groups in the fiber. Phloxine B is one of the most widely use stains in fluorescence microscopy (Lh et. al., 1997). The dye is an active component of a photoreactive insecticide (Heitz, 1997). It is used as an intermediate for making photosensitive dyes and drugs since it is able to transfer the excitation energy to molecular oxygen, which gives rise to singlet oxygen. Since phloxine B has a high triplet quantum yield and shows temperature sensitive delayed fluorescence it can be used as a dye to monitor temperature changes.

1.5.3 Fluorescein and Tetramethylrhodamine

In order to make nanoparticle sensors for detection of bacteria in food, we have used the phenomenon of fluorescence resonance energy transfer (FRET) between two chromophores which are attached to gelatin nanoparticles and which work as donor and

acceptor on the same molecule. Tetramethylrhodamine and fluorescein are among the most common fluorophores used as labeling probes for FRET studies.

They are important xanthene dyes with a large range of technical applications due to their high quantum yield of fluorescence, and large absorption in the visible range (Neckers and Valdes-Aguilera, 1993). Fluorescein isothiocyanate and tetramethylrhodamine isothiocyanate react with amino groups such as aliphatic amines, amino acids, peptides, and proteins to form highly fluorescent compounds (Babia, et al. 2001). They have been widely used to label peptides (Mchedlov-Petrossyan, 2003), proteins (Kohl et al., 2002), drugs and other biomolecules (Wang et al., 2004). Fluorescein isothiocyanate (FITC) is a derivative of fluorescein used in wide-ranging applications. FITC is the original fluorescein molecule functionalized with an isothiocyanate reactive group (**-N=C=S**), substituting for a hydrogen atom on the bottom ring of the structure (Figure 1-3). This derivative of fluorescein reacts with nucleophiles including amine and sulfhydryl groups on proteins (Kohl et al., 2002, Wang et al., 2004). FITC has excitation and emission spectrum peak wavelengths of approximately 495 nm and 521 nm, respectively.

TMR-ITC is the base tetramethylrhodamine molecule with functional reactive group of isothiocyanate at one of two hydrogen atoms on the bottom ring of the structure (Figure 1-4). TMR-ITC has its excitation peak at approximately 544 nm and maximum emission peak at approximately 572 nm.

1.5.4   Texas red

Sulforhodamine 101 acid chloride is a red-emitting fluorophore, and it is now commercially available under name Texas red (Figure 1-5). Its molecular formula is $C_{31}H_{29}C_lN_2O_6S_2$, and its molecular weight is 625.2. Texas red has maximum absorption at 578 nm and fluorescence emission at 623 nm. It has been covalently bound to primary amino functions in proteins and other biological substrates due to having free sulfonate residues (Titus et al., 1982). Protein modifications using this compound are best done at low temperatures. Once it is conjugated, however, the sulfonamides that are formed are extremely stable, even surviving complete protein hydrolysis. Texas red is a mixture of two mono-sulfonylchloride derivatives of sulforhodamine 101. Texas red bleaches more slowly than fluorescein and tetramethyrodamine; moreover, the free sulfonic acid groups cause Texas red to be conjugate with more hydrophilic compounds containing free amino groups. This makes Texas red an excellent reagent for single or double labeling of proteins in fluorescence studies (Titus et al., 1982). In this project we have used TMR-ITC and Texas red as donor and acceptor, respectively, to double label gelatin nanoparticles and studied the FRET property of these dyes to detect the possibility of hydrolysis of gelatin by food spoiling bacteria.

1.6   Basic Photophysics

The photophysical processes that occur following the absorption of a photon can be shown graphically in a Jablonski energy level diagram (Figure 1-6). This is perhaps the

most important diagram in photochemistry for the understanding of photoexcited states. Following the absorption of light, a molecule may be raised from the singlet ground state S_0 to singlet exited state S_1. Emission from S_1 to S_0 is called fluorescence (rate k_{RF}) and usually occurs with a lifetime of 10^{-9} to 10^{-8} s. Some non-radiative deactivation processes are also significant here such as internal conversion, intersystem crossing and vibrational relaxation. Along with fluorescence (k_{RF}), internal conversion from S_1 to S_0 (rate k_{IC}), intersystem crossing from S_1 to T_1 (rate k_{ST1}) and collisional quenching by oxygen (rate $k_Q[O_2]$), occur. Phosphorescence (rate k_{RP}) happens when emission is from the excited triplet state T_1 to S_0 with a longer lifetime of 10^{-5} to 1 s. Along with phosphorescence (k_{RP}) non-radiative decay from T_1 to S_0 (rate k_{TS0}), collisional quenching ($k_Q[Q]$) and reverse intersystem crossing from T_1 to S_1 (k_{TS1}), which gives rise to delayed fluorescence, occur. Rate constants k_{RF}, k_{RP}, and k_{ST1} are fixed by the molecular structure of the probe and are not influenced by environmental conditions (Turro, 1991). Vibrational relaxation occurs very quickly ($<1 \times 10^{-12}$ seconds) and is enhanced by physical contact of an excited molecule with other particles with which energy, in the form of vibrations and rotations, can be transferred through collisions. This means that most excited state molecules never emit any energy because in liquid samples the solvent, or in gas phase samples other gas phase molecules that are present, steal the energy before other deactivation processes can occur. Generally, any increase in the molecular mobility of the local environment around the chromophore will enhance the vibrational relaxation rate and the collisional constant (Ludescher et al., 2001). Molecules which contain heavy atoms such as bromine and iodine often have phosphorescence properties

because the presence of heavy atoms enhances intersystem crossing and phosphorescence quantum yield (Lakowicz, 2006).

1.6.1   Emission Intensity:

Emission intensity is proportional to the quantum yield. Quantum yield (φ) is the ratio of emitted photons to absorbed photons. For fluorescence, the quantum yield (φ_F) is the ratio of the rate of fluorescence to the sum of all other de-excitation processes from the singlet state (Hurtubise, 1990; Lakowicz, 2006):

$$\varphi_F = \frac{k_{RF}}{k_{RF} + k_{IC} + k_{ST1} + k_Q[O_2]} \tag{1}$$

In the absence of quencher, which is mostly oxygen, Equation (1) simplifies to:

$$\varphi_F = \frac{k_{RF}}{k_{RF} + k_{IC} + k_{ST1}} \tag{2}$$

For phosphorescence emission, the quantum yield (φ_P) is the product of the quantum yield for the triplet state (φ_T) and the probability of the emission that will take place from the triplet state (q_P) (Hurtubise, 1990),

$$\varphi_P = \varphi_T q_P = \left\{ \frac{k_{ST1}}{k_{RF} + k_{IC} + k_{ST1} + k_Q[O_2]} \right\} \left\{ \frac{k_{RP}}{k_{RP} + k_{TS0} + k_{TS1} + k_Q[O_2]} \right\} \tag{3}$$

In the absence of quencher, Equation (3) simplifies to Equation (4):

$$\varphi_P = \left\{ \frac{k_{ST1}}{k_{RF} + k_{IC} + k_{ST1}} \right\} \left\{ \frac{k_{RP}}{k_{RP} + k_{TS0} + k_{TS1}} \right\} \tag{4}$$

The quantum yield for delayed fluorescence (φ_{DF}) is the product of the quantum yield for fluorescence and the probability of the intersystem crossing from S_1 to T_1 and also reverse intersystem crossing from T_1 back to S_1 (Duchowicz et al., 1998).

$$\varphi_{DF} = \varphi_F \left\{ \frac{k_{ST1}}{k_{RF} + k_{IC} + k_{ST1}} \right\} \left\{ \frac{k_{TS1}}{k_{RP} + k_{TS0} + k_{TS1}} \right\} \tag{5}$$

The ratio of emission intensities of delayed fluorescence (I_{DF}) and phosphorescence (I_P) provides information about the rate constant for reverse intersystem crossing (k_{TS1}).

$$\frac{I_{DF}}{I_P} = \frac{\phi_F \{\frac{k_{ST1}}{k_F}\} \{\frac{k_{TS1}}{k_P}\}}{\{\frac{k_{ST1}}{k_F}\} \{\frac{k_{RP}}{k_P}\}} = \phi_F \frac{k_{TS1}}{k_{RP}} \tag{6}$$

This ratio is highly temperature dependent due to the rate constant for intersystem crossing which is characterized by the Arrhenius equation (Pravinata et al., 2005):

$$k_{TS1}(T) = k_{TS1}^0 e^{\left(\frac{-\Delta E_{TS}}{RT}\right)} \tag{7}$$

where, ΔE_{TS} is the energy gap between S_1 and T_1 Therefore, Equation (6) can be described by the following equation:

$$\frac{I_{DF}}{I_P} = \varphi_F \frac{k_{TS1}}{k_{RP}} = \{\frac{\varphi_F}{k_{RP}}\} k_{TS1}^0 \exp\left(-\frac{\Delta E_{TS}}{RT}\right) \tag{8}$$

ΔE_{TS} can be calculated from the slope of a Vant Hoff plot of the natural log of the ratio of delayed fluorescence intensity (I_{DF}) to phosphorescence intensity (I_P) versus inverse temperature:

$$d[ln(I_{DF}/I_P)]/d(1/T) = -\Delta E_{TS}/R \tag{9}$$

The phosphorescence lifetime is the inverse of the total decay rate. Measuring the intensity decay as a function of time can provide phosphorescence intensity.

$$\tau = (k_P)^{-1} = (k_{RP} + k_{TS1} + k_{TS0} + k_Q[O_2])^{-1} \tag{10}$$

The phosphorescence intensity decay can be fitted with either a single exponential function (Eq. 11) or a stretched exponential function (Eq. 12) depending on the complexity of the matrix and different lifetimes of the triplet probe.

$$I_{(t)} = I_{(0)} \exp\left[-(t/\tau)\right] \tag{11}$$

where, I is intensity at time t, I_o is the initial intensity at time t=0, and τ is the lifetime.

In some cases intensity decays are non-exponential and a stretched exponential function, Kohlrausch-Williams-Watts decay model can be used to analyze the lifetime distribution (Lee et al., 2001).

$$I_{(t)} = I_{(0)} \exp\left[-(t/\tau)^\beta\right] \tag{12}$$

where, $I_{(t)}$ is the intensity as a function of time following pulsed excitation, $I_{(0)}$ is the initial intensity at time zero, τ is the lifetime, and β is the stretching exponent that characterizes the distribution of the decay times.

1.6.2 *Emission Energy:*

Absorption and emission are distributed over a wide range of energies, and the energetic interactions are sensitive to dipolar interactions between the polar chromophore and the immediate environment (Ludescher et al., 2001). Rotational motions of small fluorophores in fluid solution are rapid, typically occurring on a time scale of 40 ps or less. The relatively long timescale of fluorescence allows ample time for the solvent molecules to reorient around the excited state dipole, which can lower its energy and shift the emission to longer wavelengths. High temperatures can also result in thermal disruption of dipole-dipole orientations and shift of the fluorescence emissions to higher wavelengths (Lakowicz and Cherek, 1980). This process is called solvent relaxation and occurs in 10^{-10} s in fluids. In vitrified solvents emission occurs prior to relaxation, and the spectrum of the unrelaxed fluorophore is observed. Under conditions of no relaxation and complete relaxation, the fluorescence lifetimes are relatively constant across the emission spectrum since a single excited state is being observed (Lakowicz and Cherek, 1980).

1.6.3 Stokes' Shift

The energy of emission is typically less than that of absorption. Thus, fluorescence occurs at longer wavelengths (Figure 1-7). The phenomenon is known as the Stokes shift and can be caused by energy losses due to relaxation to ground vibrational states, solvent effects, excited state reactions, complex formation, and energy transfer. (Lakowicz, 2006).

1.7   Fluorescence Resonance Energy Transfer

Fluorescence resonance energy transfer (FRET) is a physical phenomenon first described over 50 years ago. Fluorescence resonance energy transfer has become popular in biological and biophysical applications to qualitatively and quantitatively measure the distance between molecular sites (Kenworthy, 2001; Gordon et al., 1998). The mechanism of fluorescence resonance energy transfer involves a donor (D) fluorophore in an excited electronic state, which may transfer its excitation energy to a nearby acceptor (A) chromophore in a non-radiative fashion through long-range dipole-dipole interactions as shown in Figure 1-8 (Lakowicz, 2006). This process occurs when the emission spectrum of a donor overlaps with the absorption spectrum of the acceptor (Figure 1-9). In the majority of cases the acceptor is a fluorescent dye, although this is not necessary (Berney and Danuser, 2003). The extent of resonance energy transfer is determined by the distance between the donor and acceptor and the extent of spectral overlap. The range over which the energy transfer can take place is limited to

approximately 10 nanometers (100 angstroms), and the efficiency of transfer is extremely sensitive to the separation distance between fluorophores. This distance is called Förster distance and is denoted as R_0.

In order to develop a sensor to detect the secretion of proteases by some food spoilage organisms we have used sensitivity of FRET to proteolysis of peptides. A fluorescent donor attached to one of the amino acid residues of the peptide transfers energy to a quenching acceptor attached to another residue after the resonance mechanism takes place. Therefore, the quenched fluorescence can be detected in case of cleavage of any peptide bond between the donor/acceptor pair.

1.8   Hypothesis

Edible hydrocolloid luminescent nanoparticles which are sensitive to specific properties of food can be used as sensors for temperature, oxygen and bacteria.

1.9   Research Objectives

1.9.1   Objective 1:

1.9.1.1   Nanoparticle Sensor for Temperature

Develop a hydrocolloid nanoparticle sensor to detect temperature change in food. To achieve this goal we have used the phosphorescence sensitivity of a chromophore such as erythrosin-B to temperature to show the correlation between the ratio of delayed fluorescence to phosphorescence (I_{DF}/I_P) and temperature.

1.9.2   Objective 2:

1.9.2.1   Nanoparticle Sensor for Oxygen

This project has investigated the use of a hydrocolloid nanoparticle sensor for detecting the presence of oxygen in food based on the phosphorescence quenching property of the chromophore in the presence of oxygen.

1.9.3   Objective 3:

1.9.3.1   Nanoparticle Sensor for Bacteria

This project studied the feasibility of developing a hydrocolloid nanoparticle sensor for detection of food spoilage organisms based on fluorescence resonance energy transfer between two chromophores which work as donor and acceptor on the same molecule.
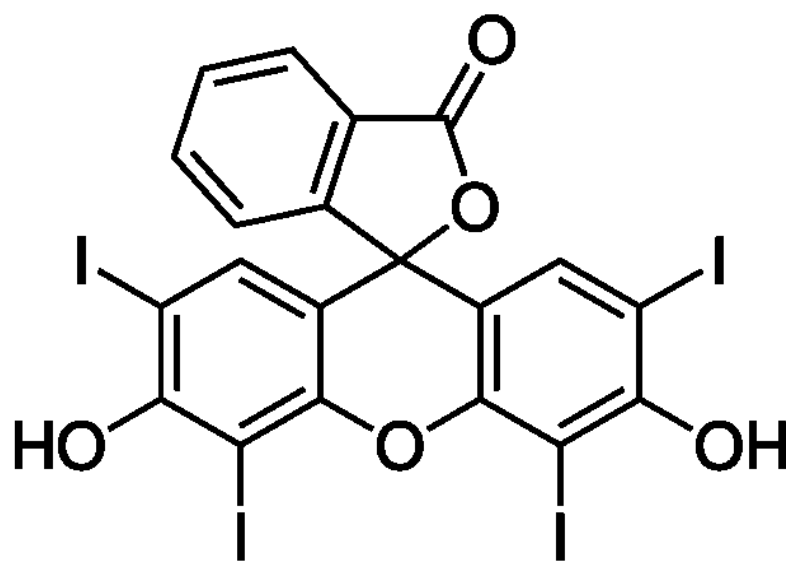
Figure 1-1: Erythrosin-B molecular structure (www.sigmaaldrich.com).
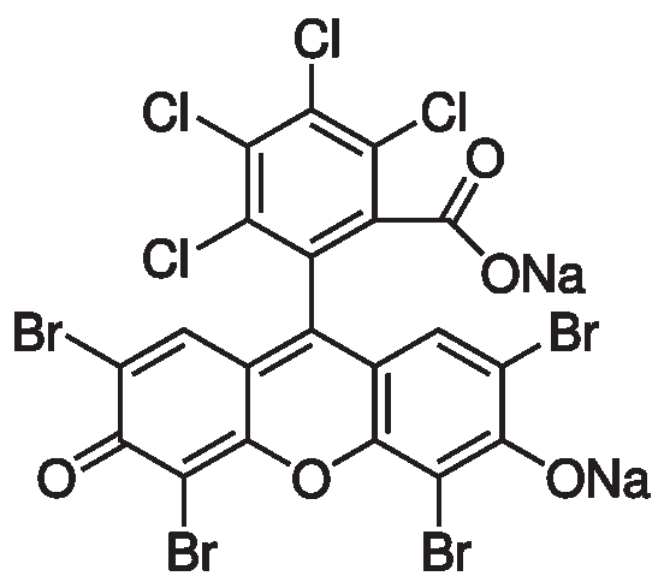
Figure 1-2: Erythrosin-B molecular structure (www.sigmaaldrich.com).
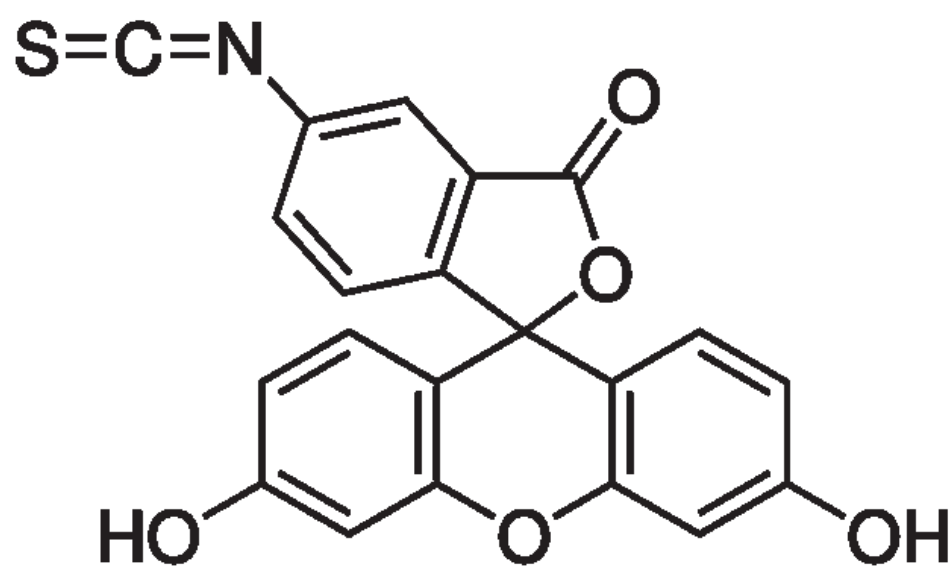
Figure 1-3: Fluorescein-ITC molecular structure (www.sigmaaldrich.com).
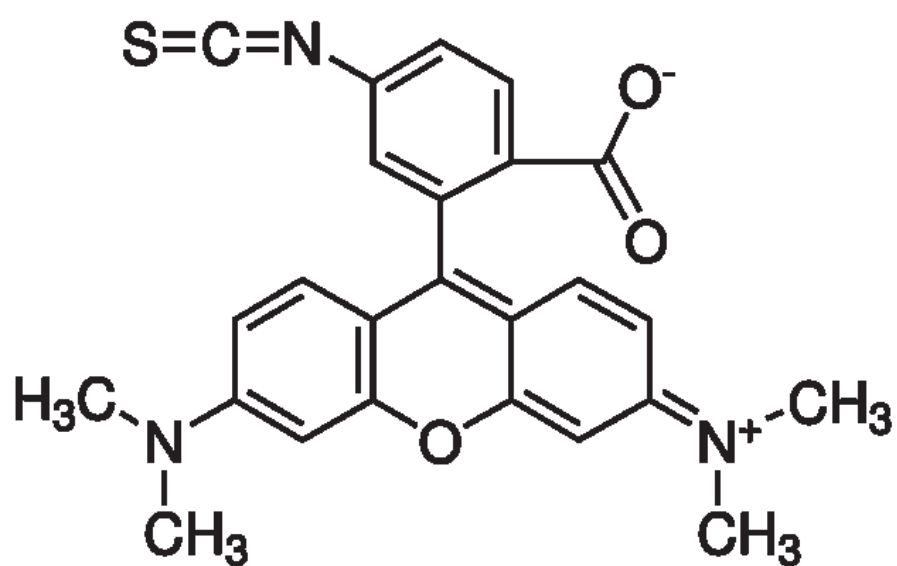
Figure 1-4: Tetramethylrodamine-ITC molecular structure (www.sigmaaldrich.com).
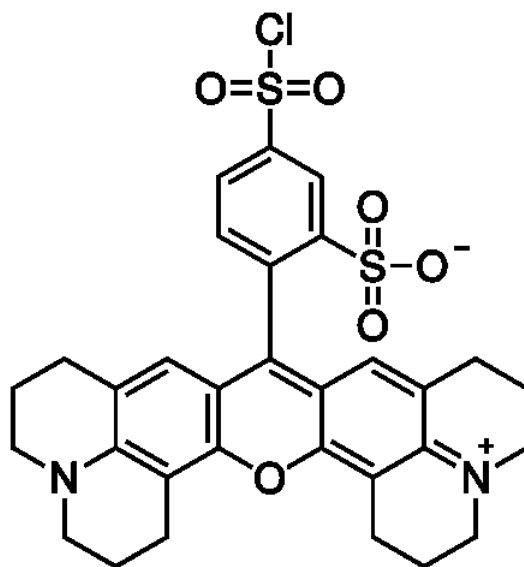
Figure 1-5: Texas Red molecular structure (www.sigmaaldrich.com).
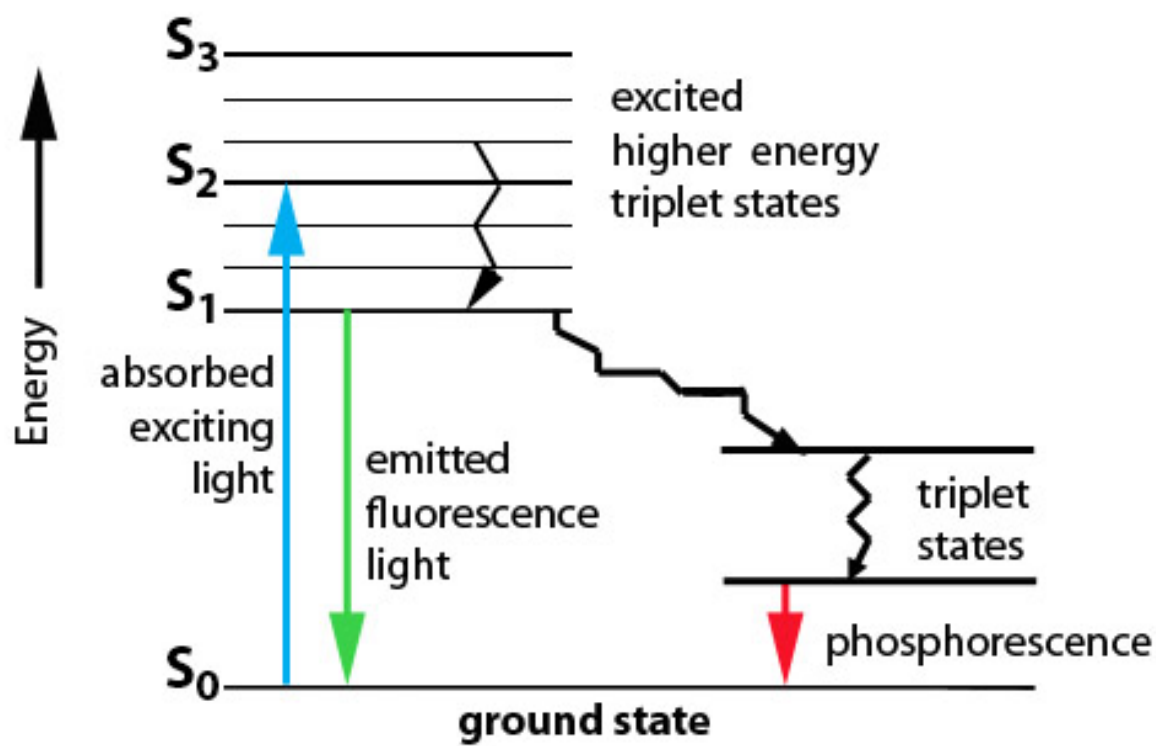
Figure 1-6 : Jablonski diagram (University of Victoria, Advance Imaging Laboratory).
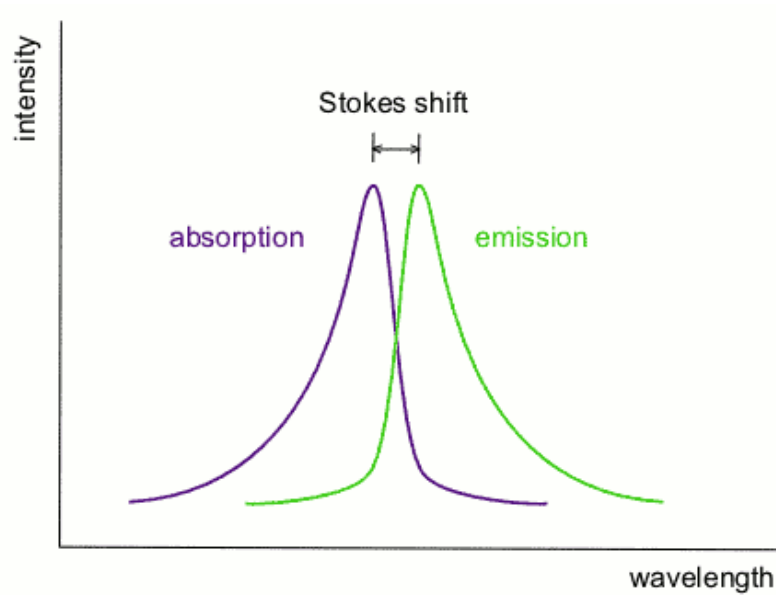
Figure 1-7 : Stokes shift (Wikipedia).
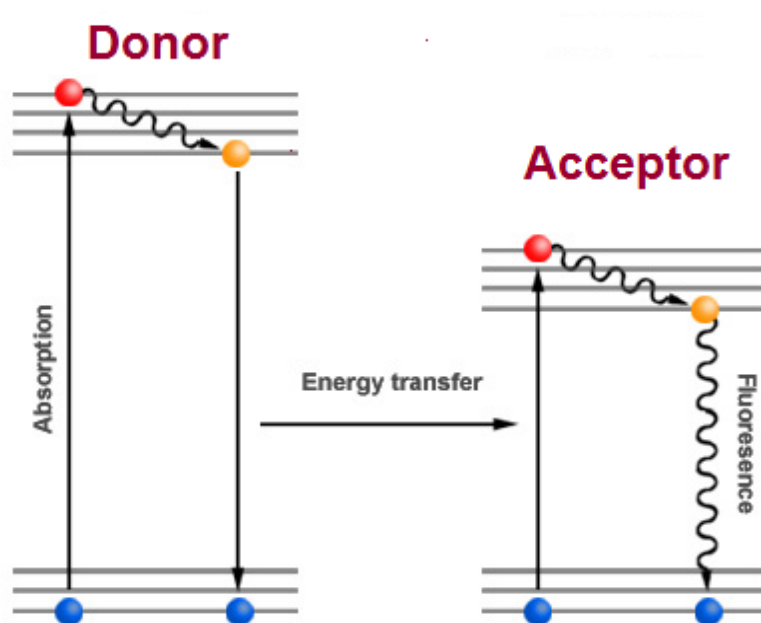
Figure 1-8 : Jablonski diagram illustrating the FRET process (Hussain, 2012).
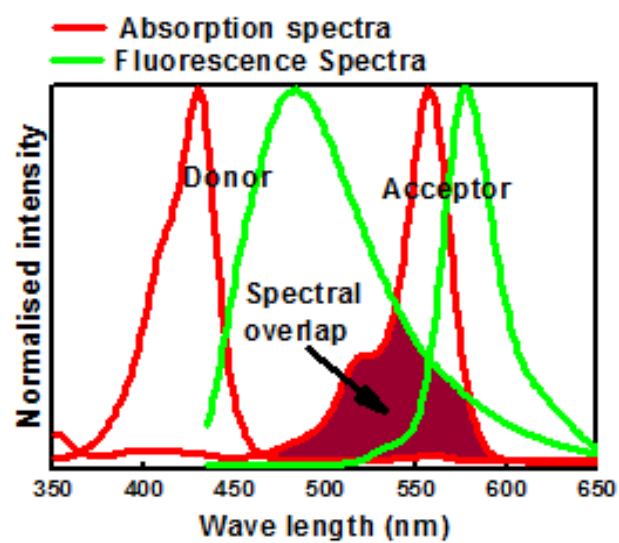
Figure 1-9 : Absorption and fluorescence spectra of an ideal donor-acceptor pair. Brown colored region is the spectral overlap between the fluorescence spectrum of donor and absorption spectrum of acceptor. (Hussain, 2012).

References

Adler, J., Baldwin, P., Melia, C., Starch damage. Part 2: types of damage in ball-milled starch, upon hydration observed by confocal microscopy. Starch/ Staerke 47, 252-256, (1995).

Aynie I, vauthier C, chacun H, Fattal E, Couvreur P. Spongelike alginate nanoparticles as a new potential system for the delivery of antisense oligonucleotides. Antisense Nucleic Acid Drug Dev. 9(3), 301-12, 1999.

Azarmi Shirzad, Huanga Yuan , Chend Hua, McQuarriea Steve , Abramse Douglas, Road Wilson , Finlayf Warren H., Millera Gerald G. Löbenberga Raimar. Optimization of a two-step desolvation method for preparing gelatin nanoparticles and cell uptake studies in 143B osteosarcoma cancer cells. J Pharm Pharmaceut Sci 9(1),124-132, 2006.

Babia T, Ledesma M.D., Saffrich R, Kok J.W, Dotti C.G., Egea G.. Endocytosis of NBD-Sphingolipids in Neurons: Exclusion from Degradative Compartments and Transport to the Golgi Complex, Traffic, 2, 395-405, 2001.

Badenhuizen, N., Detection of changes in the paracrystalline pattern of starch granules by means of acridine orange. Starch- Staerke 17(3), 69-74,1965.

Barone, P., Baik, S., Heller, D., Strano, M. Modulating single walled carbon nanotube fluorescence in response to specific molecular adsorption. AIP Conf. Proc., 786, 193-197, 2005a.

Barone, P., Baik, S., Heller, D., Strano, M. Near-infrared optical sensors based on single-walled carbon nanotubes. Nature Materials, 4, 86-92, 2005b.

Berney C.and Danuser D., FRET or No FRET: A Quantitative Comparison, Biophysical Journal, 84, 3992–4010, 2003.

Cascone M., Lazzeri L., Carmignani C., Zhu Z. Gelatin nanoparticles produced by a simple W/O emulsion as delivery system for methotrexate. J. Material Sci. Mat. Med. 13, 523-526. 2002.

Chavanpatil M. D., Khdair A., Panyam J. Surfactant-polymer : A Novel Platform for Sustained and Enhanced Cellular Delivery of Water-soluble Molecules. Pharm. Res. 24, 803–810, 2007.

Ciofani, G., Raffa, V., Menciassi, A., Micera, S., Takeoka S. Magnetic Driven Alginate Nanoparticles for Targeted Drug Delivery. Current Nanoscience, 4 (2), 212-218, 2008.

Coester CJ, Langer K, Van Briesen H, Kreuter J. Gelatin nanoparticles by two-step desolvation-a new preparation method, surface modifications and cell uptake. J Microencapsul, 17, 187-193, 2000.

Daniel M.-C. and Astruc D., "Gold nanoparticles: assembly, supramolecular chemistry, quantum-size related properties, and applications toward biology, catalysis, and nanotechnology," Chem. Rev. 104, 293- 346, 2004.

Duchowicz, R., Ferrer M.L. and Acuna A.U. Kinetic spectroscopy of erythrosin phosphorescence and delayed fluorescence in aqueous solution at room temperature. Photochem. Photobiol, 68, 494-501, 1998.

Dziechciarek Y.,. van Schijndel R. J. G , Gotlieb K. F., Feil H. , van Soest J. J. G., ATO-DLO, Wageningen, The Netherlands, Dutch Society of Rheology (NRV), October 22nd, 1998 (http://www.mate.tue.nl/nrv/ede/dziechciarek.html).

Elysee-Collen, B., Lencki, R. W. Protein ternary phase diagrams. Effect of ethanol, ammonium sulfate, and temperature on the phase behavior of type B gelatin. J. Agric. Food Chem. 44, 1651±1657, 1996.

Farrugia CA and Groves MJ, Gelatin Behaviour in Dilute Aqueous Solution: Designing a Nanoparticulate Formulation, J. Pharm. Pharmacol., 51, 643-649, 1999

Garland, P. B. and Moore, C. H. (1979). Phosphorescence of Protein-Bound Eosin and Erythrosin. Biochemical Journal 183, 561-572.

Gershkovich A.A., Kholodovych V.V., Fluorogenic substrates for proteases based on intramolecular fluorescence energy transfer (IFETS), J. Biochem. Biophys. Methods, 33, 135-162, 1996.

Gordon, G. W., Berry G., Liang X. H., Levine B. and Herman B.. Quantitative fluorescence resonance energy transfer measurements using fluorescence microscopy. Biophys. J., 74, 2702–2713, 1998.

Gupta, A., Gupta, M., Yarwood, S., Curtis, A. Effect of cellular uptake of gelatin particles on adhesion, morphology, and cytoskeleton organization of human fibroblasts. J. Controlled Release 95, 197-207, 2004.

Haessig A. and Stampfli K., Plasma substitutes past and present. Bibliotheca Haematologica, 33, 1- 8, 1969.

He, X., Wang, K., Tan, W., Li, J., Yang, X., Huang, S., Li, D., Xiao, D. Photostable luminescent nanoparticles as biological label for cell recognition of systemic lupus erythematosus. J. Nanosci. Nanotech., 2, 317-320, 2002.

Heitz, J. R. 1995. Pesticidal applications of photoactivated molecules, 1-16. In J. R. Heitz and K. R. Downum [eds.], Light activated pest control. ACS Symposium Series 616. American Chemical Society, Washington, DC.

Hurtubise R.J. Phosphorimetry : Theory Instrumentation, and Applications. New York: VCH Publishers, Inc, 1990.

Hurtubise R.J. Solid matrix luminescence analysis: photophysics, physicochemical interactions and applications. Analytical Chimica Acta 351, 1-22, 1997.

Hussain SA, An Introduction to Fluorescence Resonance Energy Transfer (FRET) Science Journal of Physics ISSN:2276-6367, Volume 2012, Article ID sjp-268, 4 Pages, 2012.

Inbaraj J J., Kukielczak B M., Chignell C F., Phioxine B Phototoxicity: A Mechanistic Study Using HaCaT Keratinocytes Journal of Photochemistry and Photobiology, 81(1), 81-88, 2005.

Jahanshahi, M., Sanati, M. H., Hajizadeh, S., Babaei, Z. Gelatin nanoparticle fabrication and optimization of the particle size. Physica Status Solidi A: Applications and Materials Science, 205(12), 2898-2902, 2008.

Jain AK, Khar RK, Ahmed FJ, Diwan PV., Effective insulin delivery using starch nanoparticles as a potential trans-nasal mucoadhesive carrier. European Journal of Pharmaceutics and Biopharmaceutics , 69(2), 426-435, (2008).

Jang KI, Lee HG. Stability of chitosan nanoparticles for L-ascorbic acid during heat treatment in aqueous solution. J Agric Food Chem. 56(6), 1936–1941, 2008.

Kamat P. V., "Photophysical, photochemical and photocatalytic aspects of metal nanoparticles," J. Phys. Chem. B 106 (32), 7729 -7744, 2002.

Kataoka K, Kwon GS, Yokoyama M, Okano T, Sakurai Y. Block copolymer micelles as vehicles for drug delivery. J Controlled Release 24(1-3),119- 132, 1993.

Kaul G, Amiji M. Biodistribution and targeting potential of poly(ethylene glycol)-modified gelatin nanoparticles in subcutaneous murine tumor model. J Drug Target, 12(9–10), 585–91, 2004.

Kenworthy, A. K. Imaging protein-protein interactions using fluorescence resonance energy transfer microscopy. Methods. 24, 289–296, 2001.

Kim, K., Byun, Y. Controlled release of all-trans retinoic acid from PEGylated gelatin nanoparticles by enzymatic degradation. Biotech. Bioproc. Eng., 4, 215-218, (1999).

Kohl T., Heinze K.G., Kuhlemann R., Koltermann A. and Schwille P., A protease assay for two-photon crosscorrelation and FRET analysis based solely on fluorescent proteins. PNAS, 99(19), 12161–12166, 2002

Kommareddy S., Amiji M. Poly(Ethylene Glycol)-Modified Thiolated Gelatin Nanoparticles for Glutathione-Responsive Intracellular DNA Delivery. Nanomedicine 3(1), 32–42, 2007.

Kommareddy S., Tiwari SB., Amiji M. Long-circulating polymeric nanovectors for tumor-selective gene delivery. Technol Cancer Res Treat, 4(6), 615–625, 2005.

Kommareddy, S., Amiji, M., Preparation and evaluation of thiol-modified gelatin nanoparticles for intracellular DNA delivery in response to glutathione. Bioconj. Chem., 16, 1423-1432, (2005)

Lakowicz J. and Cherek H., Dipolar Relaxation in Proteins on the Nanosecond Timescale Observed by Wavelength-resolved Phase Fluorometry of Tryptophan Fluorescence. Journal of Biological Chemistry, 255(3)3, 831-834, 1980.

Lakowicz, J. R. Principles of Fluorescence Spectroscopy.Plenum Press, NY., 2006

Lee K.C.B, Siegel J, Webb S.E.D, Leveque-Fort S, Cole M.J, Jones R, Dowling K, Leve M.J, and French P.M.W. Applications of the stretched exponential function to fluorescence lifetime imaging. Biophysical Journal 81, 1265-74, 2001.

Leo E, Vandelli MA, Cameroni R, Forni F. Doxorubicin-loaded gelatin nanoparticles stabilized by glutaraldehyde: Involvement of the drug in the cross-linking process. Int J Pharm 12, 75-82, 1997.

Lh HQ, Schmitz U, Niggemann B, Zanker KS: Computer-assisted molecular design for the determination of structure-activity relationships for chemopreventive agents. In: Cancer: Genetics and the environment. Ann NYAcad Sci 833,147-153, 1997.

Li, J., Wang, N., Wu, X. Gelatin nanoencapsulation of protein/peptide drugs using an emulsifier-free emulsion method. J. Microencap. 14, 163-172, 1998.

Ludescher R.D, Shah N.K, McCaul C.P, and Simon K.V. Beyond Tg: optical luminescence measurements of molecular mobility in amorphous solid foods. Food Hydrocolloids 15, 331-39, 2001.

Lukasik K. V. & Ludescher, R. D. "Molecular Mobility in Water and Glycerol Plasticized Cold and Hot-Cast Gelatin Films, 20, 96-105, 2006.

Mchedlov-Petrossyan N.O, Kukhtik V.I, Bezugliy V.D., Dissociation, tautomerism and electroreduction of xanthene and sulfonephthalein dyes in N,N-dimethylformamide and other solvents. Journal of Physical Organic Chemistry, 16(7), 380–397, 2003.

Muller RH, Mader K, Gohla S. Solid lipid nanoparticles (SLN) for controlled drug deliveryreview of the state of the art. Eur J Pharm Biopharm 50:161-177, 2000.

Murphy, C. Optical sensing with quantum dots. Anal. Chem., 74, 520A-526A, 2002.

Nack, T. J., & Ludescher, R. D. Molecular mobility and oxygen permeability in amorphous bovine serum albumin films. Food Biophysics, 1, 151–162, 2006.

Neckers D.C., Valdes-Aguilera OM. Photochemistry of the xanthene dyes, Adv. Photochem. 18, 315–394, 1993.

Oldmixon E H., Mallory's Phloxine B-Methylene Blue-Azure II Stain Emphasizes Elastin and Collagen Bundles in Epoxy Embedded Lung, Biotechnic & Histochemistry, 63(3), 165-170, 1988

Oppenheim, R.C., Stewart, N.F., The manufacture and tumor cell uptake of nanoparticles labeled with fluoroscein isothiocyanate. Drug Dev. Ind. Pharm. 5, 583–591, 1979.

Parker C.A. Photoluminescence of Solutions. Amsterdam: Elsevier Pub Co., 1968.

Pravinata, L.C., You, Y., & Ludescher, R.D. Erythrosin B phosphorescence monitors molecular mobility and dynamic site heterogeneity in amorphous sucrose. Biophysical Journal, 88, 3551-3561, 2005.

Qi H,Takano H, Kato Y, Wu Q, Ogata C, Zhu B, Murata Y, Nakamura Y, Hydogen peroxide-dependent photocytotoxicity by phloxine B, a xanthene-type food colorant Bioche Biophys Act 1810(7), 704-12, 2011.

Qi L-F, Xu Z-R, Li .Y , Jiang X, Han X-Y, In vitro effects of chitosan nanoparticles on proliferation of human gastric carcinoma cell line MGC803 cells. World J Gastroenterology. 11(33), 5136-5141, 2005.

Rasooly, R. Phloxine B, aversatile bacterial stain. International Journal of Food Microbiology.157, 29-34, 2007.

Rosi N. L., and Mirkin C. A., "Nanostructures in biodiagnostics," Chem. Rev. 105, 1547-1562, 2005.

Schwick H. G. and Heide K., Immunochemistry and immunology of collagen and gelatin [Review]. Bibliotheca Haematologica, 3, 111-125, 1969.

Seguchi, M. Dye binding to the surface of wheat starch granules. Cereal Chem. 64, 518-520, 1986.

Simon-Lukasik, K. V., & Ludescher, R. D. Erythrosin B phosphorescence as a probe of oxygen diffusion in amorphous gelatin films. Food Hydrocolloids, 18, 621–630, 2004.

Sundaresan, K. & Ludescher, R. D. "Molecular Mobility and Oxygen Permeability in Amorphous β-Lactoglobulin." Food Hydrocolloids 22, 403–413, 2008.

Titus, J. A., et al., Texas Red, a hydrophilic, red-emitting fluorophore for use with fluorescein in dual parameter flow microfluorometric and fluorescence microscopic studies. J. Immunol. Methods, 50(2), 193-204 (1982).

Vanderkooi J.M., Maniara G., Green T. and Wilson D. An Optical Method for Measurement of Dioxygen Concentration Based upon Quenching of Phosphorescen. The Journal of Biological Chemistry, 262, 5476-5482, 1987.

Verma AK, Sachin K, Saxena A, Bohidar HB. Release kinetics from bio polymeric nanoparticles encapsulating protein synthesis inhibitor -Cycloheximide, for possible therapeutic applications. Curr Pharm Biotech, 6(2), 121-130, 2005.

Wang L., Gaigalas A.K., Blasic J., Holden M.J., Spectroscopic characterization of fluorescein- and tetramethylrhodamine-labeled oligonucleotides and their complexes with a DNA template. Spectrochimica Acta Part A 60, 2741–2750, 2004.

Wang, L., Wang, L., Xia, T., Bian, G., Dong, L., Tang, Z., Wang, F. A highly sensitive assay for spectrofluorimetric determination of reduced glutathione using organic nano-probes. Spectrochim. Acta, Part A: Molec. Biomolec. Spectro, 61A, 2533-2538, 2005.

Weber C., Kreuter J., La K. Desolvation process and surface characteristics of HSA-nanoparticles, International Journal of Pharmaceutics 196,197–200, 2000.

Wen-Li Du, Ying-Lei Xu, Zi-Rong Xu, Cheng-Li F., Preparation, characterization and antibacterial properties against E. coli K88 of chitosan nanoparticle loaded copper ions. Nanotechnology, 19, 085707 (5pp) 2008.

www.sigmaaldrich.com

www.wikipedia.org

Xiao Sy., Tong Cy., Liu Xm., Yu D., Liu Ql., Xue Cg., Tang Dy., Zhao Lj., Preparation of folate-conjugated starch nanoparticles and its application to tumor-targeted drug delivery vector. Chin Sci Bull, 51(14), 1693-1697, 2006.

Ye, Z., Tan, M., Wang, G., Yuan, J. Preparation, characterization and application of fluorescent terbium complex-doped zirconia nanoparticles. J. Fluor. 15, 499-505, 2005.

Yeh TK, Lu Z, Wientjes MG, Au JLS. Formulating paclitaxel in nanoparticles alters its disposition. Pharm Res, 22(6), 867-874, 2005.

Zhai F, Li D, Zhang C, Wang X, Li R, Synthesis and characterization of polyoxometalates loaded starch nanocomplex and its antitumoral activity. European Journal of Medicinal Chemistry, 43(9), 1911-1917, 2008.

Zwiorek K., kloeclner J., Wagner E., Coester C., Gelatin nanoparticles as a new and simple gene delivery system. J pharm Pharmaceuti Sci., 7(4), 22-28, 2004.

2 TEMPERATURE SENSOR

2.1 Nanoparticle Sensor for Temperature

Goal: To develop a hydrocolloid nanoparticle sensor to detect temperature change in food.

To achieve this goal we used the phosphorescence sensitivity of a chromophore such as erythrosine B and phloxine B to temperature to show the correlation of the delayed fluorescence and phosphorescence ratio (I_{DF}/I_P) with temperature.

2.2 Background

A temperature sensor is a device that collects data regarding the temperature from a source and converts it to a form that can be understood either by an observer or another device. Temperature sensors have been made in many different forms and of different materials and have been used for a wide variety of purposes, from simple home and personal use to very accurate and precise scientific use. This project has developed a novel class of edible hydrocolloid food nanosensors such as gelatin nanoparticles and starch nanoparticles which are doped with luminescent chromophores and can be used to provide information about the local food matrix such as temperature. The luminescence properties of the probes such as phosphorescence and delayed fluorescence provide the sensor sensitivity to the temperature.

The xanthene dyes are an extremely helpful group of luminescent and triplet forming dyes for practical applications and theoretical studies. The rate of intersystem crossing for triplet forming xanthene dyes is measured in different environments such as liquid, amorphous solid and solid (Pravinata et al., 2005, Nack & Ludescher 2006). This family of fluorescein derivatives includes erythrosine B, phloxine B, eosin and rose bengal. These dyes are mostly in the form of sodium salts of their sulfonic or carboxylic acids, and they are water-soluble (Duarte et al. 2012). They are anionic, and can be attached to cationic groups in solid matrices and thus, they can be applied to all kind of natural fibers like wool, cotton and silk as well as to synthetics like polyesters, acrylic and rayon (Duarte et al, 2012). They can be also applied to food matrices like gelatin, BSA, milk proteins, and amorphous sucrose (Simon-Lukasik & Ludescher, 2004; Nack & Ludescher, 2006; Sundaresan & Ludescher, 2008; and Pravinata et al., 2005). Starch granules have been non-covalently labeled with eosin Y (Seguchi, 1986). They are also used in plastics, inks, paints and leather.

Erythrosine B is an E-type luminescent chromophore which shows delayed fluorescence, because the first exited singlet state (S_1) and the triplet state (T_1) are close in energy (Parker, 1968). Erythrosine B has 98% of excited molecules converting to the triplet state and has high quantum yield and is considered as an ideal probe for phosphorescence studies (Garland and Moore, 1979). The phosphorescence of erythrosine B is due to the xanthene ring with four iodine atoms. When erythrosine B is thermally activated it goes through reverse intersystem crossing from triplet state to singlet and generates delayed fluorescence. If the ratio of delayed fluorescence (I_{DF}) to phosphorescence (I_P)

monotonically changes with temperature (T), it can perform as a temperature sensor. In this case, the relationship between I_{DF}/I_P and T is obtained from the analysis of test data as described in the following sections.

Phloxine B is a derivative of fluorescein with noticeably bluish shade used for disinfection and detoxification of wastewater through photooxidation. The difference between this molecule and fluorescein is the presence of four bromine atoms at positions 2, 4, 5 and 7 of the xanthene ring and four chlorine atoms in the carboxyphenyl ring (Duarte et al, 2012). The phosphorescence of phloxine B is due to the xanthene ring with four bromine atoms. When phloxine B is thermally activated, it goes through reverse intersystem crossing from the triplet to the singlet state and generates delayed fluorescence. Phloxin its the maximum emission about 710 nm, absorption about 500nm and shows delayed fluorescence at about 570 nm.

2.3   Material and Methods

2.3.1   Preparation of gelatin nanoparticles

Gelatin nanoparticles were prepared by the two-step desolvation method (Azarmi et al. 2006). 1.25 g of type A gelatin (100 Bloom) from Vyse Gelatin Company (Schiller Park, IL), was dissolved in 25 mL distilled water [Milli-Q water (18.3 MΩ) was used in all experiments]. The solution was stirred under constant heating until a clear solution was obtained. 25 ml acetone from VWR International was added to the gelatin solution to precipitate the higher molecular weight gelatin (HWG) and yield more homogeneous

gelatin nanoparticles. The removal of the low molecular weight gelatin in the supernatant after the first desolvation step reduced the formation of aggregates during cross-linking due to an enhanced stability of particles formed before cross-linking, and prevented further secondary aggregation and flocculation of particles during storage. The solution was left at room temperature for 3 hr. Then the supernatant was discarded and the sediment re-dissolved in 25 ml distilled water under constant heating. The solution was stirred until a clear solution was obtained. HCL 1N from Sigma-Aldrich was added drop-wise to adjust the pH of gelatin solution to 2.5. At the second step desolvation, 75 ml acetone was added drop-wise to form nanoparticles. At the end, 250 μL of 25% glutaraldehyde solution from Sigma-Aldrich was added to crosslink the nanoparticles, and the solution was stirred for 12h. The remaining solvent was evaporated by a rotary evaporator. The nanoparticles were transferred to a dialysis membrane tube having 1000 Da molecular weight cutoff and dialyzed against distilled water for 24 hr to remove unreacted cross-linking (glutaraldehyde) agent and other impurities. The nanoparticles were then freeze-dried and stored in refrigerator for further experiments. The particle size was measured by particle size analyzer 90 Plus (Brookhaven Instruments Corporation).

2.3.2   *Preparation of Starch Nanoparticles*

Starch nanoparticles were prepared by a water/oil (W/O) nanoemulsion. In this method, phosphoryl chloride was used as a cross-linker (Wang et al., 2004). 0.5 g of soluble starch was added to 5 ml distilled water and heated in a boiling water-bath until a clear

solution was obtained. This aqueous solution was cooled to room temperature, and 100 mg of K_2SO_4 was added. The aqueous phase was added drop-wise to an oil-phase (containing 100 mL of $C_6H_5CH_3$, 100 mL of $CHCl_3$ and 4 mL of surfactant Span-80) with constant stirring until a microemulsion was formed. Then the microemulsion was treated by Sonifier cell disruptor W185 from Heat Systems-Ultrasonics Inc (Farmingdale, NY), for 5 min in order to obtain a nanoemulsion. 600 μL of $POCl_3$ was added to this nanoemulsion and stirring was continued for another 1 h. The nanoemulsion was washed three times with acetone and then ethanol respectively, to obtain white solid starch nanoparticles. Solid starch nanoparticles were dissolved in distilled water and then passed through 0.2 μm Whatman® PES filters to remove any particle with a diameter larger than 200 nm. Then dissolved nanoparticles were dialyzed against 1.5 L distilled water for 2 days using a dialysis membrane tube with a 1000 Da molecular weight cutoff. After dialysis nanoparticles were freeze-dried to obtain dry powder and the dry powder of starch nanoparticles was kept in a refrigerator for further use. In the original method, polyoxometalates, instead of K_2SO_4, was added and encapsulated in starch nanoparticles. However, with removal of polyoxometalates, there were no white solid starch nanoparticles precipitated upon washing the nanoemulsion with acetone and ethanol. Therefore, K_2SO_4 was added as a substitute for polyoxometalates. Other salts may also work but have not been tried.

Washing the nanoemulsion with acetone and ethanol is important because they cause precipitation of the nanoparticles from the W/O emulsion. They also help remove any remaining phosphoryl chloride and dilute the acidity of the nanoparticles solution, which

results from the reaction of phosphoryl chloride with water. Solid starch nanoparticles can simply turn dark when dissolved in water if not well washed by acetone and ethanol. The high acidity of the nanoparticle solutions may be a reason for this observation. The nanoparticles were transferred to a dialysis membrane tube having 1000 Da molecular weight cutoff and dialyzed against distilled water for 24 hr to remove unreacted phosphoryl chloride and other impurities like potassium sulfate. Removing the unreacted phosphoryl chloride can minimize over-cross-linking of nanoparticles, which would decrease the solubility of the nanoparticles in water during storage. The dry powder of starch nanoparticles can be then stored in refrigerator for a few months.

Soluble starch from potato, toluene, chloroform, sodium phosphate dibasic heptahydrate, sodium phosphate monobasic anhydrous, sodium acetic trihydrate, potassium sulfate, Span-80, Trizma® base, phosphoryl chloride, harmane and quinine hemisulfate monohydrate were purchased from Sigma-Aldrich. Phosphoric acid (85%), hydrochloric acid, glacial acetic acid, acetone and ethanol were obtained from Fisher Scientific.

2.3.3   Determining Nanoparticles Size

Gelatin or starch nanoparticle solutions were diluted in distilled water 1:400 and transferred into small testing tubes. The diluted sample was tested using a 90Plus Particle Size Analyzer from Brookhaven Instruments Corporation (Holtsville, NY) before labeling to determine particle sizes. The diluted samples were measured at a temperature of 25°C and a scattering angle of 90°.

2.3.4   Labeling Gelatin Nanoparticles and Starch Nanoparticles

10 mg of freeze-dried gelatin nanoparticels was dissolved in 10 ml DI water and stirred under constant heating until a clear solution was obtained. Erythrosine B was dissolved in spectrophotometric grade dimethylformamide to prepare a 10 mM stock solution. Erythrosine B from the stock solution was added to 10 ml gelatin nanoparticle solution to make 10 μM erythrosine B solution. This solution was stored overnight at room temperature. Then the erythrosine B labeled nanoparticles were transferred to a dialysis membrane tube having 1000 Da molecular weight cutoff and dialyzed against distilled water for 48 hr to remove unreacted, free dye. The dialysis water was changed every 6 to 8 hr. this procedure attached erythrosine B to gelatin nanoparticles. In order to attach other luminescence probes to gelatin nanoparticles the same method was applied. For the purpose of labeling starch nanoparticles with a luminescence probe such as erythrosine B and phloxine B a similar procedure was followed.

The dialysis during the labeling process aims to remove unlabeled free probe. Detectable phosphorescence and fluorescence signals of unreacted probes were observed normally in the first two batches of dialysis water and almost disappeared or became very weak after 24 hr of dialyzing, indicating that 48 hours of dialyzing can eliminate all free dyes from the nanoparticle solution.

2.3.5   Preparing Sample for Temperature Sensor

1 ml of erythrosine B or phloxine B labeled gelatin nanoparticles was transferred into a cylinder and diluted with DI water with relative ratio of 1:10 to obtain a pale pink solution. This solution was used for the experiments. Two types of samples were prepared in order to study the application of nanoparticle sensors in liquid and solid foods.

2.3.6   Liquid Samples

Prior to any experiments cuvettes were washed in the cuvette washer with soap; rinsed with DI water, ethanol and acetone; and dried for few minutes. 40 μL of the diluted pale pink solution of erythrosine B or phloxine B labeled gelatin nanoparticles was added to 2 ml of any liquid food solution and placed in a clean standard 1cm x 1cm fluorescence cuvette for luminescence measurement. Liquid food solutions included buffer solutions of pH 3 and pH 7, water, Tropicana orange juice containing no pulp (Table 2-1), Seagram's ginger ale (Table 2-2), lemonade juice drink from Brisk (Table 2-3), Red bull energy drink (Table 2-4) and Gatorade (Table 2-5). Nitrogen was purged for 30 minutes through the prepared sample in cuvette before starting and during the experiment to prevent oxygen quenching of the triplet state.

2.3.7   Solid Samples

In the case of solid samples, 20 μL of the diluted pale pink solution of erythrosine B or phloxine B labeled gelatin nanoparticles was dropped on the surface of approximately 1 to 1.5 cm^2 solid samples including Doritos cheese nacho (Table 2-6), Tostitos scoop nacho (Table 2-7), Nabisco unsalted top saltine cracker (Table 2-8), SunTree banana chips (Table 2-9), Lays classic potato chips (Table 2-10) and white pita bread (Table 2-11). Samples were dried by a heat gun for few minutes and fitted diagonally into a standard 1cm x 1cm fluorescence cuvette for luminescence measurement. Nitrogen was purged for 30 minutes through the cuvette containing the sample prior to the experiment and during the experiment to prevent oxygen quenching of the triplet state. The effect of relative humidity on the behavior of nanoparticle sensors in solid foods was investigated by subjecting some of the food samples to various levels of relative humidity as described below.

2.3.8   Relative Humidity

Four saturated salt solutions with different relative humidities, namely lithium chloride with RH=11.3%, potassium acetate with RH=23.4%, magnesium chloride with RH=33.5% and potassium carbonate with RH =43% were used for this experiment. 10 gr of each salt were added into small desiccators, and a small amount of water was added to the desiccators in order to make a saturated salt solution. All 4 desiccators were monitored everyday, and water or salts were added as needed to facilitate making a stable

saturated salt solution. Erythrosine B labeled gelatin nanoparticles were added to small pieces of solid samples of cheese nacho, nacho, dried banana and potato chips. The samples were dried by heat gun for 5 minutes. 4 aluminum containers were weighed. Then 4 to 5 small pieces of one sample - for example potato chips were placed into the aluminum containers and were weighed again and weights were recorded. The aluminum containers which contained potato chips were placed into the 4 different desiccators with different relative humidity and equilibraed for 3 days. The aluminum containers which contained potato chips were weighed again after 3 days and weights were recorded. They were placed into the same desiccators, where they stayed for another 2 days and weighed again. The samples were weighed every 2 days until 3 constant weight measurements were achieved consecutively. When the samples reached the target humidity, their weights were stabilized and they were ready for further tests. This test was performed on Doritos cheese nacho (Table 7), Tostitos scoop nacho (Table 8), SunTree banana chips (Table 9), and Lays classic potato chips (Table 10). Duration of stabilization was different for each sample.

2.4   Data Analysis

The emission spectra were analyzed by fitting a lognormal function to both the delayed fluorescence and phosphorescence over the temperature range of 3°C to 60°C.

$$I(\nu) = I_0 \exp\left\{ -\ln(2)\left(\frac{\ln[1 + 2b(\nu - \nu_p)/\Delta]}{b} \right)^2 \right\}$$

Where, I_0 is the maximum intensity value of the emission spectra, ν_P is the frequency in cm^{-1} of the maximum emission, Δ is the line width parameter, and b is the asymmetry parameter.

2.5 Instrumentation

Luminescence measurements were made using Cary Eclipse (Varian Instruments, Walnut Creek, CA) fluorescence spectrophotometer equipped with a temperature controller and multi-cell holder. This instrument, which collects data in analog mode, uses a high intensity pulsed lamp. A time delay was employed to avoid any fluorescence during the lamp pulse. Temperature was controlled using a thermoelectric temperature controller (Varian Instruments). The measurements were made in the absence of oxygen. Nitrogen was purged for 30 min before and during the experiment to prevent oxygen quenching of the triplet state. Nitrogen flow was generated by passing high purity nitrogen through a Supelco (Bellefonte, PA) carrier gas purifier. The standard 1cm x 1cm quartz fluorescence cuvette was capped with a lid having inlet and outlet ports for gas lines.

2.6 Luminescence Measurements

Emission spectra were measured as a function of temperature. Delayed fluorescence spectra were collected over a 2 ms time window. Phosphorescence and delayed fluorescence emission scans were performed over the range of 520-800 nm with an excitation wavelength of 510 nm. The emission is characterized by a delayed fluorescence band with peak at ~550 nm and a phosphorescence band with peak at ~690 nm.

The excitation and emission monochromators were both set at 20 nm band pass. Each data point (collected at 1 nm intervals with a 0.1 s averaging time) was collected from a single flash with a 0.2 ms total decay time. Emission spectra were fitted using the program Igor (Wavemetrics, Inc., Lake Oswego, OR). All the measurements were made in triplicate at least.

2.7 Results and Discussion

2.7.1 Nanoparticle Size

The dimensions of nanoparticles varied in different batches. However, most gelatin nanoparticles were within the range of 70-140 nm, and most starch nanoparticles were within the range of 100-200 nm (Figure 2-1).

2.7.2   Erythrosine B Labeled Gelatin Nanoparticles in Solution

Figure 2-2 shows the emission spectra of erythrosine B labeled gelatin nanoparticles as a function of temperature in water. Each spectrum shows the variation of intensity with wavelength. Erythrosine B labeled gelatin nanoparticles showed delayed fluorescence spectra when collected over a 2 ms time window at temperatures ranging from 3 to 60°C. The emission is characterized by a delayed fluorescence bandwidth peak at ~550 nm and a phosphorescence bandwidth peak at ~690 nm. The longer wavelength band is phosphorescence from the excited triplet state (T_1) while the shorter wavelength band is delayed fluorescence from the excited singlet state (S_1) that has been repopulated from the triplet state by thermally activated reverse intersystem crossing (Parker, 1968). The intensity of the phosphorescence band decreased, while the intensity of the delayed fluorescence band increased with increasing temperature as shown in Figure 2-2. Phosphorescence showed a red shift around room temperature which is mainly attributed to solvent dipolar relaxation (Lakowicz and Cherek, 1980). Solvent relaxation is the reorientation of adjacent dipoles around the excited states of fluorophores and causes shifts of the fluorescence emissions to longer wavelengths (Lakowicz and Cherek, 1980). These relaxation processes and the spectral shifts in fluid solvents near room temperature are accomplished prior to fluorophore emission (Lakowicz and Cherek, 1980). Luminescence spectra composed of both delayed fluorescence and phosphorescence were fitted using the sum of two lognormal functions. The intensity plot of erythrosine B labeled gelatin nanoparticles showed a decrease in the intensity of phosphorescence and

an increase in the intensity of delayed fluorescence as a function of temperature over the temperature range of 3 to 60°C (Figure 2-3).

The Van't Hoff plot of erythrosine B labeled gelatin nanoparticles showed that the ratio $\ln(I_{DF}/I_P)$ versus $1/T$ decreased as a function of $1/T$ as shown in Figure 2-4. The data points exhibit an approximately linear trend; therefore, the linear best fit to the data was calculated in the form of $\ln(I_{DF}/I_P) = m (1/T) + C$. In this equation, m denotes the slope and C denotes the y-intercept of the regression line. The correlation coefficient (R) is 0.9987 which is an indication of good fit. This plot shows the sensitivity of delayed fluorescence to temperature and demonstrates that erythrosine B can serve as a temperature sensor by using the relationship between intensity ratio and temperature.

The effect of different pH values on erythrosine B labeled gelatin nanoparticles was also studied. Figure 2-5 is Van't Hoff plot of erythrosine B labeled gelatin nanoparticles in buffer solutions of pH 3 and pH 7 over the temperature range of 3 to 60°C along with the best fit lines. This figure shows that the pH of solution did not significantly affect the behavior of erythrosine B labeled gelatin nanoparticles and its sensitivity to temperature. The regression lines which approximate the relationship between intensity ratio and temperature in solutions with different pH are almost identical.

Erythrosine B labeled gelatin nanoparticles were added to different liquid food samples including water, orange juice, ginger ale, lemonade, Red Bull and Gatorade. Figure 2-6 shows the Van't Hoff plot of erythrosine B labeled gelatin nanoparticles in orange juice, ginger ale, lemonade, red bull, Gatorade, water, buffer solution pH 3 and buffer solution

pH 7 over the temperature range of 3 to 60°C. This figure demonstrates that the ratio of $\ln(I_{DF}/I_P)$ varied monotonically and decreased as a function of 1/T for all solutions. This figure shows the sensitivity of delayed fluorescence to temperature and indicates that erythrosine B can act as a temperature sensor in a variety of food solutions by using the relationship between intensity ratio and temperature. Erythrosine B labeled gelatin nanoparticles are sensitive to temperature change, in different solutions with different compositions when there is no oxygen present in the solution.

In an attempt to find a simple correlation between intensity ratio and temperature, the data were plotted in three different ways: $\ln(I_{DF}/I_P)$ vs. 1/T (Figure *2-6*), $\ln(I_{DF}/I_P)$ vs. T (Figure 2-7), and I_{DF}/I_P vs. T (Figure 2-8). The Van't Hoff plots shown in Figure 2-6 and Figure 2-7 exhibit some curvature but can be approximated by a straight line due to small curvature. Figure 2-6 was selected as the preferred presentation of data for analysis. Analysis of the Van't Hoff plot provides the constants for temperature calculation from a measurement of the delayed phosphorescence luminescence based on the linear best fit to the test data points obtained for each sample in the form of $\ln(I_{DF}/I_P) = m \, (1/T) + C$. In this equation, m denotes the slope and C denotes the y-intercept of the regression line. The slope m provides an estimate of the energy gap, ΔE_{TS}, between the lowest triplet (T_1) and singlet state (S_1). The y-intercept C can be regarded as a measure of the ultimate intensity ratio (limit of intensity ratio as the temperature increases). Due to the practical upper bound on the temperature values that are of interest in food sensory applications, the measured intensity ratios are expected to remain well below C. Once determined for

each liquid sample, m and C can be used to calculate the temperature at any given intensity ratio according to the following equation:

$T_{calc} = m/(\ln (I_{DF}/ I_P) - C$

Table 2-12 presents the calculated constants m and C for each liquid sample along with the associated energy gap (ΔE_{TS}). The range of parameter m is from -4,061 to -3,880. Parameter C varies from 12.10 to 12.74. The relatively narrow range of variation of these parameters suggests that a single regression line may be appropriate for all liquid samples. Constants m and C defining the best fit line to all data points shown in Figure 2-6 are -3,806.8 and 11.917, respectively. The correlation coefficient value $R^2=0.99$ is an indication of good fit. The calculated temperature (T_{calc}) was compared with the actual temperature for each liquid sample in order to assess the accuracy of the estimation. Table 2-13 shows the error in estimating the temperature in liquid samples resulting from the use of a single regression line for all data points. The error is defined as,

$$e = \frac{|T_{act} - T_{calc}|}{T_{act}}$$

where, T_{act} denotes the actual temperature. In this equation, T_{act} and T_{calc} are in degrees Kelvin (K).

According to this table, the estimation error is relatively small and comparable to the practical precision with which the temperature is generally measured and recorded. The largest errors are in most cases associated with the lowest temperature (3°C). This can be attributed to the condensation around the cuvette during the experiment. Note that a

higher degree of accuracy can be obtained by using a bilinear approximation. In this case, a single regression line (one set of m and C values) may be fitted to the data points at temperatures below 10°C and another set of m and C values may be used to approximate the trend at temperatures above 10°C.

Labeled gelatin nanoparticles were tried in some other liquid samples such as apple juice, pomegranate juice and green tea, but gelatin nanoparticles were precipitated after few minutes. This was due to the presence of tannin and anthocyanins in the composition of those samples. Both tannins and anthocyanins in beverages are molecules containing benzene rings with adjacent hydroxyl groups as shown in Figure 2-26 by the galloyl group (Cole, 1986). These molecules are the major source of hydrogen bonds which are the basis of complex formation between gelatin and tannins or anthocyanins in beverages (Figure 2-27) (Cole, 1986). Greater precipitation occurs with high molecular weight gelatin (Van Buren and Robinson, 1969). Since gelatin nanoparticles used in the experiments were made from high molecular weight gelatin, they caused precipitation. Tannic acid contains a mixture of phenolics which develop a strong bond with gelatin.

2.7.3 Phloxine B Labeled Gelatin Nanoparticles in Liquid Samples

Emission spectra of phloxine B labeled gelatin nanoparticles in water as a function of temperature are shown in Figure 2-9. Phloxine B labeled gelatin nanoparticles showed delayed fluorescence spectra when collected over a 2 ms time window and the temperature range of 3 to 60°C. The emission is distinguished by a delayed fluorescence bandwidth peak at ~567 nm and a phosphorescence bandwidth peak at ~710 nm. The

longer wavelength band is phosphorescence from the excited triplet state (T_1) while the shorter wavelength band is delayed fluorescence from the excited singlet state (S_1) that has been repopulated from the triplet state by thermally activated reverse intersystem crossing (Parker, 1968). The intensity of the phosphorescence band decreased and the intensity of delayed fluorescence band increased with increasing temperature (Figure 2-9). The variation of delayed fluorescence and phosphorescence intensity of phloxine B labeled gelatin nanoparticles as a function of temperature is shown in Figure 2-10. The data points plotted on this chart correspond to the peak intensities shown in Figure 2-9 (7 data points corresponding to the 7 temperature values used in the experiments). Extrapolating the trend of variation of phosphorescence intensity with temperature, it appears that the probe may be functional up to a temperature of 80°C. Beyond this temperature, the intensity will be too low to allow easy measurement.

Van't Hoff plot of $\ln(I_{DF}/I_P)$ vs. $1/T$ is shown in Figure 2-11 along with the linear best fit to the data following the same analysis procedure as for erythrosine B labeled gelatin nanoparticles reported earlier in this chapter. For reference, the Van't Hoff plot of erythrosine B labeled gelatin nanoparticles shown in Figure 2-4 is superimposed on Figure 2-11 (Figure 2-12). It is noted that the two plots are nearly identical.

In order to observe the behavior of phloxine B labeled gelatin nanoparticles in liquid food samples, they were added to water, Gatorade, lemonade and ginger ale. Figure 2-13 shows the Van't Hoff plot of phloxine B labeled gelatin nanoparticles in ginger ale, lemonade, Gatorade, water, over the temperature range of 3 to 60°C. This figure

demonstrates that ratio of $\ln(I_{DF}/I_P)$ varied monotonically as a function of $1/T$ for all solutions.

Unlike the Van't Hoff plots obtained for erythrosine B labeled gelatin nanoparticles, these van't hoff curves for phloxine B show significant curvature, making the linear approximation of their behavior perhaps inappropriate, as it introduces systematic error. It is noted that the linearity of the relationship between intensity and temperature, although desirable for calculation, is not needed for this probe to be useful as a temperature sensor.

Two additional presentations of data as shown in Figure 2-14 and Figure 2-15 were also considered in order to seek a simple correlation between intensity ratio and temperature but did not reveal any advantage over the van't hoff plot. Therefore, the van't hoff plot shown in Figure 2-13 was used for the analysis. A quadratic polynomial fit to the data points was derived to approximate the relationship between $\ln(I_{DF}/I_P)$ and $1/T$ as shown in Figure 2-13.

Analysis of the Van't Hoff plot provides the constants for calculating the temperature from a measurement of the delayed phosphorescence luminescence.

$$T_{calc} = \frac{2a}{-b + \sqrt{b^2 - 4a\left[c - \ln\left(\frac{I_{DF}}{I_P}\right)\right]}}$$

In this equation, a, b, and c are the constant coefficients of the quadratic best fit polynomial, $\ln\left(\frac{I_{DF}}{I_P}\right) = a\left(\frac{1}{T}\right)^2 + b\left(\frac{1}{T}\right) + c$

ΔE_{TS} was calculated using straight line approximation. Table 2-14 shows the constants m, C and the energy gap ΔE_{TS} calculated for for each solid sample.The range of parameter m is from -3,356 to -3,500. Parameter C varies from 10.54 to 10.90.

Table 2-15 shows the error in estimating the temperature (degrees Kelvin) in liquid samples with phloxine B resulting from the use of a quadratic best fit curve for all data points.

Since both erythrosine B and phloxine B have shown very similar behaviors, it is expected that the effect of pH on the response of phloxine B labeled gelatin nanoparticles is negligible; therefore, the pH test was not performed for phloxine B.

2.7.4   Erythrosine B Labeled Gelatin Nanoparticles on Solid Samples

Figure 2-16 shows the emission spectra of erythrosine B labeled gelatin nanoparticles as a function of temperature on potato chips when collected over a 2 ms time window and the temperature range of 3 to 60°C. The emission is characterized by a delayed fluorescence bandwidth peak at ~550 nm and a phosphorescence bandwidth peak at ~690 nm which are the same as the values observed for erythrosine B labeled gelatin nanoparticles in solution (Figure 2-2).

It is important to note that the behavior of erythrosine B labeled gelatin nanoparticles on solids (Figure 2-17) is similar to their behavior in solution.

The solid food samples used in the experiments were cheese nacho, nacho, banana chips, cracker, potato chips and white bread. Figure 2-18 shows the Van't Hoff plot of erythrosine B labeled gelatin nanoparticles on these samples over the temperature range

of 3 to 60°C. As can be seen in Figure 2-18, the variation of intensity ratio with temperature is similar to the behavior observed in liquid samples. In the case of solid samples a wider range of intensity ratios is noted compared to liquid samples.

It is also noted that the Van't Hoff curves of white bread and cheese nacho exhibited a parallel shift compared to the other samples (same m but smaller C). The ratio of $\ln(I_{DF}/I_P)$ was smaller for these two samples indicating that the delayed fluorescence was quenched. It is suspected that this different behavior might be caused by the higher water activity of bread which quenched the delayed fluorescence, since the water activity for all solid samples were between 0.2 -0.4 except for bread which had a water activity of 0.9. However; water activity tests (reported in a subsequent section of this chapter) indicated that the water activity of the samples did not have any effect on the behavior of erythrosine B labeled gelatin nanoparticles on solid samples. Other factors may have contributed to the different behaviors of erythrosine B labeled gelatin nanoparticles on white bread and cheese nacho such as porosity, smoothness of the sample surface, sample thickness, different compositions in the sample and some seasoning on the sample surface and interaction of these materials with labeled gelatin nanoparticles. This different behavior can also be due to the interaction of proteins on the surface of the sample and the way they bond to each other since the labeled gelatin nanoparticles were applied on the surface of each sample.

Following the same procedure used to analyze the liquid data, Table 2-16 presents the calculated constants m and C for each solid sample along with the associated energy gap (ΔE_{TS}). The range of parameter m is from -4,239 to -3,730. Parameter C varies from

11.90 to 13.88. The range of these parameters exhibits a wider variation compared to the range observed for liquid samples; therefore, a single regression line is not suggested for all solid samples. Table 2-17 shows the error in estimating the temperature (degrees Kelvin) in solid samples resulting from the use of linear approximation for each sample. According to this table, the error in estimating the temperature is relatively small over the range of temperatures encountered in the experiments.

It is further noted that a unified trend line or curve for both solid and liquid samples may not be useful due to increased error in measuring the temperature.

2.7.5   Phloxine B Gelatin Nanoparticles on solid samples

Figure 2-19 shows the emission spectra of phloxine B labeled gelatin nanoparticles as a function of temperature on potato chips which are similar to those obtained for liquid samples (Figure 2-9).

The intensity plot of phloxine B labeled gelatin nanoparticles as a function of temperature is shown in Figure 2-20. Unlike the variation of I_P in liquid samples, the range of I_p variation in solid samples is relatively small indicating a lower signal compared with liquid samples.

Phloxine B labeled gelatin nanoparticles were added to different solid food samples of dried banana, cheese nacho, potato chips and white bread. Figure 2-21 shows the Van't Hoff plot of phloxine B labeled gelatin nanoparticles in dried banana, cheese nacho, potato chips, and white bread over the temperature range of 3 to 60°C. It is noted that the

intensity ratio varies over a smaller range compared to the data previously obtained for liquid samples. The slope of regression lines for various data sets is between -2630 and -2155 and the y-intercept varies from 7.80 to 9.10 (Table 2-18). The difference between these values and the values obtained for liquid samples is relatively significant suggesting that separate calibrations are required for application in solution and on solids.

Table 2-19 shows the error in estimating the temperature (degrees Kelvin) in solid samples with phloxine B resulting from the use of linear approximation for each sample. The errors are generally larger than those calculated for erythrosine B labeled gelatin nanoparticles on solid samples.

2.7.6   Water Activity Test

Water activity tests were performed on solid food samples (cheese nacho, nacho, banana chips and potato chips) with four different water activities using erythrosine B labeled gelatin nanoparticles. Figure 2-22 and Figure 2-23 show the Van't Hoff plot for cheese nacho, nacho, dried banana and potato chips with water activities of 11.3% aw, 23.1% aw, 33.5% aw, and 43.1% aw over the temperature range of 3 to 60°C.

These plots indicate that the change in intensity ratio due to changes in relative humidity is generally negligible. Only dried banana sample showed a slightly increased response at low temperatures associated with 11.30% aw. These tests demonstrated that different relative humidifies did not affect the behavior of erythrosine B labeled gelatin nanoparticles on different solid samples

2.7.7   Starch Nanoparticles:

Labeling the starch nanoparticles with erythrosine B and phloxine B was not successful. After labeling the starch nanoparticle with erythrosine B and phloxine B they were transferred to a dialysis membrane tube having 1000 Da molecular weight cutoff and dialyzed against distilled water for 48 hr to remove unreacted, free dyes as explained in Material and Method. During the dialyses most of the probe migrated to the water and left very pale starch nanoparticles. These starch nanoparticles were not able to show a good signal for this experiment.

2.8   Summary:

Experiments with two different probes, namely erythrosine B labeled gelatin nanoparticles and phloxine B labeled gelatin nanoparticles have demonstrated that both probes can be effectively used as temperature sensors in liquid and solid food. The Van't Hoff plots of $\ln(I_{DF}/I_P)$ versus $1/T$ vary monotonically over a relatively wide temperature range and thus provide a basis for estimating temperature from measurements of phosphorescence and delayed fluorescence.

Depending on the desired level of accuracy in temperature estimation, different data processing approaches are possible. A linear best fit to the data offers the most advantage in terms of ease of use but may introduce a larger error compared with polynomial curve fits. As shown in Table 12b, the use of a single regression line to approximate Van't Hoff plots obtained for different food samples, has yielded reasonable results.

Both probes showed stability during the time of storage in the solution or in freeze dried form in the refrigerator and responded well to the changes in temperature. Comparison of the emission spectra for phloxine B and erythrosine B labeled gelatin nanoparticles (Figure 2-16 and Figure 2-19) showed that the erythrosine B provided a better signal on solid samples than phloxine B. This is due to the smaller molecular weight of phloxin B (829.63 g mol^{-1} vs. 879.86 g mol^{-1} for erythrosine B). The smaller molecular weight of phloxin B is a result of 4 molecules of bromine in its structure vs. 4 molecules of iodine in erythrosine B.

The tests indicated that the presence of some ingredients such as tannin and anthocyanins in the composition of the food may prohibit the use of gelatin nanoparticle probes due to precipitation of gelatin nanoparticles.

sample2a01/11/06 (Combined)

Effective Diameter: 89.3 nm
Polydispersity: 0.287
Avg. Count Rate: 3.4 Mcps
Sample Quality: 9.9
Elapsed Time: 00:09:00

Run	Eff. Diam. (nm)	Half Width (nm)	Polydispersity	Sample Quality
1	90.3	48.0	0.282	9.7
2	89.3	47.4	0.281	9.8
3	88.8	48.1	0.293	9.8
Mean	89.5	47.8	0.286	9.8
Std. Error	0.4	0.2	0.004	0.0
Combined	89.3	47.9	0.287	9.9

sample red 12/19/06 (Combined)

Effective Diameter: 139.7 nm
Polydispersity: 0.167
Avg. Count Rate: 139.2 kcps
Sample Quality: 8.2
Elapsed Time: 00:09:00

Run	Eff. Diam. (nm)	Half Width (nm)	Polydispersity	Sample Quality
1	139.5	54.9	0.155	6.0
2	139.3	58.6	0.177	8.2
3	140.0	58.0	0.172	8.8
Mean	139.6	57.2	0.168	7.7
Std. Error	0.2	1.1	0.007	0.8
Combined	139.7	57.1	0.167	8.2

Figure 2-1: Representative data set for gelatin nanoparticle size which was measured by 90Plus Particle Size Analyzer from Brookhaven Instruments.
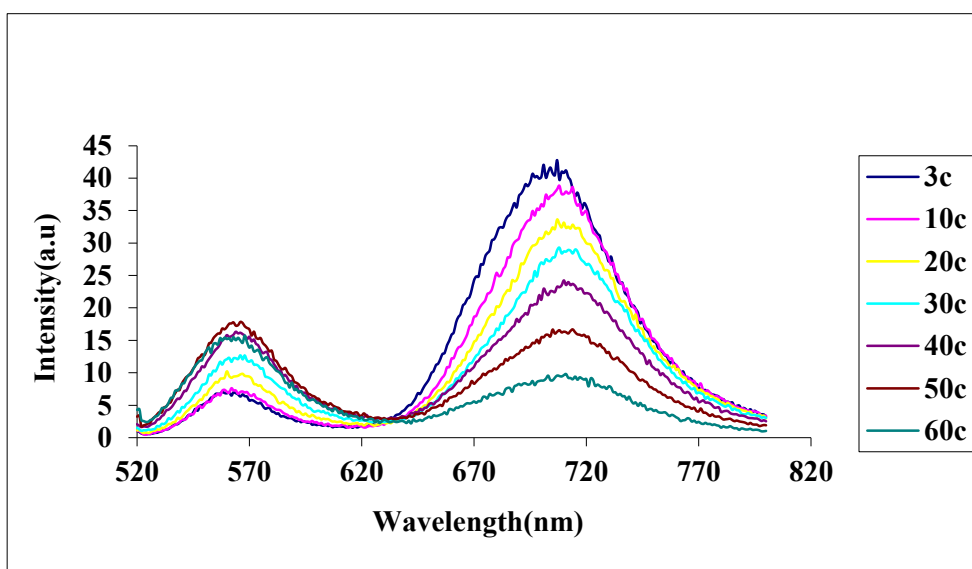
Figure 2-2 : Emission intensity for delayed fluorescence and phosphorescence of erythrosine B labeled gelatin nanoparticles in water when collected over a 2 ms time window over the temperature range of 3 to 60°C.
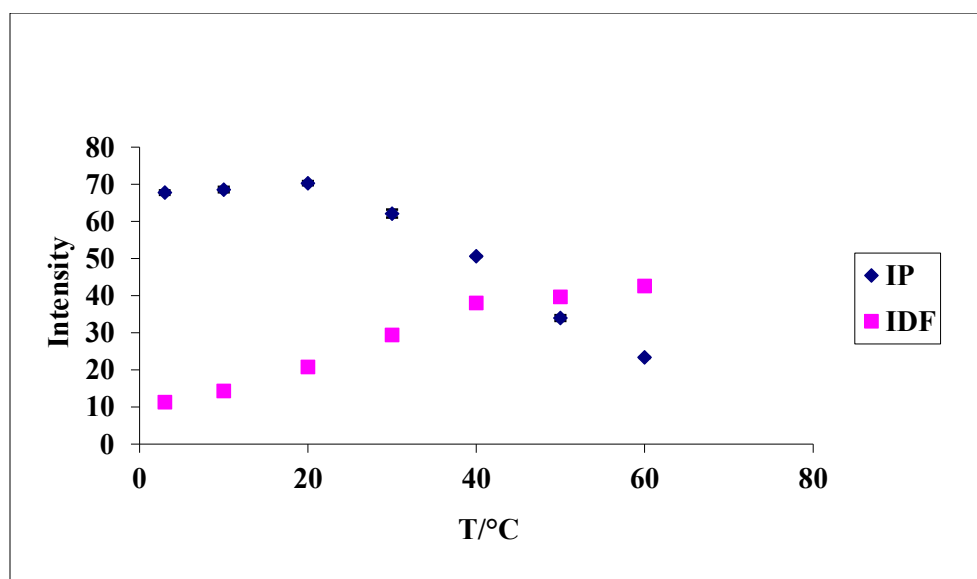
Figure 2-3: The intensity plot of erythrosine B labeled gelatin nanoparticles in water showed a decrease in intensity of delayed phosphorescence (I_p) and an increase in the intensity of delayed fluorescence (I_{DF}) as a function of temperature over the temperature range of 3 to 60°C.
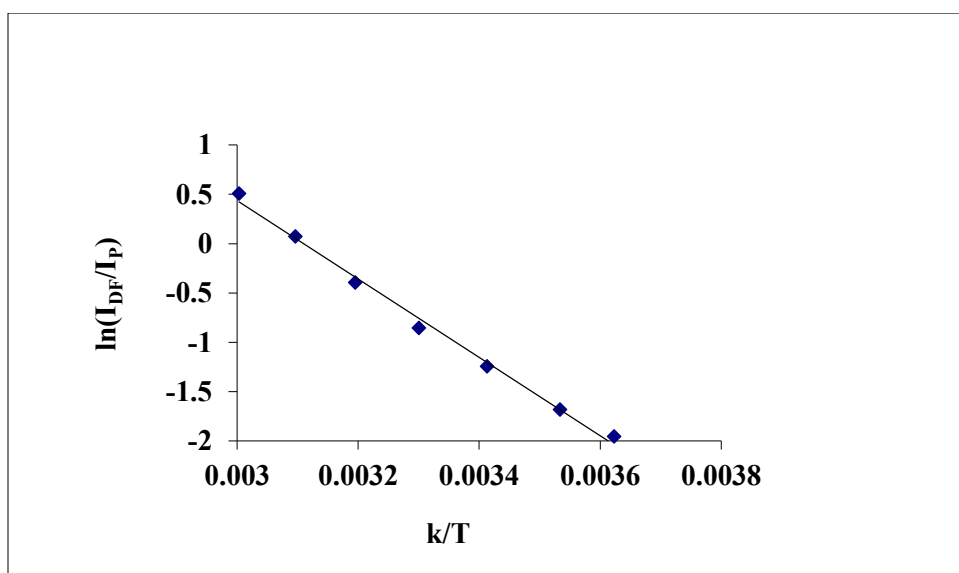
Figure 2-4: Van't Hoff plot of erythrosine B labeled gelatin nanoparticles in water shows that the ratio $\ln(I_{DF}/I_P)$ decreased as a function of $1/T$. The linear best fit to the data is also shown in this figure.
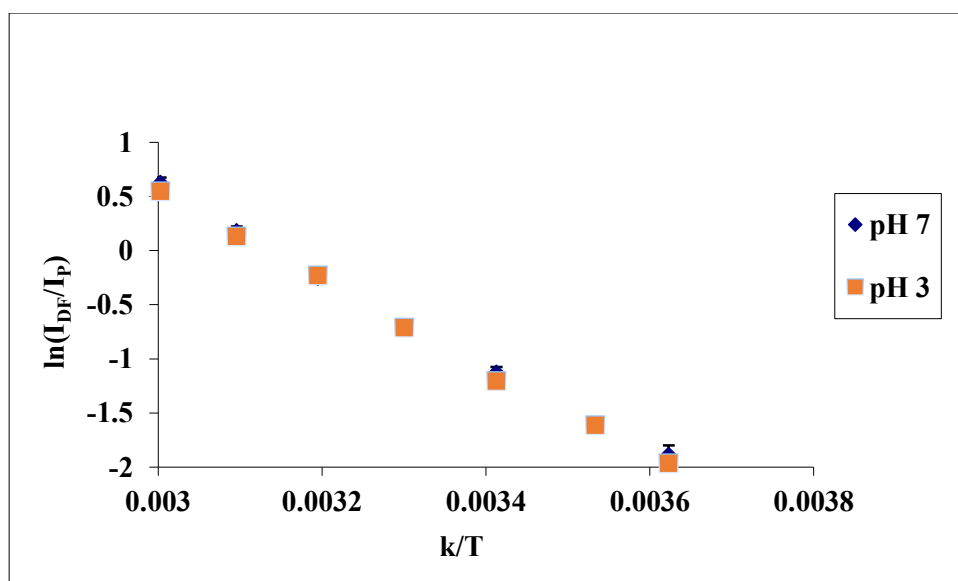
Figure 2-5: Van't Hoff plot of erythrosine B labeled gelatin nanoparticles in buffer solutions of pH 3 and pH 7. It shows the ratio of $\ln(I_{DF}/I_P)$ varied almost linearly and decreased as a function of $1/T$ for both solutions.
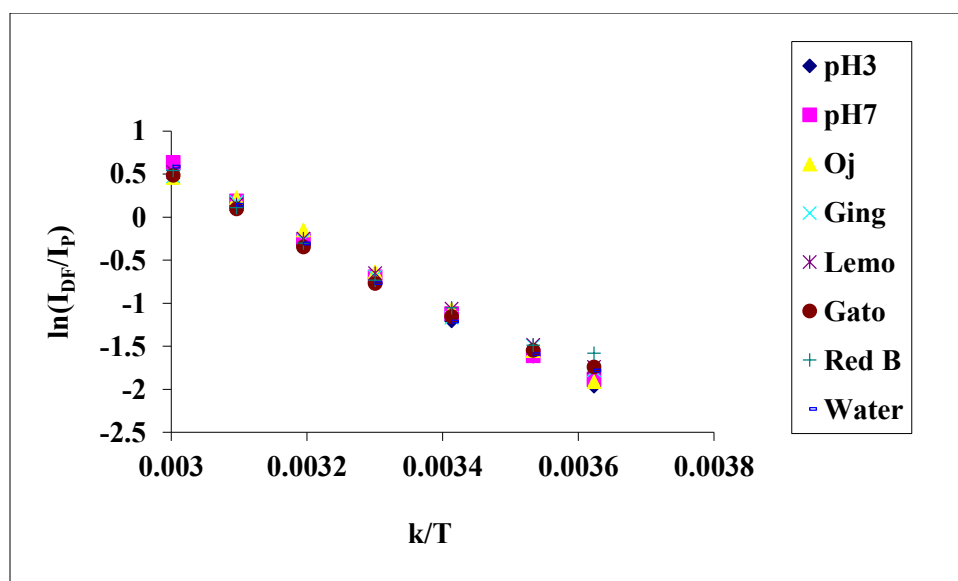
Figure 2-6: The Van't Hoff plot of erythrosine B labeled gelatin nanoparticles in orange juice, ginger ale, lemonade, Red Bull, Gatorade, water, buffer solution pH 3 and buffer solution pH 7 over the temperature range of 3 to 60°C.
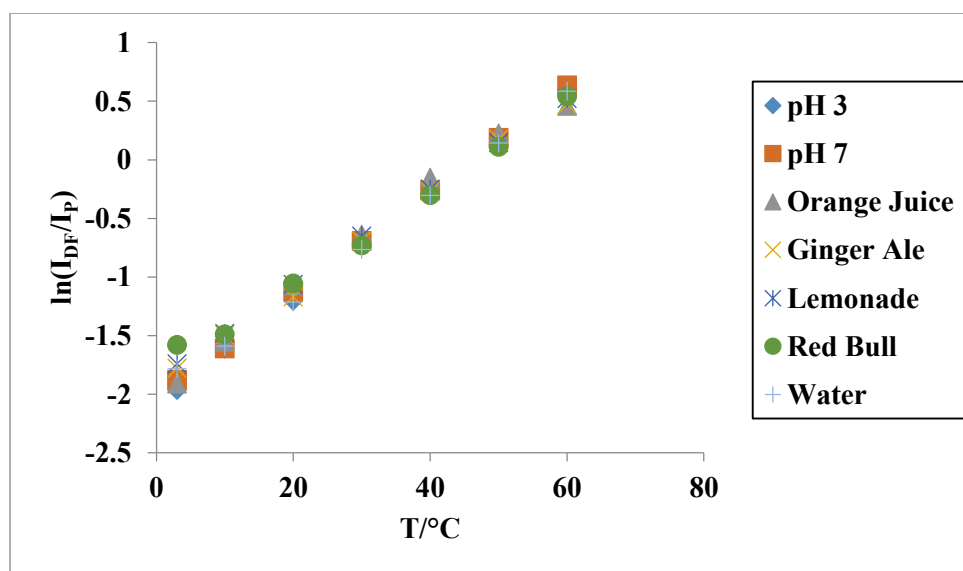
Figure 2-7: Plot of log normal ratio of delayed fluorescence intensity over phosphorescence intensity versus temperature(°C) for erythrosine B labeled gelatin nanoparticles in water, Gatorade, lemonade and ginger ale over the temperature range of 3 to 60°C.
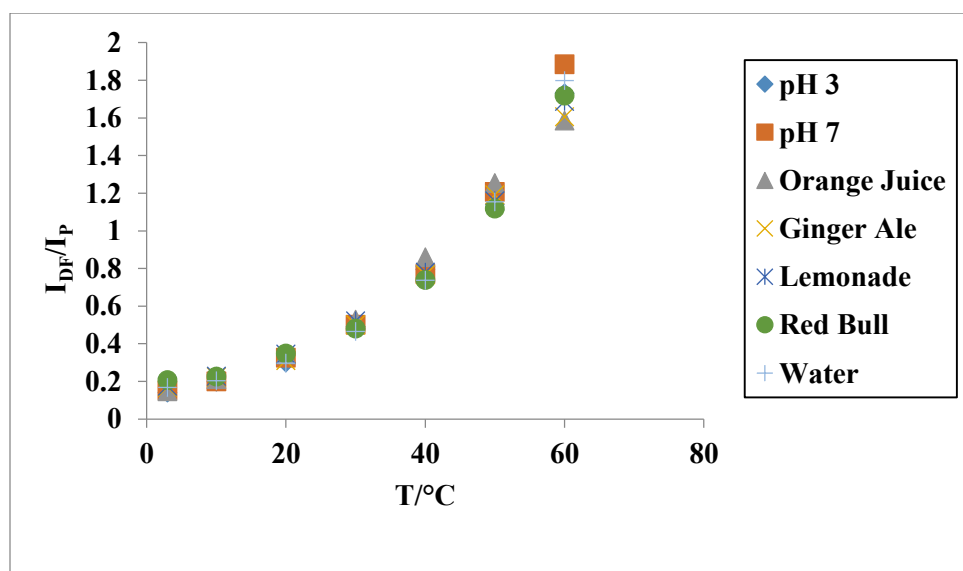
Figure 2-8: Plot of delayed fluorescence intensity over phosphorescence intensity versus temperature(°C) for of erythrosin B labeled gelatin nanoparticles in water, Gatorade, lemonade and ginger ale over the temperature range of 3 to 60°C.
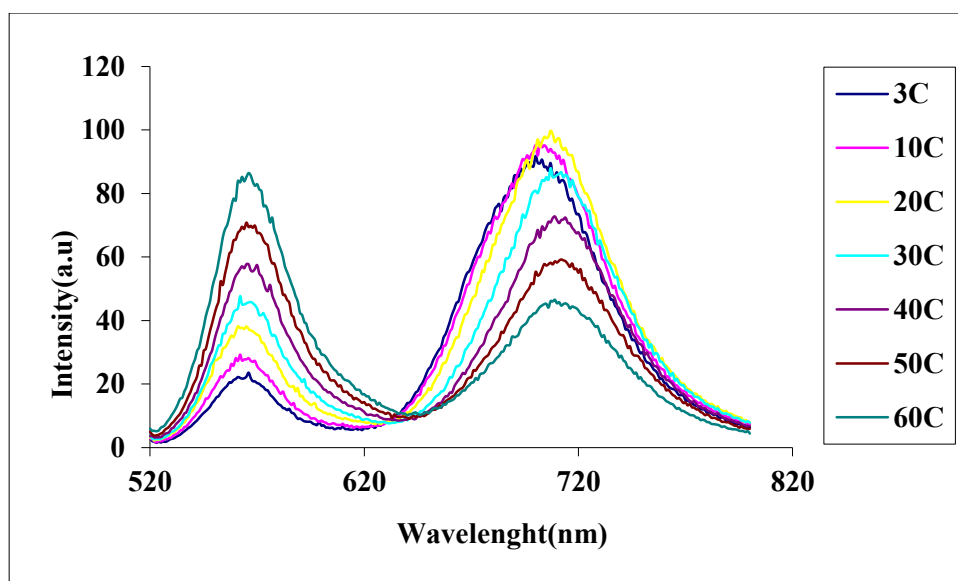
Figure 2-9: Emission spectra of phloxine B labeled gelatin nanoparticles as a function of temperature in water when collected over a 2 ms time window and the temperature range of 3 to 60°C.. The longer wavelength band is phosphorescence while the shorter wavelength band is delayed fluorescence.
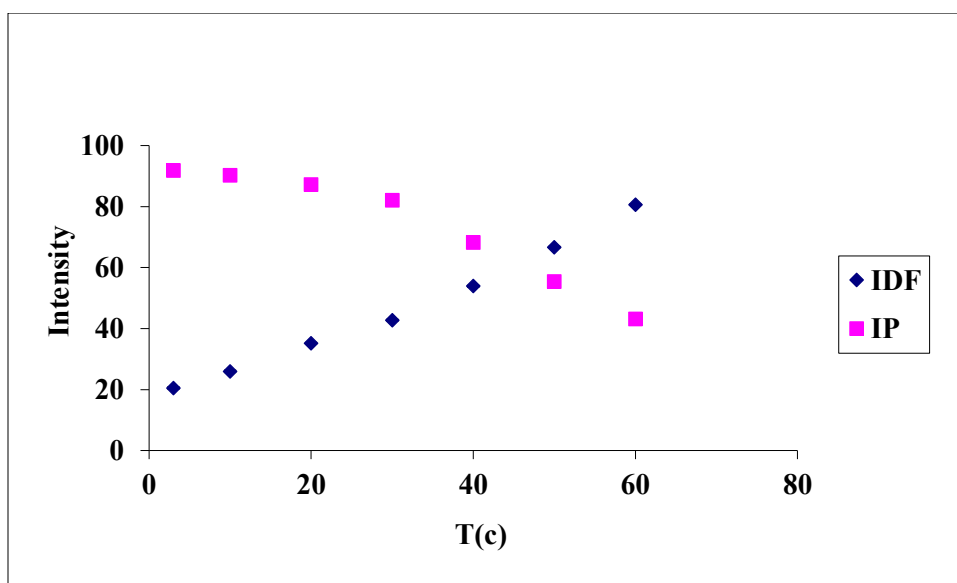
Figure 2-10: The intensity plot of phloxine B labeled gelatin nanoparticles in water as a function of temperature shows the decrease in intensity of phosphorescence and increase in delayed fluorescence as a function of temperature over the temperature range of 3 to 60°C.
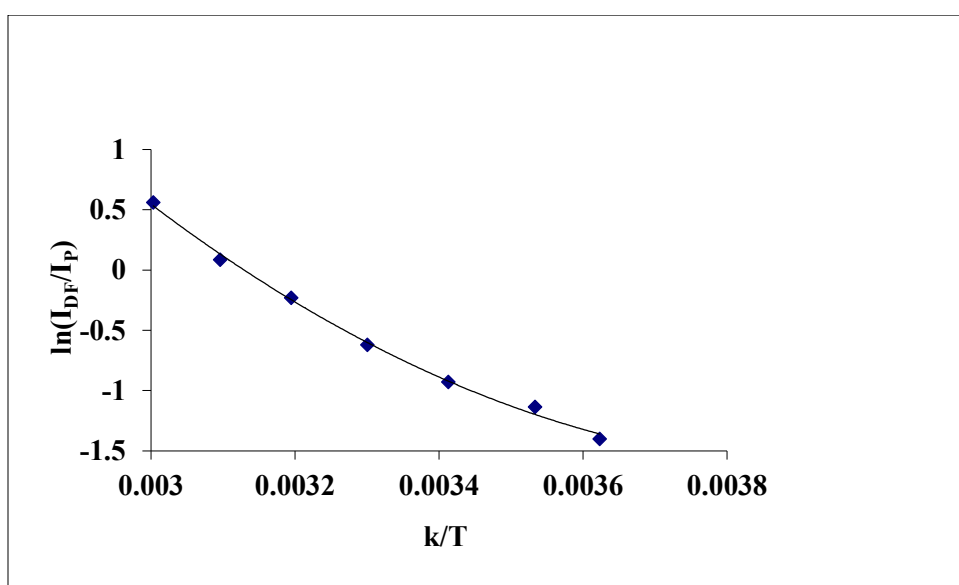
Figure 2-11: Van't Hoff plot of phloxine B labeled gelatin nanoparticles in water shows the variation of $\ln(I_{DF}/I_P)$ ratio versus $1/T$.
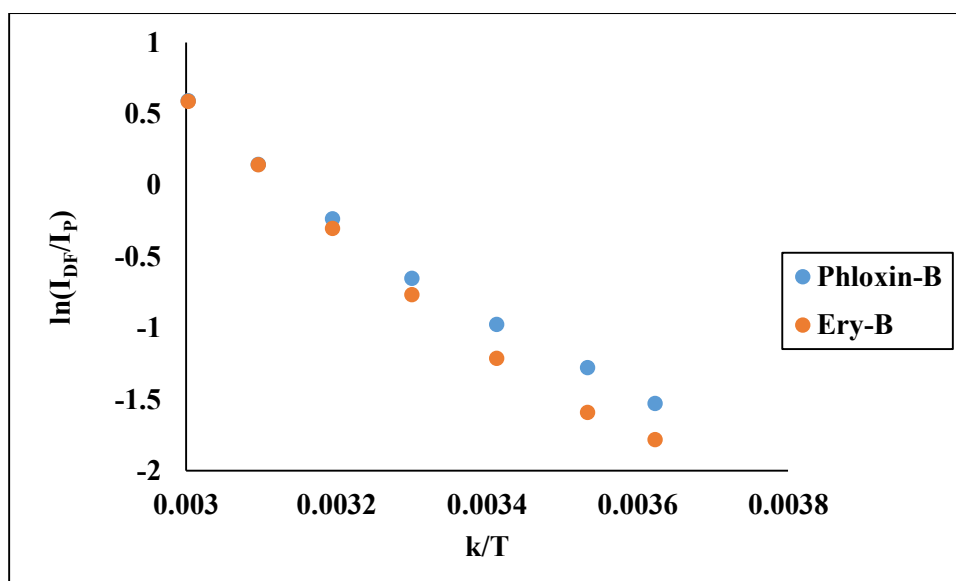
Figure 2-12: Van't Hoff plot of erythrosine B labeled gelatin nanoparticles in water is superimposed on Van't Hoff plot of phloxine B labeled gelatin nanoparticles in water.
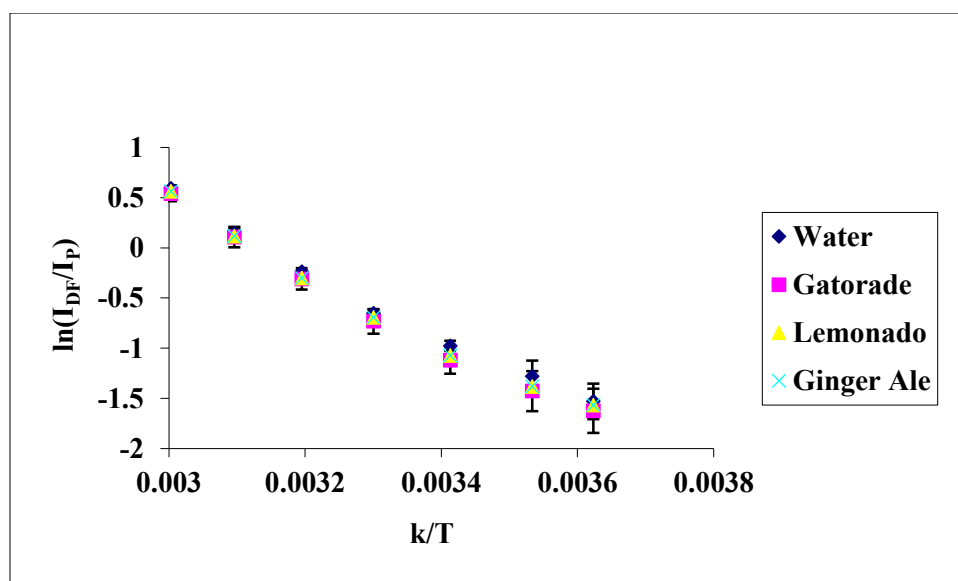
Figure 2-13: The Van't Hoff plot of phloxine B labeled gelatin nanoparticles in water, Gatorade, lemonade and ginger ale over the temperature range of 3 to 60°C.
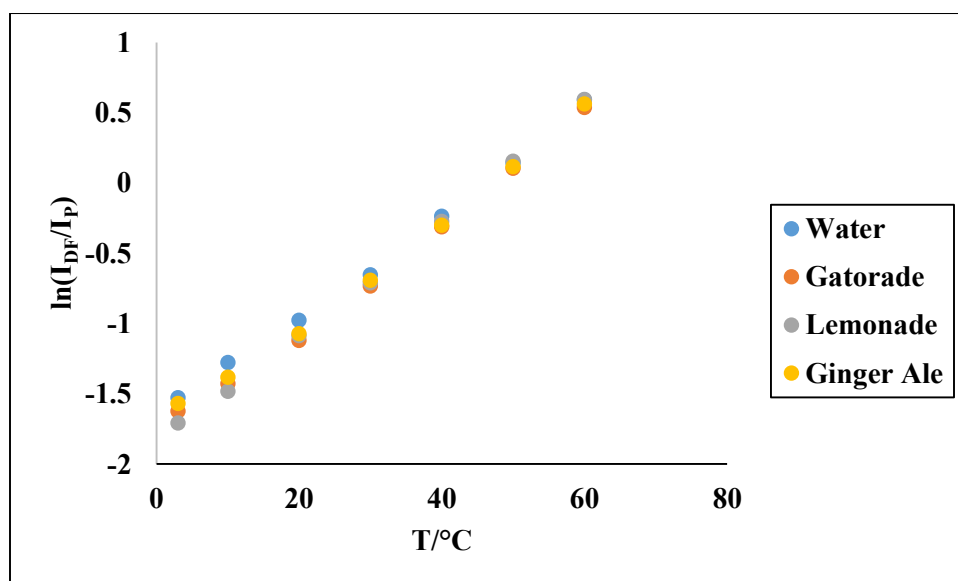
Figure 2-14: Plot of log normal ratio of delayed fluorescence intensity over phosphorescence intensity versus temperature (°C) for phloxine B labeled gelatin nanoparticles in water, Gatorade, lemonade and ginger ale over the temperature range of 3 to 60°C.
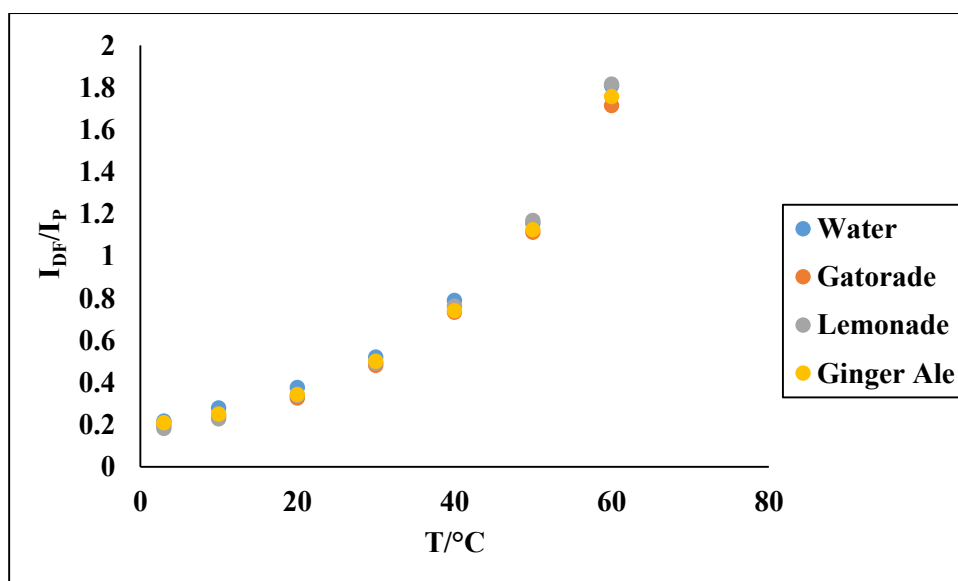
Figure 2-15: Plot of delay fluorescence intensity over phosphorescence intensity versus temperature (°C) for phloxine B labeled gelatin nanoparticles in water, Gatorade, lemonade and ginger ale over the temperature range of 3 to 60°C.
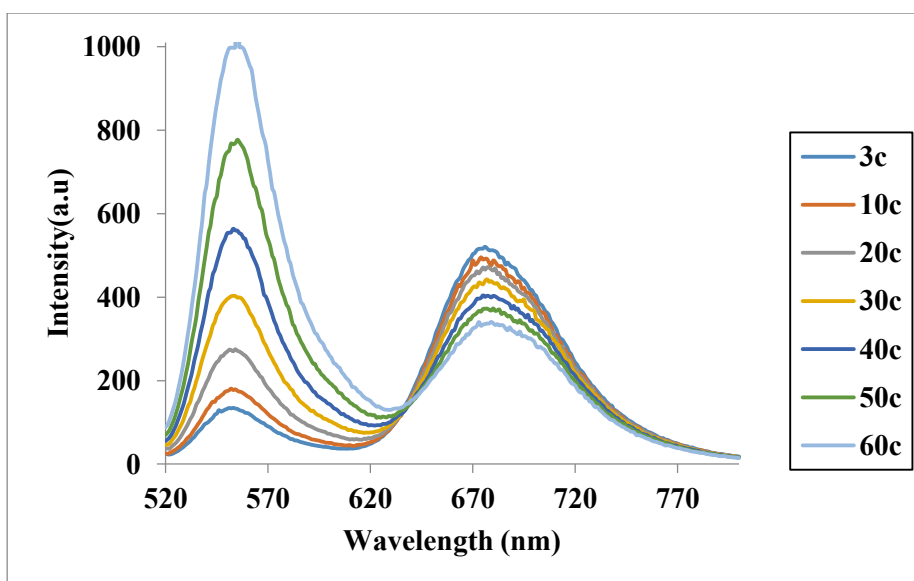
Figure 2-16: Emission spectra of erythrosine B labeled gelatin nanoparticles as a function of temperature on potato chips. The longer wavelength band is phosphorescence while the shorter wavelength band is delayed fluorescence when collected over a 2 ms time window and the temperature range of 3 to 60°C.
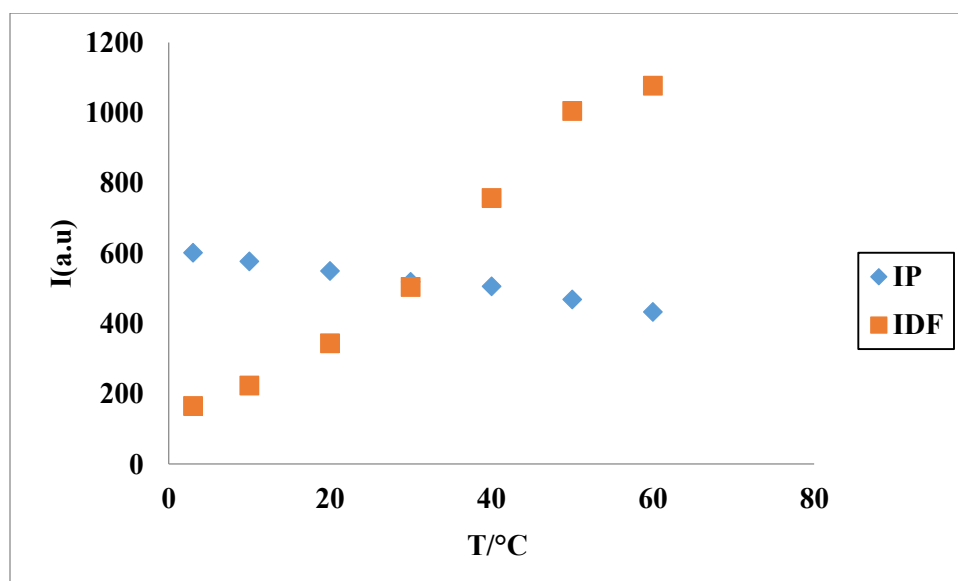
Figure 2-17:The intensity plot of erythrosine B labeled gelatin nanoparticles on potato chips shows a decrease in the intensity of phosphorescence and an increase in the intensity of delayed fluorescence as a function of temperature over the temperature range of 3 to 60°C.
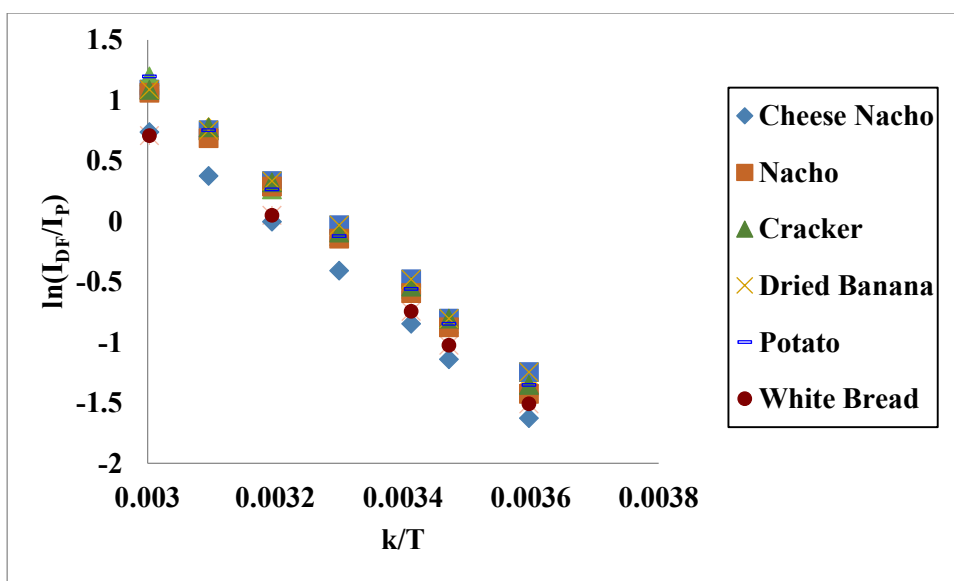
Figure 2-18: Van't Hoff plot of erythrosine B labeled gelatin nanoparticles on cheese nacho, nacho, cracker, dried banana, potato chips, and white bread over the temperature range of 3 to 60°C.
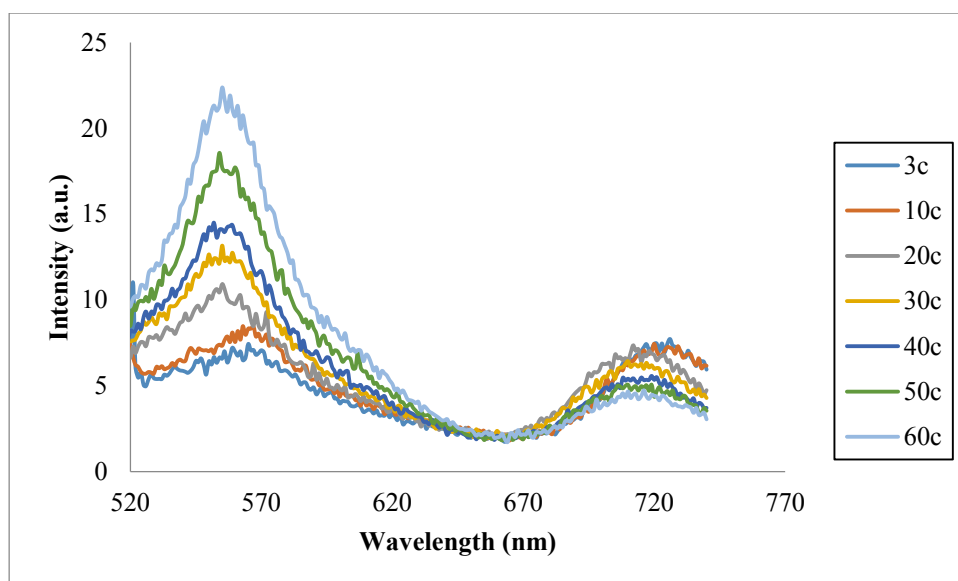
Figure 2-19: Emission spectra of phloxine B labeled gelatin nanoparticles as a function of temperature on potato chips. The longer wavelength band is phosphorescence while the shorter wavelength band is delayed fluorescence when collected over a 2 ms time window and the temperature range of 3 to 60°C.
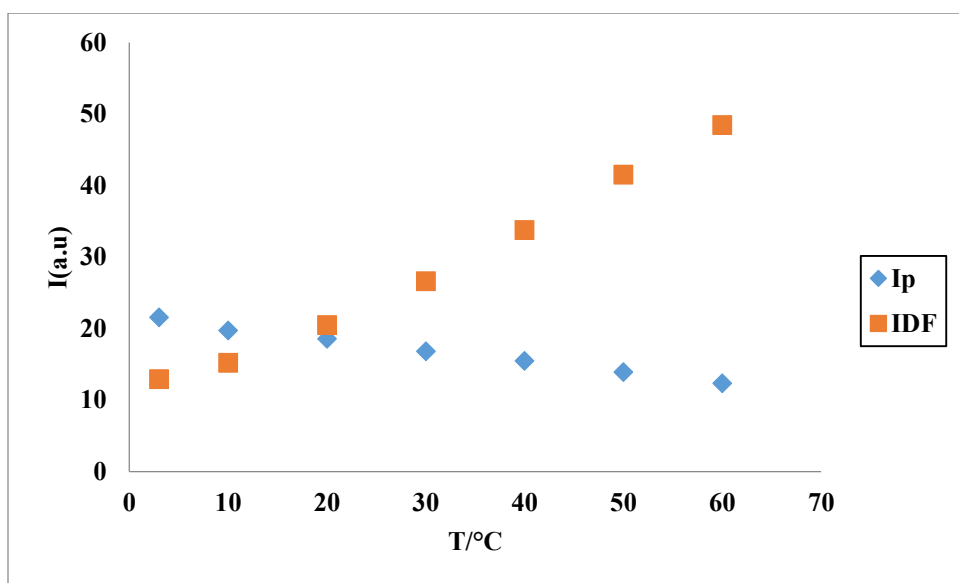
Figure 2-20: The intensity plot of phloxine B labeled gelatin nanoparticles on potato chips shows a decrease in the intensity of phosphorescence and an increase in the intensity of delayed fluorescence as a function of temperature over the temperature range of 3 to 60°C.
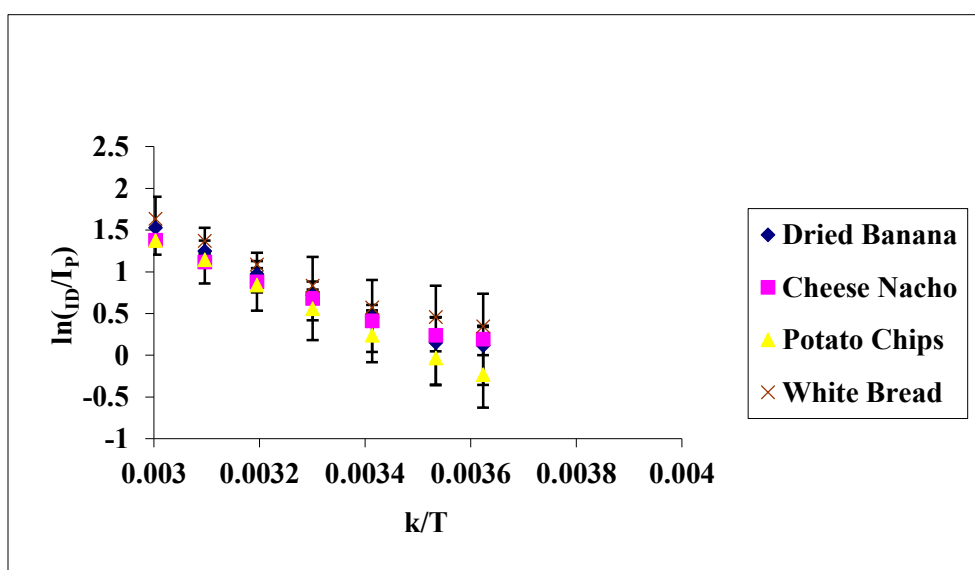
Figure 2-21: Van't Hoff plot of phloxine B labeled gelatin nanoparticles in dried banana, cheese nacho, potato chips, and white bread over the temperature range of 3 to 60°C.
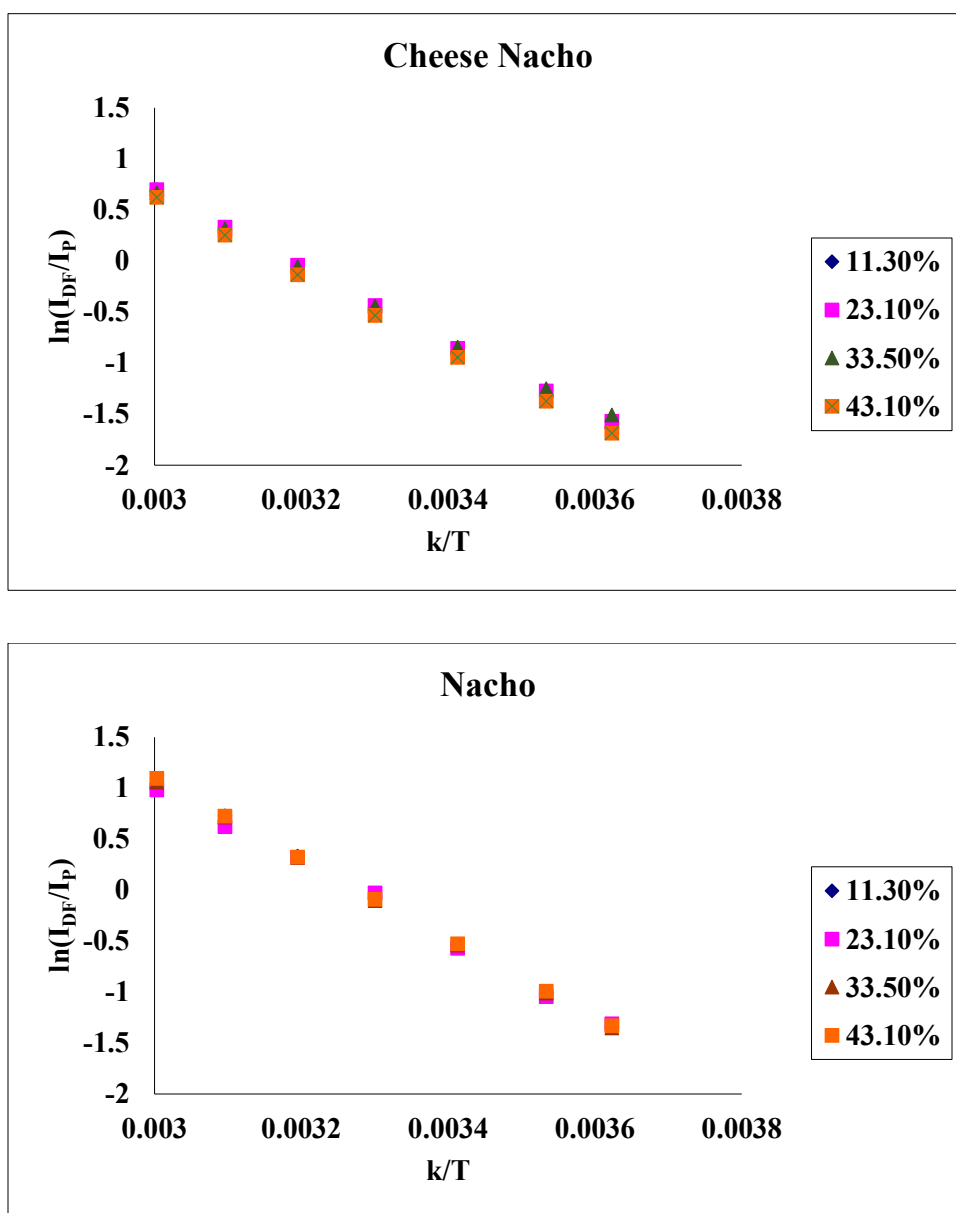
Figure 2-22: Van't Hoff plot for cheese nacho and nacho with water activities of 11.3% aw, 23.1% aw, 33.5% aw, and 43.1% aw over the temperature range of 3 to 60°C using erythrosine B labeled gelatin nanoparticles.
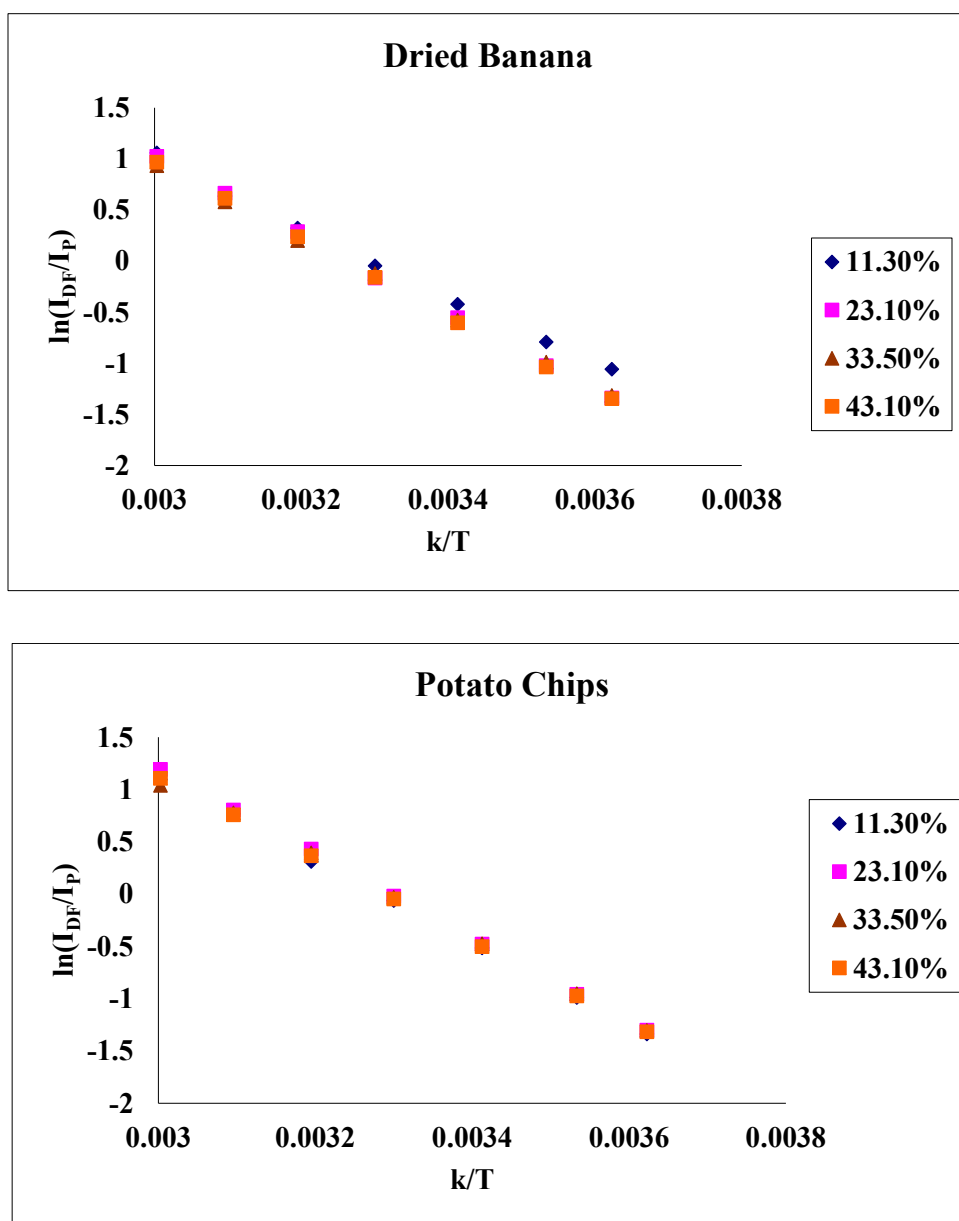
Figure 2-23: Van't Hoff plot for dried banana and potato chips with water activities of 11.3% aw, 23.1% aw, 33.5% aw, and 43.1% aw over the temperature range of 3 to 60°C using erythrosine B labeled gelatin nanoparticles.
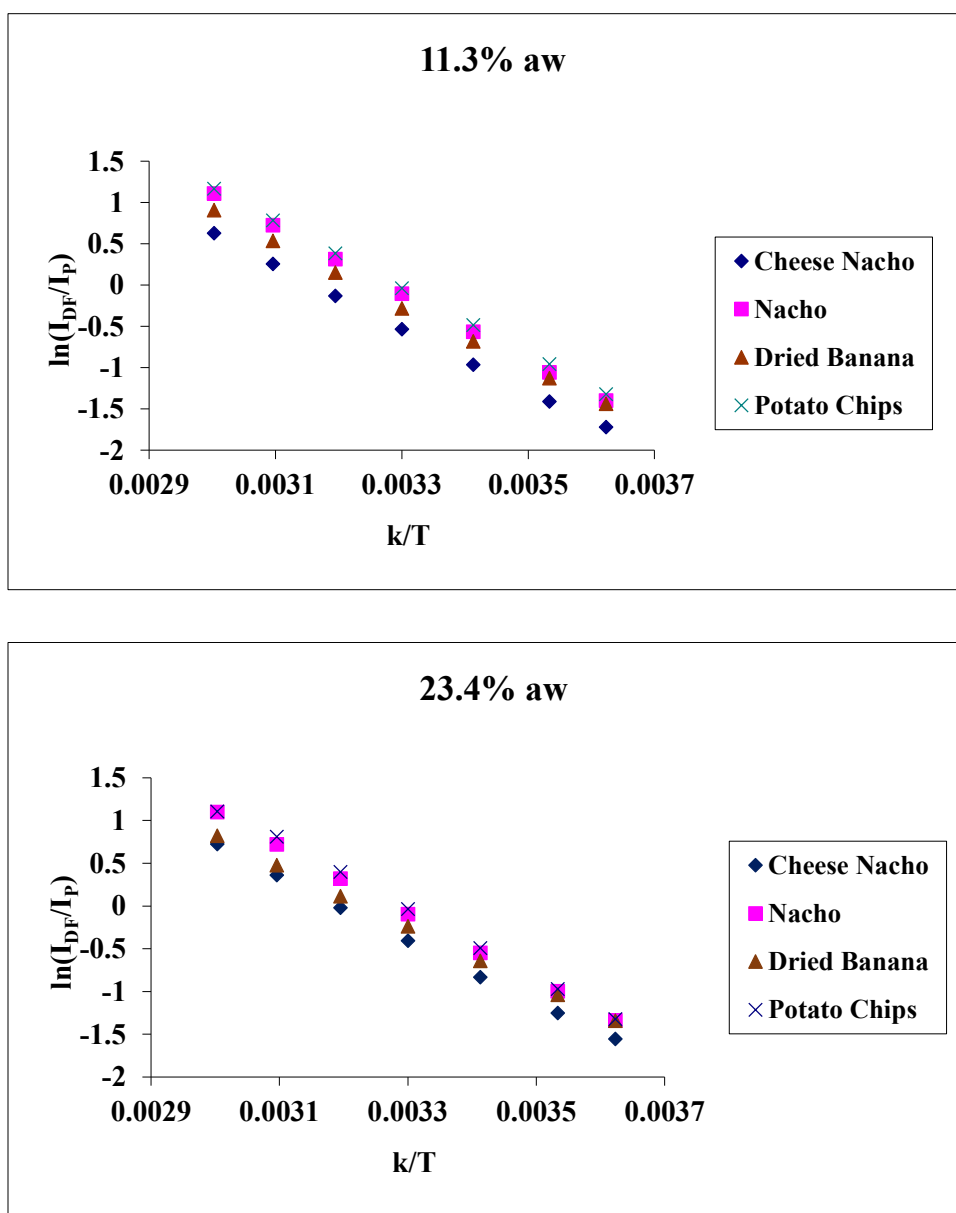
Figure 2-24: Van't Hoff plot for cheese nacho, nacho, dried banana and potato chips with water activities of 11.3% aw and 23.1% aw over the temperature range of 3 to 60°C using erythrosine B labeled gelatin nanoparticles.
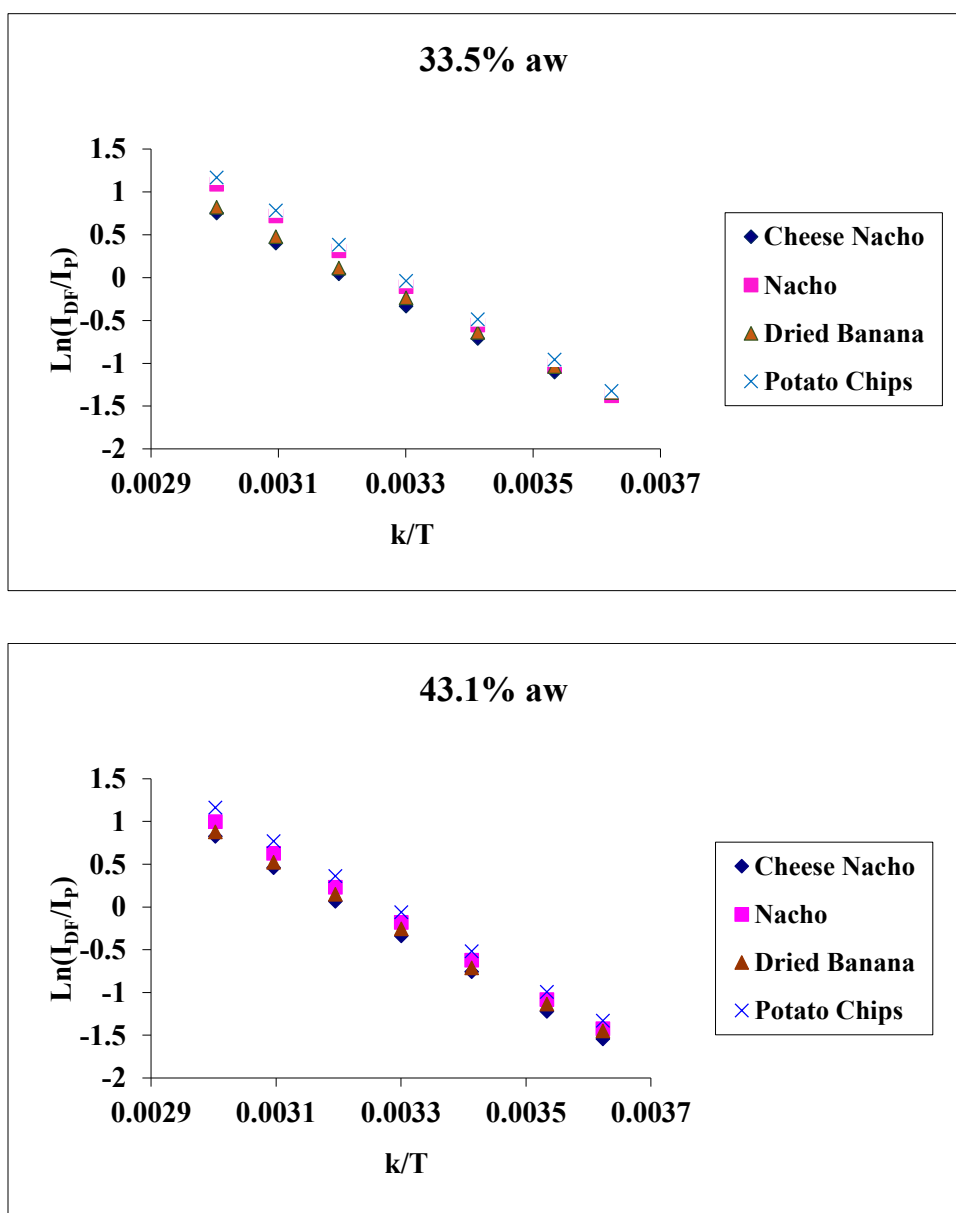
Figure 2-25: Van't Hoff plot for cheese nacho, nacho, dried banana and potato chips with water activities of 33.5% aw and 43.1% aw over the temperature range of 3 to 60°C using erythrosine B labeled gelatin nanoparticles.
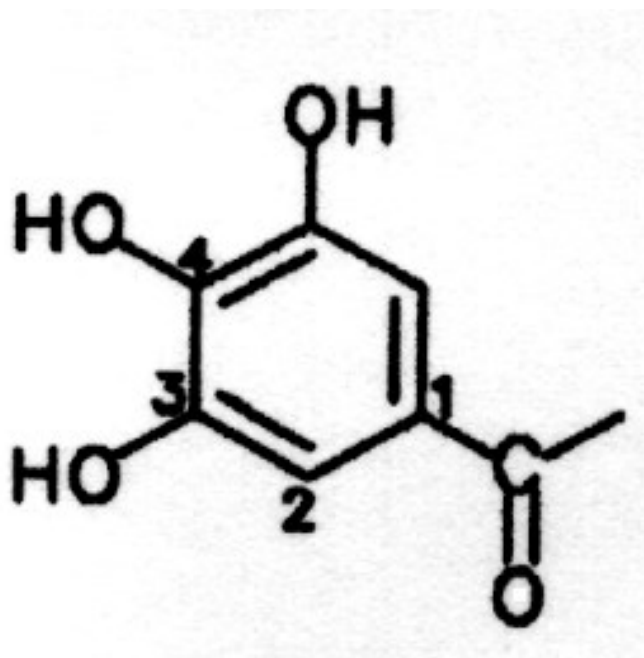
Figure 2-26: Galloyl group, a major constituent of tannins (Cole, 1986).
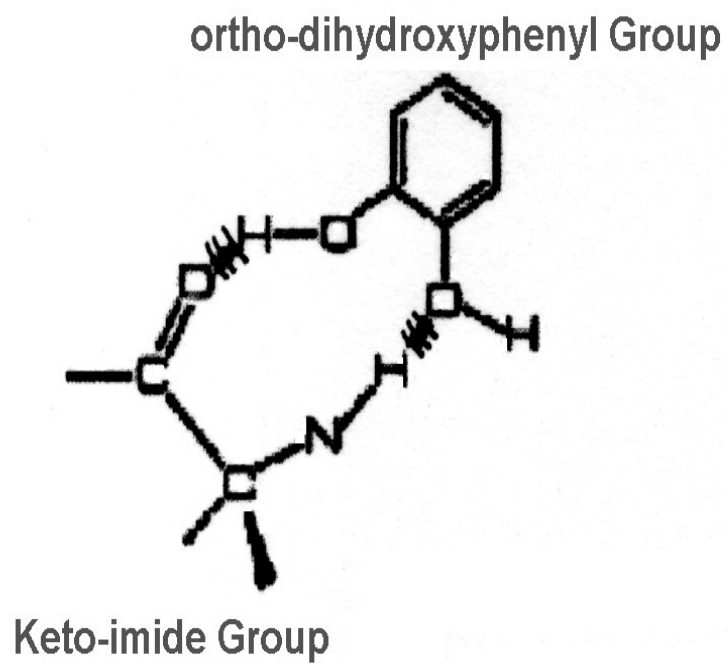
Figure 2-27: Polyphenol - peptide hydrogen bonding (Cole, 1986).

Vitamin A	0%	Vitamin C	120%
Calcium	2%	Iron	0%
Thiamin	10%	Riboflavin	4%
Niacin	4%	Vitamin B$_6$	6%
Folic Acid	15%	Magnesium	6%

* Percent Daily Values are based on a 2,000 calorie diet.

Contains orange juice from the U.S. and Brazil.
Tropicana Manufacturing Company, Inc.
Bradenton, Florida 34206 USA
©2007 Tropicana Products, Inc.

Tropicana Pure Premium
No Pulp Orange Juice

"CONTAINS ORANGE JUICE FROM THE U.S. AND BRAZIL": While HomeMaker uses only Florida oranges, other brands — including Tropicana — get juices from elsewhere. The fine print on this Tropicana carton shows that the contents do contain Brazilian juices.

Table 2-1: Tropicana orange juice (no pulp).

Nutrition Facts

Serving Size 8 fl oz (240 mL)
Servings Per Container about 4

Amount Per Serving

Calories 90

	% Daily Value*
Total Fat 0g	0%
Sodium 25mg	1%
Total Carbohydrate 24g	8%
Sugars 24g	
Protein 0g	

Not a significant source of calories from fat, saturated fat, trans fat, cholesterol, dietary fiber, vitamin A, vitamin C, calcium and iron.

*Percent Daily Values are based on a 2,000 calorie diet.

Ingredients:

Carbonated water, high fructose corn, syrup, citric acid, natural flavors, potassium sorbate and sodium benzoate (to protect taste), caramel color.

Table 2-2: Seagram's ginger ale (http://www.seagramsgingerale.com).

Serving Size: 8 fl oz • 240 mL	
Amount Per Serving	
Calories 0	Calories from Fat 0
	% DV
Total Fat 0g	0%
Saturated Fat 0g	0%
Trans Fat 0g	
Polyunsaturated Fat 0g	
Monounsaturated Fat 0g	
Cholesterol 0mg	0%
Sodium 25mg	1%
Potassium 45mg	1%
Total Carbohydrate 0g	0%
Dietary Fiber 0g	0%
Sugars 0g	
Other Carbohydrate 0g	
Protein 0g	0%
Unofficial Pts+: 0 (Old Pts: 0)	©DietFacts.com

Table 2-3: Brisk lemonade Drink.

RED BULL Energy Drink ● Improves performance, especially during times of increased stress or strain ● Increases endurance ● Increases concentration and improves reaction speed ● Stimulates the metabolism

Nutrition Facts
Serving Size 1 Can

Amount Per Serving:

Calories 110

	% Daily Value*
Total Fat 0 g	0%
Sodium 200 mg	8%
Total Carb. 28 g	9%
Sugars 27 g	
Protein less than 1g	

Niacin 100%	Vitamin B6 250%
Vitamin B12 80%	Pantothenic Acid 50%

Not a significant source of sat. fat, cholest., fiber, vitamin A, vitamin C, calcium and iron.

* Percent Daily Values are based on a 2,000 calorie diet.

CARBONATED WATER, SUCROSE, GLUCOSE, SODIUM CITRATE TAURINE, GLUCURONOLACTONE, CAFFEINE, INSTOL, NIACINAMIDE, CALCIUM-PANTOTHENATE, PYRIDOXINE HCl, VITAMIN B12, ARTIFICIAL FLAVORS, COLORS.

DISTRIBUTED BY:
RED BULL N.A., INC.
SANTA MONICA, CA 90404
© 1996, 2003

MADE IN AUSTRIA

Lightly carbonated.
Serve chilled.

Red Bull®

ENERGY DRINK

With Taurine. | Vitalizes body and mind.

8.3 FL OZ (250mL)

PLEASE RECYCLE

REXAM RB-US & SR33DOSC

Table 2-4: Red Bull Energy Drink (http://healthpsych.psy.vanderbilt.edu).

Nutrition Facts

Per 355 mL / par 355 mL

Amount / Teneur	% Daily Value / % valeur quotidenne
Calories / Calories 90	
Fat / Lipides 0 g	0 %
Sodium / Sodium 160 mg	7 %
Potassium / Potassium 40 mg	1 %
Carbohydrate / Glucides 23 g	8 %
Sugars / Sucres 21 g	
Protein / Protéines 0 g	

INGREDIENTS: WATER, LIQUID SUGAR, GLUCOSE-FRUCTOSE, CITRIC ACID, NATURAL AND ARTIFICIAL STRAWBERRY FLAVOUR, SALT, SODIUM CITRATE, MONOPOTASSIUM PHOSPHATE, COLOUR.

Table 2-5: Gatorade G Series (http://www.chemistryland.com).

Nutrition Facts

Serving Size 1 oz (28g/About 11 chips)

Amount Per Serving

Calories 150   Calories from Fat 70

	% Daily Value*
Total Fat 8g	**12%**
Saturated Fat 1.5g	**6%**
Trans Fat 0g	
Cholesterol 0mg	**0%**
Sodium 210mg	**9%**
Total Carbohydrate 17g	**6%**
Dietary Fiber 1g	**4%**
Sugars 1g	
Protein 2g	

Vitamin A 2%	•	Vitamin C 0%
Calcium 0%	•	Iron 0%
Thiamin 2%	•	Vitamin B6 2%

* Percent Daily Values are based on a 2,000 calorie diet. Your daily values may be higher or lower depending on your calorie needs:

		Calories:	2,000	2,500
Total Fat	Less than		65g	80g
Sat Fat	Less than		20g	25g
Cholesterol	Less than		300mg	300mg
Sodium	Less than		2,400mg	2,400mg
Total Carbohydrate			300g	375g
Dietary Fiber			25g	30g

Calories per gram:
Fat 9 • Carbohydrate 4 • Protein 4

Ingredients: Whole Corn, Vegetable Oil (Sunflower, Canola, Corn, and/or Soybean Oil), Maltodextrin (Made From Corn), and Less Than 2% of the Following: Wheat Flour, Salt, Cheddar Cheese (Milk, Cheese Cultures, Salt, Enzymes), Whey, Monosodium Glutamate, Buttermilk, Romano Cheese (Part-Skim Cow's Milk, Cheese Cultures, Salt, Enzymes), Whey Protein Concentrate, Onion Powder, Partially Hydrogenated Soybean and Cottonseed Oil, Corn Flour, Natural and Artificial Flavor, Dextrose, Tomato Powder, Lactose, Spices, Artificial Color (Including Yellow 6, Yellow 5, Red 40), Lactic Acid, Citric Acid, Sugar, Garlic Powder, Skim Milk, Whey Protein Isolate, Corn Syrup Solids, Red and Green Bell Pepper Powder, Sodium Caseinate, Disodium Inosinate, and Disodium Guanylate.

CONTAINS MILK AND WHEAT INGREDIENTS.

Table 2-6: Doritos Cheese Nacho (http://www.fritolay.com).

Nutrition Facts

Serving Size 1 oz (28g/About 13 chips)

Amount Per Serving

Calories 140	Calories from Fat 60

	% Daily Value*
Total Fat 7g	**11%**
Saturated Fat 1g	**5%**
Trans Fat 0g	
Cholesterol 0mg	**0%**
Sodium 120mg	**5%**
Total Carbohydrate 19g	**6%**
Dietary Fiber 2g	**7%**
Sugars 0g	
Protein 2g	

Vitamin A 0%	•	Vitamin C 0%
Calcium 2%	•	Iron 0%
Vitamin E 4%	•	Thiamin 2%
Riboflavin 2%	•	Vitamin B6 4%
Phosphorus 6%	•	Magnesium 4%
Zinc 2%		

* Percent Daily Values are based on a 2,000 calorie diet. Your daily values may be higher or lower depending on your calorie needs:

	Calories:	2,000	2,500
Total Fat	Less than	65g	80g
Sat Fat	Less than	20g	25g
Cholesterol	Less than	300mg	300mg
Sodium	Less than	2,400mg	2,400mg
Total Carbohydrate		300g	375g
Dietary Fiber		25g	30g

Calories per gram:
Fat 9 • Carbohydrate 4 • Protein 4

INGREDIENTS: Whole White Corn, Vegetable Oil (Corn, Canola and/or Sunflower Oil), and Salt.

No Preservatives.

Table 2-7: Tostitos Scoop Nacho (http://www.fritolay.com).

Nutrition Facts
Serving Size 5 crackers (16g)
Servings Per Container About 28

Amount Per Serving

Calories 70   Calories from Fat 15

	% Daily Value*
Total Fat 1.5g	**2%**
Saturated Fat 0g	**0%**
Trans Fat 0g	
Polyunsaturated Fat 0.5g	
Monounsaturated Fat 0g	
Cholesterol 0mg	**0%**
Sodium 150mg	**6%**
Potassium 15mg	**0%**
Total Carbohydrate 12g	**4%**
Dietary Fiber 0g	**0%**
Sugars 0g	
Protein 1g	

Vitamin A 0%	•	Vitamin C 0%	
Calcium 0%	•	Iron 4%	

*Percent Daily Values are based on a 2,000 calorie diet. Your daily values may be higher or lower depending on your calorie needs:

		Calories:	2,000	2,500
Total Fat	Less than		65g	80g
Sat Fat	Less than		20g	25g
Cholesterol	Less than		300mg	300mg
Sodium	Less than		2,400mg	2,400mg
Potassium			3,500mg	3,500mg
Total Carbohydrate			300g	375g
Dietary Fiber			25g	30g

INGREDIENTS: UNBLEACHED ENRICHED FLOUR (WHEAT FLOUR, NIACIN, REDUCED IRON, THIAMINE MONONITRATE (VITAMIN B1), RIBOFLAVIN (VITAMIN B2), FOLIC ACID), SOYBEAN OIL, PARTIALLY HYDROGENATED COTTONSEED OIL, SEA SALT, SALT, MALTED BARLEY FLOUR, BAKING SODA, YEAST.

CONTAINS: WHEAT.

KRAFT FOODS GLOBAL, INC.
NORTHFIELD, IL 60093-2753 USA
© KRAFT FOODS

kraft foods

VISIT US AT: www.nabiscoworld.com
OR CALL WEEKDAYS: 1-800-622-4726

FOR BEST WHEN USED BY INFORMATION, PLEASE SEE DATE PRINTED ON PACKAGE.

CARTON MADE FROM 100% RECYCLED PAPERBOARD
MINIMUM 35% POST-CONSUMER CONTENT

Table 2-8: Nabisco unsalted tops saltine crackers (http://www.nabiscoworld.com).

Nutrition Facts

Serving Size 1/3 cup (30g)
Servings Per Container About 6

Amount Per Serving

Calories 160	Calories from Fat 80

	% Daily Value*
Total Fat 9g	**14%**
Saturated Fat 7g	**35%**
Trans Fat 0g	
Cholesterol 0mg	**0%**
Sodium 0mg	**0%**
Potassium 140mg	**4%**
Total Carbohydrate 19g	**6%**
Dietary Fiber 4g	**16%**
Sugars 5g	
Protein 0g	

Vitamin A 2%	•	Vitamin C 2%
Calcium 0%	•	Iron 2%
Riboflavin 2%	•	Niacin 2%
Vitamin B6 2%	•	Folate 8%
Pantothenic Acid 4%	•	Phosphorus 2%
Magnesium 6%	•	Manganese 20%

*Percent Daily Values are based on a 2,000 calorie diet. Your daily values may be higher or lower depending on your calorie needs:

	Calories:	2,000	2,500
Total Fat	Less than	65g	80g
Saturated Fat	Less than	20g	25g
Cholesterol	Less than	300mg	300mg
Sodium	Less than	2,400mg	2,400mg
Potassium		3,500 mg	3,500 mg
Total Carbohydrate		300g	375g
Dietary Fiber		25g	30g

Calories per gram:
Fat 9 • Carbohydrate 4 • Protein 4

Ingredients:

Banana Chips (Contains bananas, coconut oil, sugar and natural banana flavor).

Table 2-9: SunTree Banana Chips (http://www.nutrientfacts.com).

Nutrition Facts

Serving Size 1 oz. (28g/About 15 chips)

Amount Per Serving

Calories 160	Calories from Fat 90

	% Daily Value*
Total Fat 10g	**16%**
Saturated Fat 1g	**5%**
Trans Fat 0g	
Polyunsaturated Fat 2.5g	
Monounsaturated Fat 5g	
Cholesterol 0mg	**0%**
Sodium 170mg	**7%**
Potassium 350mg	**10%**
Total Carbohydrate 15g	**5%**
Dietary Fiber 1g	**5%**
Sugars less than 1g	
Protein 2g	

Vitamin A 0%	•	Vitamin C 10%
Calcium 0%	•	Iron 2%
Vitamin E 6%	•	Thiamin 4%
Niacin 6%	•	Vitamin B₆ 10%
Magnesium 4%	•	Zinc 2%

* Percent Daily Values are based on a 2,000 calorie diet. Your daily values may be higher or lower depending on your calorie needs:

	Calories:	2,000	2,500
Total Fat	Less than	65g	80g
Sat Fat	Less than	20g	25g
Cholesterol	Less than	300mg	300mg
Sodium	Less than	2,400mg	2,400mg
Potassium		3,500mg	3,500mg
Total Carbohydrate		300g	375g
Dietary Fiber		25g	30g

Calories per gram:
Fat 9 • Carbohydrate 4 • Protein 4

Ingredients: Potatoes, Vegetable Oil (Sunflower, Corn and/or Canola Oil), and Salt.
No Preservatives.

Table 2-10: Lays Classic Potato Chips (http://www.fritolay.com).

Nutrition Facts

Serving Size: 1 oz (28g)

Amount Per Serving

Calories 78   Calories from Fat 3

	% Daily Value*
Total Fat 0.34 g	1%
Saturated Fat 0.05 g	0%
Trans Fat	
Cholesterol 0 mg	0%
Sodium 151.96 mg	6%
Potassium 34.02 mg	1%
Total Carbohydrate 15.79 g	5%
Dietary Fiber 0.62 g	2%
Sugars	
Sugar Alcohols	
Protein 2.58 g	
Vitamin A 0 IU	0%
Vitamin C 0 mg	0%
Calcium 24.38 mg	2%
Iron 0.4 mg	2%

INGREDIENTS: Unbleached Enriched Wheat Flour [Flours, Malted Barley Flour, Reduced Iron, Niacin, Thiamin Mononitrate (Vitamin B1), Riboflavin (Vitamin B2), Folic Acid], Water, High Fructose Corn Syrup, Yeast, Soybean Oil, Salt, Malted Barley Flour, Calcium Propionate (Preservative), Monoglycerides, Guar Gum.

Table 2-11: White Pita Bread (http://nutritiondata.self.com).

Liquid Sample	m $x10^3$	c $x10$	ΔE kJ/mol
Buffer pH3	-4.061	1.272	33.7632
Buffer pH7	-4.055	1.274	33.7133
Ginger Ale	-4.017	1.265	33.3973
Lemonade	-3.950	1.235	32.8403
Orange Juice	-3.929	1.234	32.6657
Water	-3.880	1.210	32.2583

Table 2-12: Analysis of the Van't Hoff plot of erythrosine B labeled gelatin nanoparticles provides the constant for calculating the temperature from a measurement of the delayed phosphorescence. $T_{calc} = m/(\ln (I_{DF}/ I_P) - C)$. In this equation m = slope and C = y – intercept of the ln (I_{DF}/I_P) versus 1/T calibration plot.

Temperature (°C)	Water	Ginger Ale	Lemonade	Orange Juice	Red Bull	Gatorade	Buffer pH 3	Buffer pH 7
3	0.69%	0.70%	0.98%	0.25%	2.19%	0.98%	0.63%	0.01%
10	0.42%	0.30%	0.39%	0.13%	0.35%	0.09%	0.58%	0.56%
20	1.05%	0.72%	0.10%	0.03%	0.16%	0.59%	0.98%	0.34%
30	0.95%	0.35%	0.03%	0.07%	0.67%	0.97%	0.52%	0.35%
40	0.48%	0.17%	0.03%	0.78%	0.47%	0.84%	0.13%	0.12%
50	0.10%	0.37%	0.14%	0.81%	0.17%	0.31%	0.01%	0.48%
60	0.90%	0.09%	0.34%	0.21%	0.50%	0.00%	0.56%	1.32%

Table 2-13: Percent error in estimating the temperature (degrees Kelvin) in liquid samples with erythrosine B resulting from the use of a single regression line for all data points.

Liquid Sample	m $x10^3$	c $x10$	ΔE kJ/mol
Gatorade	-3.500	1.090	29.101
Ginger Ale	-3.430	1.070	27.908
Lemonade	-3.430	1.070	30.911
Water	-3.356	1.054	28.532

Table 2-14: Analysis of the Van't Hoff plot of phloxine B labeled gelatin nanoparticles provides the constants for calculating the temperature from a measurement of the delayed phosphorescence luminescence. $T_{calc} = m/(\ln (I_{DF}/ I_P) - C)$. In this equation m = slope and C = y – intercept of the $\ln (I_{DF}/I_P)$ versus 1/T calibration plot.

Temperature (°C)	Water	Ginger Ale	Lemonade	Gatorade
3	0.25%	0.48%	1.43%	0.48%
10	0.33%	0.17%	0.98%	0.17%
20	0.56%	0.09%	0.21%	0.09%
30	0.37%	0.03%	0.17%	0.03%
40	0.17%	0.09%	0.12%	0.09%
50	0.20%	0.12%	0.15%	0.12%
60	0.22%	0.06%	0.16%	0.06%

Table 2-15: Percent error in estimating the temperature (degrees Kelvin) in liquid samples with phloxine B resulting from the use of a quadratic best fit curve for all data points.

Solid Sample	m $x10^3$	c $x10$	ΔE kJ/mol
Cheese Nacho	-3.981	1.27	33.106
Nacho	-4.170	1.36	34.674
Potato Chips	-4.239	1.38	35.244
Cracker	-4.120	1.35	34.266
Dried Banana	-3.968	1.3	32.99
White Bread	-3.73	1.19	31.014

Table 2-16: Analysis of the Van't Hoff plot of erythrosine B labeled gelatin nanoparticles provides the constant for calculating the temperature from a measurement of the delayed phosphorescence. $T_{calc} = m/(\ln (I_{DF}/ I_P) - C)$. In this equation m = slope and C = y – intercept of the ln (I_{DF}/I_P) versus $1/T$ calibration plot.

Temperature (°C)	Cheese Nacho	Nacho	Cracker	Banana Chips	Potato Chips
3	0.67%	0.67%	0.50%	0.91%	1.35%
10	1.64%	1.64%	1.77%	1.56%	2.27%
20	0.29%	0.29%	0.15%	0.47%	0.76%
30	0.23%	0.23%	0.04%	0.49%	0.48%
40	0.12%	0.12%	0.11%	0.08%	0.05%
50	0.01%	0.01%	0.26%	0.32%	0.60%
60	0.05%	0.05%	0.33%	0.06%	1.02%

Table 2-17: Percent error in estimating the temperature (degrees Kelvin) in solid samples with erythrosine B resulting from the use of linear approximation for each sample.

Solid Sample	m $x10^3$	c $x10$	ΔE kJ/mol
Banana chips	-2.563	0.910	17.918
Cheese Nacho	-2.155	0.780	21.311
Potato Chips	-2.630	0.900	21.872
White Bread	-2.428	0.880	20.192

Table 2-18: Analysis of the Van't Hoff plot of phloxine B labeled gelatin nanoparticles provides the constant for calculating the temperature from a measurement of the delayed phosphorescence. $T_{calc} = m/(\ln (I_{DF}/ I_P) - C)$. In this equation m = slope and C = y – intercept of the ln (I_{DF}/I_P) versus 1/T calibration plot.

Temperature (°C)	Cheese Nacho	White Beard	Banana Chips	potato Chips
3	2.62%	4.07%	3.36%	3.19%
10	0.69%	2.81%	1.18%	2.88%
20	0.48%	0.70%	1.18%	2.45%
30	0.09%	0.60%	0.93%	2.82%
40	0.50%	0.56%	0.75%	2.96%
50	0.15%	1.18%	1.05%	3.63%
60	0.76%	1.75%	1.64%	3.55%

Table 2-19: Percent error in estimating the temperature (degrees Kelvin) in solid samples with phloxine B resulting from the use of linear approximation for each sample.

References

Azarmia Shirzad, Huanga Yuan , Chend Hua, McQuarriea Steve , Abramse Douglas, Road Wilson , Finlayf Warren H., Millera Gerald G. Löbenberga Raimar. Optimization of a two-step desolvation method for preparing gelatin nanoparticles and cell uptake studies in 143B osteosarcoma cancer cells. J Pharm Pharmaceut Sci 9(1),124-132, 2006.

Cole C.G.B. The use of gelatin in wine fining, Published in the Proceedings of the 1st SAAFoST Technical Symposium, Emulsifiers, Stabilisers and Thickeners in the Food Industry 1, held in Durban, RSA, in April 1986.

Duarte P., Ferreira D. P. , Machado I. F., Ferreira L. F. V., Rodríguez H. B. and Román E. S., Phloxine B as a Probe for Entrapment in Microcrystalline Cellulose, Molecules, 17, 1602-1616, 2012.

Garland, P. B. and Moore, C. H. Phosphorescence of Protein-Bound Eosin and Erythrosine. Biochemical Journal 183, 561-572. 1979.

http://healthpsych.psy.vanderbilt.edu

http://nutritiondata.self.com

http://www.chemistryland.com

http://www.fritolay.com

http://www.nabiscoworld.com

http://www.nutrientfacts.com

http://www.seagramsgingerale.com

Inbaraj J. J., Kukielczak B. M. and Chignell C. F. Phloxine B Phototoxicity: A Mechanistic Study Using HaCaT Keratinocyted, Photochemistry and Photobiology, , 81, 81-88, 2005.

Lakowicz J. and Cherek H., Dipolar Relaxation in Proteins on the Nanosecond Timescale Observed by Wavelength-resolved Phase Fluorometry of Tryptophan Fluorescence. Journal of Biological Chemistry, 255(3)3, 831-834, 1980.

Nack, T. J., & Ludescher, R. D. Molecular mobility and oxygen permeability in amorphous bovine serum albumin films. Food Biophysics, 1, 151–162, 2006.

Parker C.A. Photoluminescence of Solutions. Amsterdam: Elsevier Pub Co., 1968.

Pravinata, L.C., You, Y., & Ludescher, R.D. Erythrosine B phosphorescence monitors molecular mobility and dynamic site heterogeneity in amorphous sucrose. Biophysical Journal, 88, 3551-3561, 2005.

Rasooly, R. Phloxine B, aversatile bacterial stain. International Journal of Food Microbiology.157, 29-34, 2007.

Simon-Lukasik, K. V., & Ludescher, R. D. Erythrosine B phosphorescence as a probe of oxygen diffusion in amorphous gelatin films. Food Hydrocolloids, 18, 621–630, 2004.

Sundaresan, K. & Ludescher, R. D. "Molecular Mobility and Oxygen Permeability in Amorphous β-Lactoglobulin." Food Hydrocolloids 22, 403–413, 2008.

Van Buren J. P. and Robinson W. B. Formation of Complexes between Protein and Tannic Acid). J. Agr. Food Chem, 17, 4, 772 777, July-Aug. 1969.

Wang L., Gaigalas A.K., Blasic J., Holden M.J., Spectroscopic characterization of fluorescein- and tetramethylrhodamine-labeled oligonucleotides and their complexes with a DNA template. Spectrochimica Acta Part A 60, 2741–2750, 2004.

3   OXYGEN SENSOR

3.1   Introduction

Measuring oxygen concentration by quenched luminescence has become popular in different applications including packaging. This technique is based upon the oxygen-dependent quenching of phosphorescence. Examples of this application are the use of an optical sensor which monitors the oxygen content in foods packaged under modified atmosphers (Mills, 2005); biomedical applications such as fluorescence-based optical sensor for blood gas analysis (Wolfbeise, 1996); and environmental monitoring such as sensor in an accelerated bioremediation process in water, air and soil (Hill et al., 2001). Oxygen quenching luminophores have been studied for a long time. The application of luminophores has become increasingly advanced, including new optical sources, detectors, and data processing; also measurement of oxygen concentrations in liquids has resulted in bench top instruments and optodes (Lübbers and Opitz, 1975; Bergman 1986; Bacon and Demas, 1987), with significant advances made in the 1990's (Lübbers, 1992; Gruber et al 1993; Weigl et al. 1994). Lifetime measurements form the basis of the O_2xyDot™ oxygen indicator sold by OxySense, Inc. (Dallas, TX; http://www.oxysense.com). O_2xyDots consist of small (0.5 mm diameter) silicon rubber disks impregnated with the ruthenium(II) phenanthroline chromophore $Ru(dpp)_3ClO_4$ as described in detail by Mills (2005). Quenching of phosphorescence from porphyrins (Papkovsky et al., 2000a) and other aromatics (Papkovsky et al., 2000b) has also been shown to detect oxygen under conditions suitable for food applications.

The intensity of fluorescence or phosphorescence can be decreased by different processes such as collisional quenching (dynamic), static quenching (non-fluorescent complex), self-quenching or other absorbing species. Collisional quenching takes place when the exited triplet state fluorophore is deactivated upon contact with a quencher like oxygen and transfers its energy to a ground state oxygen molecule and returning from the excited triplet state to the ground state without emission of light (Lakowicz, 1999 and Lo et al. 1996). In this process the molecules are not chemically altered. Collisional quenching decreases the intensity of fluorescence and the overall amount of phosphorescence emitted due to quenching and increases the rate of decay of the triplet state; therefore, decreases the phosphorescence lifetime. The quenching of phosphorescence by oxygen is diffusion limited and follows the Stern-Volmer relationship (Mills, 2005):

$$I_o/I = \tau_o/\tau = 1 + K_{SV} [O_2] \tag{1}$$

$$K_{SV} = k_q \tau_0$$

where I, I_0, τ, and τ_0 denote the luminescence intensities and lifetimes of the luminophore in the presence and absence of oxygen, respectively. K_{SV} is the Stern–Volmer constant for the quenching reaction, which depends on the biomolecular quenching rate k_q and exited state lifetime (τ_0) in the absence of quencher and $[O_2]$ is the oxygen concentration in solution.

Erythrosin B was used in this study as an oxygen probe because of its phosphorescence lifetime sensitivity to oxygen. This probe is chemically stable, and the phosphorescence

emission is in the red or near infrared where biological molecules absorb very little (Vanderkooi et al. 1987). Its lifetime in aqueous solution at room temperature is long, ~0.2 ms (Duchowicz et al., 1998) and increases to ~0.6 ms in an immobile glassy matrix (Simon-Lukasik & Ludescher, 2004). Erythrosin B has long wavelength absorption (λ_{max} ≈ 520) nm and a large stokes shift for phosphorescence (λ_{max} ≈ 680 nm).

Erythrosin B has shown sensitivity to oxygen in food polymers such as BSA (Nack & Ludescher 2006), B-lactoglobulin (Sandarsun & Ludescher 2008), and gelatin (Simon-Lukasik & Ludescher, 2004; Lukasik & Ludescher, 2006).

3.2   Materials and Methods:

3.2.1   Preparing sample for oxygen sensor

In chapter 2, it was explained how to make gelatin nanoparticles, measure the particle size and label them with erythrosin B.

1 ml of erythrosin B labeled gelatin nanoparticles was transferred into a cylinder and diluted with DI water with relative ratio of 1:10 to obtain a pale pink solution which was used for the experiments.

The tests were performed on liquid and solid food samples as described below.

3.2.2 Liquid Samples

Prior to conducting any experiments, cuvettes were washed in the cuvette washer with soap and rinsed with DI water, ethanol, and acetone then dried for few minutes. 40 μL of the diluted pale pink solution of erythrosin B labeled gelatin nanoparticles was added to 2 ml of liquid food solutions in clean standard 1cm x 1cm fluorescence cuvettes for luminescence measurement. The liquid food samples were water, Tropicana orange juice containing no pulp, lemonade juice drink from Brisk and Gatorade. Two different concentrations of oxygen were considered in the experiments to represent the lower and upper-bound limits, namely zero and air-saturated at room temperature. Because of the sensitivity of erythrosin B labeled gelatin nanoparticles to temperature, the experiments were conducted at different temperatures.

In order to reach 0 mM oxygen concentration, nitrogen was purged for 30 minutes before starting the experiment into the sample and continued until the experiment was finished to prevent oxygen quenching of the triplet state. In order to obtain air saturated samples, the samples were purged with air for 30 minutes at room temperature. The sample was then transferred into a cuvette, and mineral oil was added on top of the sample. Since the concentration of dissolved oxygen varies with temperature, mineral oil was utilized to act as a barrier and to maintain a constant concentration of dissolved oxygen in different temperatures for this experiment. An oxygen sensor (DO-166MT-1 Miro Dissolved Oxygen Electrode) was used to verify the concentration of oxygen in each sample in cuvvet before starting the experiment.

3.2.3   Solid Samples

In the case of solid samples, 20 μL of the diluted pale pink solution of erythrosin B labeled gelatin nanoparticles was dropped on the surface of approximately 1 to 1.5 cm² solid samples of Doritos cheese nacho, Tostitos scoop nacho, SunTree banana chips, and Lays classic potato chips. Samples were dried by a heat gun for few minutes and fitted diagonally into a standard 1cm x 1cm fluorescence cuvette for luminescence measurement. For conducting the experiment without oxygen, nitrogen was purged for 30 minutes prior to the experiment and continued until the experiment was finished to prevent oxygen quenching of the triplet state. In order to make an air-saturated sample, the sample was purged with an indirect stream of air for 30 minutes after placing the sample in the cuvett, and the cuvett was closed and sealed during the experiment to keep the concentration of oxygen constant.

3.2.4   Relative Humidity

Four salts, of different relative humidity, were used for this experiment. These salts were lithium chloride with RH=11.3%, potassium acetate with RH=23.4%, magnesium chloride with RH=33.5% and potassium carbonate with RH =43%. 10 g of each salt was added into a small desiccator and small amount of water was added into the desiccators in order to make a saturated salt solution. All four (4) desiccators were monitored daily and water or salt was added as needed to facilitate making a stable saturated salt solution. Erythrosin B labeled gelatin nanoparticles were added to small pieces of solid samples.

The samples were then dried by heat gun for 5 minutes. Four aluminum containers were weighed and the weights were recorded. Then 4 or 5 small pieces of one sample - for example, potato chips - were placed into the aluminum containers and were weighed again and the weights were recorded. The aluminum containers which contained the solid food sample were placed into the four different desiccators that had different relative humidity and allowed to stabilize. The samples were weighed every 2 days until 3 consecutive constant weight measurements were achieved. When the samples reached the target humidity and their weights stabilized, they were ready for further tests. This test was applied on Doritos cheese nacho, Tostitos scoop nacho, SunTree banana chips, and Lays classic potato chips. Duration of stabilization was different for each sample.

3.3 Data Analysis

The phosphorescence intensity decays were fitted with a single exponential function for liquid samples (Eq. 2),

$$I(t) = I_0 e^{\frac{-t}{\tau}} \tag{2}$$

where I is intensity at time t, I_0 is the initial intensity at time t=0, and τ is the lifetime.

Phosphorescence intensity decay of erythrosine B labeled gelatin nanoparticles on solid samples was analyzed using a stretched exponential or Kohlrausch-Williams-Watts (KWW) decay model according to Eq. (3) (Lee et al., 2001),

$$I_{(t)} = I_{(0)} \, exp \, [-(t/\tau)^{\beta}] \tag{3}$$

where $I_{(t)}$ is the intensity as a function of time following pulsed excitation, $I_{(0)}$ is the initial intensity at time zero, τ is the KWW lifetime (τ_{KWW}), and β is the stretching exponent that characterizes the distribution of the decay times (Richert and Heuer, 1997). This stretch factor essentially expresses the width of the distribution of the lifetimes. The τ_{KWW} and stretch factors provide an estimate of the most probable lifetime and the width of the lifetime distribution. Analysis of the relaxation process as a function of time requires using a proper mean relaxation time $<\tau>$, which needs the asymmetry of the individual photophysical lifetimes by addition of the stretch factor β. This mean relaxation time can be calculated from Eq. (4),

$$<\tau> = (\tau_{KWW}/\beta)\Gamma(1/\beta) \tag{4}$$

where τ_{KWW} is the KWW lifetime, β is the stretching exponent and Γ represents the gamma function (Draganski et al, 2010).

The phosphorescence lifetime is the inverse of the total decay rate. Measuring the intensity decay as a function of time can provide phosphorescence intensity.

$$\tau = (k_{RP} + k_{TS1} + k_{TS0} + k_Q[O_2])^{-1} \tag{5}$$

k_{RP} denotes the intrinsic rate of radiative decay. It is constant, equal to 41 s^{-1} for Ery B and unaffected by temperature or environment (Duchowicz et al., 1998), k_{TS1} is the rate of reverse intersystem crossing from the excited triplet state back to the excited singlet state and k_{TS0} is the rate of collisional quenching to the ground state; this rate is altered by the physical environment of the probe and is a measure of local matrix mobility (Pravinata et al., 2005; Papp and Vanderkooi, 1989), and $k_Q[O_2]$ is the oxygen quenching rate which is zero in the absence of oxygen. $k_Q[O_2]$ is a non-radiative decay which also varies with the local physical environment of the probe (Draganski et al, 2010).

K_{TS1} is a thermally activated process that follows Arrhenius kinetics (Parker, 1968) and depends on ΔE_{TS}, the energy gap between S_1 and T_1 (Simon-Lukasik and Ludescher, 2004).

$$k_{TS1}(T) = k_{TS1}^{\circ} \, exp(\Delta E_{TS}/RT) \tag{6}$$

The slope of a Van't Hoff plot of the natural log of the ratio of delayed fluorescence (I_{DF}) to phosphorescence (I_P) intensity versus inverse temperature provides a measure of ΔE_{TS} (Duchowicz et al., 1998),

$$d[ln(I_{DF}/I_P)]/d(1/T) = -\Delta E_{TS}/R \qquad (7)$$

where I_{DF} is intensity of delayed fluorescence, I_P is intensity of phosphorescence and $R = 8.314$ J K^{-1} mol^{-1}.

Therefore, it is possible to calculate the average non-radiative decay rate ($<k_{TS0}>$) from the calculated average lifetimes using Eq. (5), the calculated values of k_{TS1}, and the known value of k_{RP} for erythrosine B.

Since the quenching of a luminescent molecule such as erythrosin B by oxygen obeys the Stern-Volmer relationship, the lifetime of erythrosin B labeled gelatin nanoparticles was fitted to the Stern-Volmer equation (1).

3.4   Instrumentation

Luminescence measurements were made using Cary Eclipse (Varian Instruments, Walnut Creek, CA) fluorescence spectrophotometer equipped with a temperature controller and multi-cell holder. This instrument, which collects in analog mode and uses a high intensity pulsed lamp and a time delay, was employed to avoid any fluorescence during

the lamp pulse. Temperature was controlled using a thermoelectric temperature controller (Varian Instruments).

3.5   Results and Discussion

3.5.1   Liquid Samples

The relationship between the phosphorescent lifetime of erythrosine B labeled gelatin nanoparticles under anoxic conditions and in air was investigated in 4 different solutions: orange juice, lemonade, water and Gatorade. Erythrosin B labeled gelatin nanoparticles were added into the solutions and lifetime was monitored using the phosphorescence intensity decay over the temperature range of 3°C to 60°C in the absence and presence of oxygen. For all solutions the intensity decays were fitted using a single exponential model. The lifetimes of erythrosin B labeled gelatin nanoparticles both in the absence and presence of oxygen decreased monotonically with increasing temperature from 3°C to 60°C (Figure 3-1, Figure 3-2, Figure 3-3, and Figure 3-4). For all 4 liquid samples (orange juice, lemonade, water and Gatorade) the lifetime in the absence of oxygen was higher than the lifetime in the presence of O_2 which was expected due to oxygen quenching in the triplet state in the presence of oxygen. It was not possible to measure the lifetime at temperatures exceeding 30 °C in the presence of oxygen due to higher mobility of matrix and oxygen quenching in the triplet state for all 4 liquid samples.

The temperature dependence of k_{TS0}, calculated as described in the Materials and Methods section, is plotted in Arrhenius format in Figure 3-5. The erythrosin B lifetime

in nitrogen is temperature-dependent and decreases as temperature increases. The values of k_{TS0} of the erythrosin B triplet state increases due to matrix-induced quenching when temperature increases (Draganski et al., 2010). The magnitude of k_{TS0} depends on two factors: first, internal factors associated with the way in which the excited triplet state of erythrosin B is vibrationally coupled to the ground singlet state, and, second, the external factors related to the way in which the ground state vibrational energy can dissipate from the excited probe into the surrounding matrix (Fischer et al., 2002; Strambini and Gonnelli, 1985). Both of these factors are sensitive to the molecular mobility in the matrix (Strambini and Gonnelli, 1985); therefore, the magnitude of k_{TS0} offers a measure of matrix mobility (Nack & Ludescher, 2006).

The values of k_{TS0} over the temperature range of 3 to 30°C are very close for orange juice, lemonade and Gatorade although this value for water is much higher than in juice at higher temperature. This could be explained by the complexity of the juice matrices.

The rate of oxygen quenching $k_Q[O_2]$, was calculated from the difference in the lifetimes in the presence and absence of oxygen. This value is dependent on the rate of diffusion of oxygen through the matrix (k_Q) and also on the oxygen solubility in the matrix ($[O_2]$) (Guillet, 1987) and is proportional to oxygen permeability. Figure 3-6 shows the Arrhenius plot of oxygen quenching rates over the temperature range of 3°C to 30°C for erythrosin B labeled gelatin nanoparticles in 4 different samples of orange juice, lemonade, water and Gatorade. These plots are almost linear with no sudden deviation in the slope across the entire temperature range and are fitted to a linear equation. The slope of these plots was used to calculate the activation energy (E_A) for oxygen quenching

(Table 3-1). The E_A values are very close for lemonade, orange juice and Gatorade ranging from 32 to 35 kJ/mol but E_A is smaller for water (22 kJ/mol).

As shown in Figure 3-6, the value of $k_Q[O2]$ for lemonade, water and Gatorade are very close and larger than that for the orange juice. This can be due to higher viscosity or thickness of orange juice compared to other liquid samples which causes a lower rate of oxygen diffusion into the liquid (Tan and Thorpe 1992, Jamnongwong et al 2010). The literature shows that the concentration of dissolved oxygen in juices is almost the same as water (Lewis and McKenzie, 1947; Ahrne et al. 1997). Sometimes, due to presence of solid parts, the concentration of dissolved oxygen is less than 10% smaller in juices than in water (Sadler et al. 1988). This small variation does not lead to a significant difference in the data obtained from the experiments because the probe is not sensitive to very small changes in oxygen concentration in the samples.

Since the quenching of luminescence by oxygen follows the Stern-Volmer relationship (Eq. 1) one might expect that a plot of τ_o/τ versus $[O_2]$ could be used to define a relationship which allows oxygen concentration to be calculated from the measured lifetime ratio. The success of this approach would depend on the ability to precisely measure the lifetime ratio for oxygen concentration values between zero and saturated. Future research may indicate the validity of the aforementioned approach; however, this study has only focused on detecting the presence of oxygen. Additional experiments performed as part of this study have shown that accurately setting the oxygen

concentration in samples is a major challenge which makes the construction of the Stern-Volmer plot difficult.

Figure 3-7 and Figure 3-8 show the probe lifetime ratio (τ_0/τ) in oxygen saturated liquid samples and anoxic condition as a function of temperature. The lifetime ratio at zero oxygen concentration is one by definition. The results show that erythrosin B labeled gelatin nanoparticles are sensitive to oxygen concentration in the solution and are able to detect the presence of oxygen. It is noted that in order to calibrate the probe for measurement of oxygen concentration, more data points will be needed to establish the trend of lifetime variation as a function of oxygen concentration

3.5.2 Solid samples

The relationship between phosphorescent lifetime of erythrosine B labeled gelatin nanoparticles under anoxic conditions and air was investigated on solid samples of cheese nacho, nacho, banana chips and potato chips. Erythrosin B labeled gelatin nanoparticles were added to the surface of samples, and the samples were dried by a heat gun. For all solid samples the intensity decay data were fitted using a stretched exponential decay model (Eq. 3, Materials and Methods section). Lifetime was monitored using phosphorescence intensity decay over the temperature range of 3°C to 60°C in the absence and presence of oxygen. The average lifetimes of erythrosin B both in the absence and the presence of oxygen decreased monotonically with increasing temperature from 3°C to 60°C and overlapped each other (Figure 3-9, Figure 3-10, Figure 3-11, and Figure 3-12). It was observed that the average lifetime under anoxic condition was not

higher than the average lifetime in the air. There are a few possible explanations for this behavior including, negligible oxygen diffusing due to the formation of a gelatin film on the surface of the samples, or collapse of some nanoparticles into the carbohydrate matrix of the food samples rather than coalescing into a film.

Review of the literature suggests that the similarity of erythrosin B phosphorescence lifetimes in the absence and presence of oxygen can be attributed to gelatin film formation. Simon-Lukasik and Ludescher (2004) showed that oxygen quenching in the erythrosin B gelatin film was negligible at 58% relative humidity as erythrosin B phosphorescence lifetimes in air and in nitrogen were similar, and oxygen quenching became more significant at higher RH. The average lifetimes of erythrosin B in all 4 samples were very close ranging from 0.98 ms to 0.74 ms over the temperature range of 3°C to 60°C. This was verified by testing the solid samples at different relative humidity values. The samples were placed in 4 different desiccators with 4 different RH values of RH=11.3%, RH=23.4%, RH=33.5% and RH =43% until they reached the target humidity and equilibrated. For all samples the intensity decays were fitted using a stretched exponential decay model (Eq. 3, Materials and Methods section). Lifetime was monitored using the phosphorescence intensity decay over the temperature range of 3°C to 60°C in the absence and presence of oxygen. The average lifetimes both in the absence and the presence of oxygen decreased monotonically with increasing temperature from 3°C to 60°C (Figure 3-13a, Figure 3-13b, Figure 3-14a, Figure 3-14b, Figure 3-15a, Figure 3-15b, Figure 3-16a, and Figure 3-16b). The average lifetimes in the absence and the

presence of oxygen were practically identical in all samples. Higher RH values were not considered for these samples, as they would lose their textures and crispiness.

The temperature dependence of k_{TS0}, calculated for 4 solid samples, is plotted in an Arrhenius format in Figure 3-17. Since the erythrosin B average lifetime in nitrogen is temperature-dependent and decreases as temperature increases, it causes an increase in the average rate of k_{TS0} of the erythrosin B triplet state due to matrix-induced quenching (Draganski et al, 2010). The values of k_{TS0} of the Arrhenius plots for all 4 samples are relatively close, ranging from 900-1340 s^{-1} over the temperature range of 3°C to 60°C. The results of experiments on liquid and solid food samples indicate that:

erythrosine B labeled gelatin nanoparticles can be used as a probe to detect the presence or absence of oxygen in some liquid foods.

The use of this probe to estimate the oxygen concentration in liquid foods will require full oxygen quenching curves to be generated with many [O_2] values to evaluate whether the S-V relationship applies. Precise control of oxygen concentration in solution will pose a challenge as has been observed in this study.

The oxygen quenching curves should be obtained at different temperatures since the phosphorescent lifetime of erythrosine B labeled gelatin nanoparticles is temperature-dependent.

The probe did not work as an appropriate sensor in the case of solid food samples with low RH possibly due to the formation of a gelatin film on the samples and negligible

diffusion of oxygen into the sample. It is recommended that future studies try to explore the exact cause of this observed behavior.

3.5.3   Comparison with Commercial Oxygen Sensors

It should be noted that the proposed gelatin nanoparticle oxygen sensors represent a promising alternative to commercially available oxygen sensors which can be potentially used by the food industry. The non-invasive commercial oxygen monitoring methods are based on utilization of oxygen-sensitive packaging material or embedded patches such as the Ocean Optics RedEye oxygen sensing patch. The commercial oxygen sensors, although claimed by the manufacturers to be suitable for food applications, have not gained popularity in the food and packaging industry mainly due to their additional cost.

The advantages of gelatin nanoparticle oxygen sensors over available commercial oxygen sensing methods can be summarized as follows:

1. The use of gelatin nanoparticle oxygen sensors does not require special packaging materials or inserts and is compatible with conventional packaging materials and procedures; therefore, these sensors will be less costly.

2. Gelatin nanoparticle oxygen sensors are edible and can be placed directly inside or on the food.

3. Gelatin nanoparticles have the ability to spread uniformly inside fluids or over surfaces, thus providing more coverage.

This study has indicated that gelation nanoparticles were not able to function properly as oxygen probes on solid food samples selected for the experiments. This is a disadvantage of gelatin nanoparticle oxygen sensors compared with commercial technology.

Therefore, it is recommended that further research be conducted on the application of gelatin nanoparticles as oxygen sensors in food, particularly focusing on reliable calibration methods.
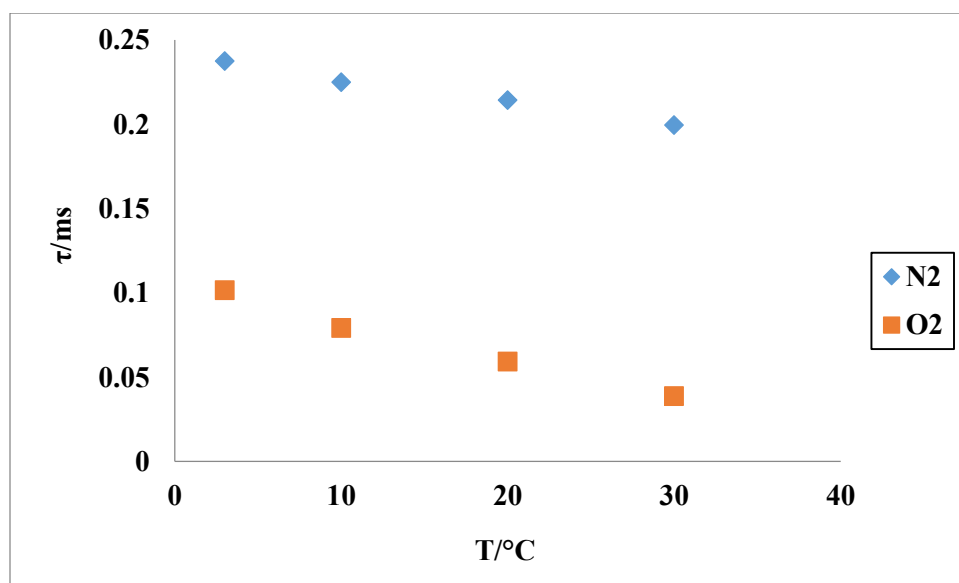
Figure 3-1: The lifetimes of erythrosin B labeled gelatin nanoparticles both in the absence and presence of oxygen (0.25 mM) in lemonade over the temperature range of 3°C to 30°C.
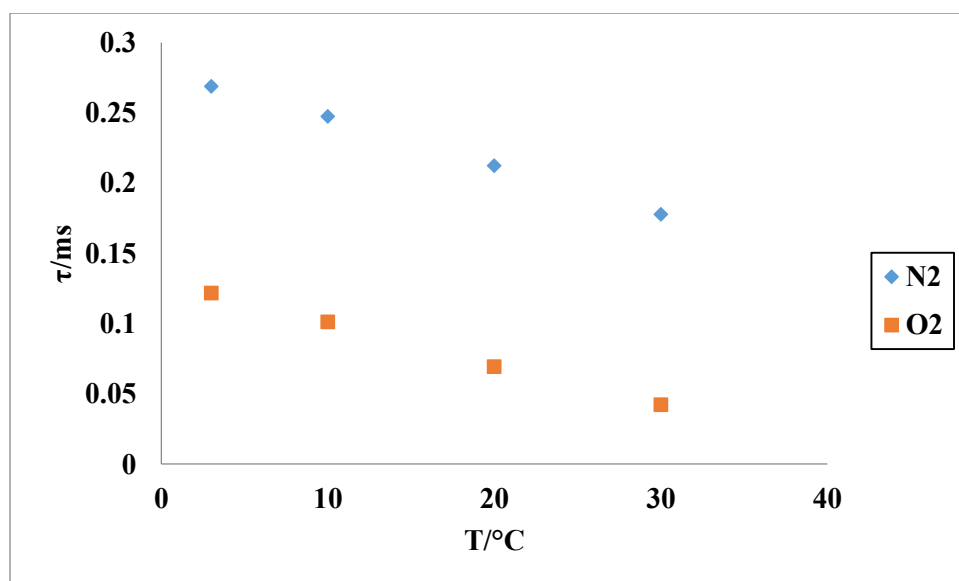
Figure 3-2: The lifetimes of erythrosin B labeled gelatin nanoparticles both in the absence and presence of oxygen (0.25 mM) in orange juice over the temperature range of 3°C to 30°C.
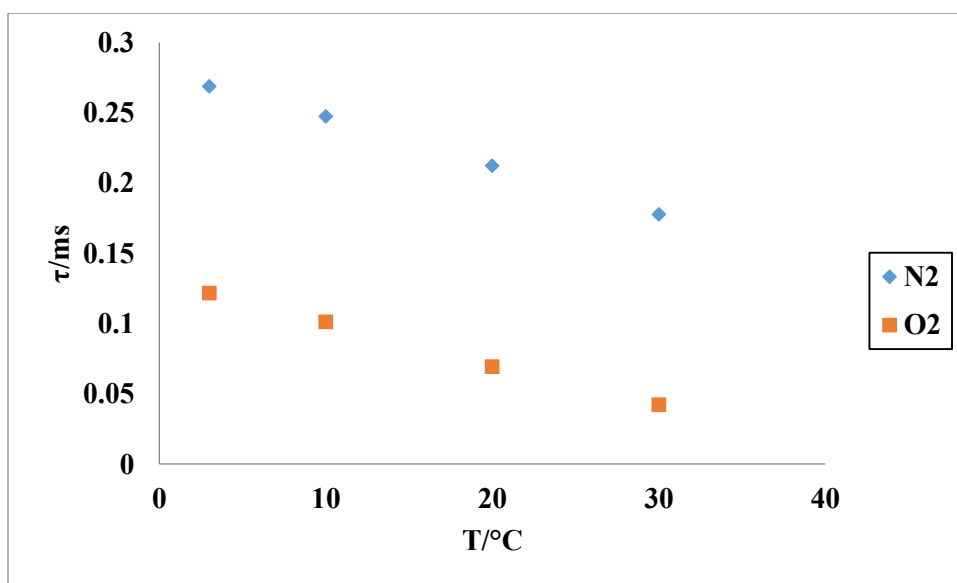
Figure 3-3: The lifetimes of erythrosin B labeled gelatin nanoparticles both in the absence and presence of oxygen (0.25 mM) in Gatorade over the temperature range of 3°C to 30°C.
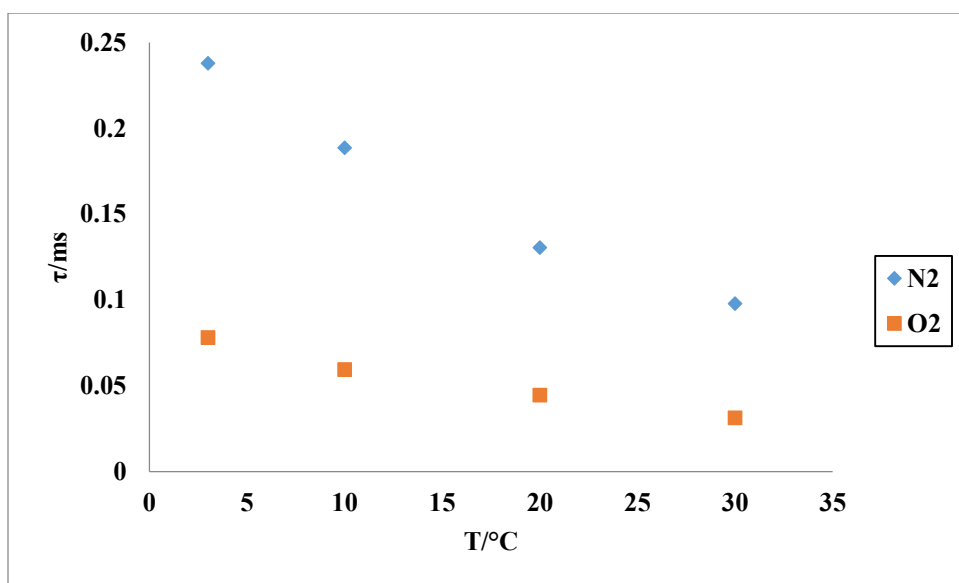
Figure 3-4: The lifetimes of erythrosin B labeled gelatin nanoparticles both in the absence and presence of oxygen (0.25 mM) in water over the temperature range of 3°C to 30°C.

Figure 3-5: Arrhenius plots of the average non-radiative rate ($<k_{TS0}>$) of erythrosin B labeled gelatin nanoparticles in orange juice, lemonade water and Gatorade over the temperature range from 3°C to 30°C.
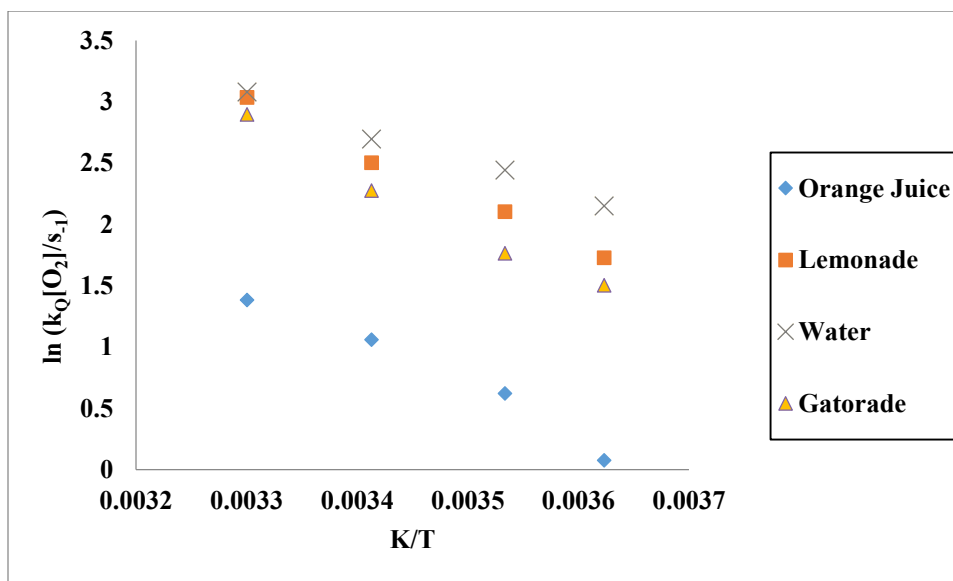
Figure 3-6: Arrhenius plot of average oxygen quenching rate $k_Q[O_2]$ over the temperature range from 3°C to 30°C for erythrosin B labeled gelatin nanoparticles in 4 different solutions of orange juice, lemonade, water and Gatorade.

a
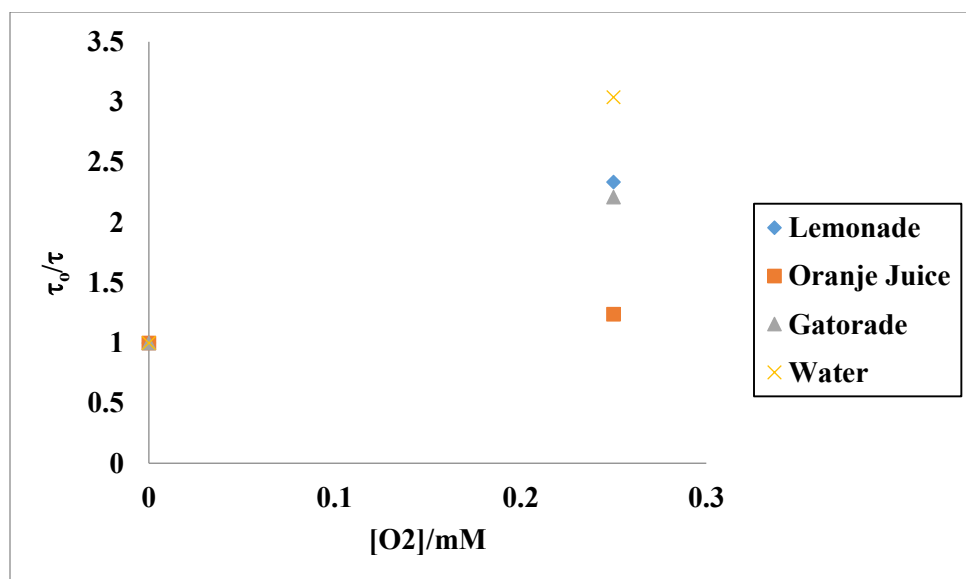
b
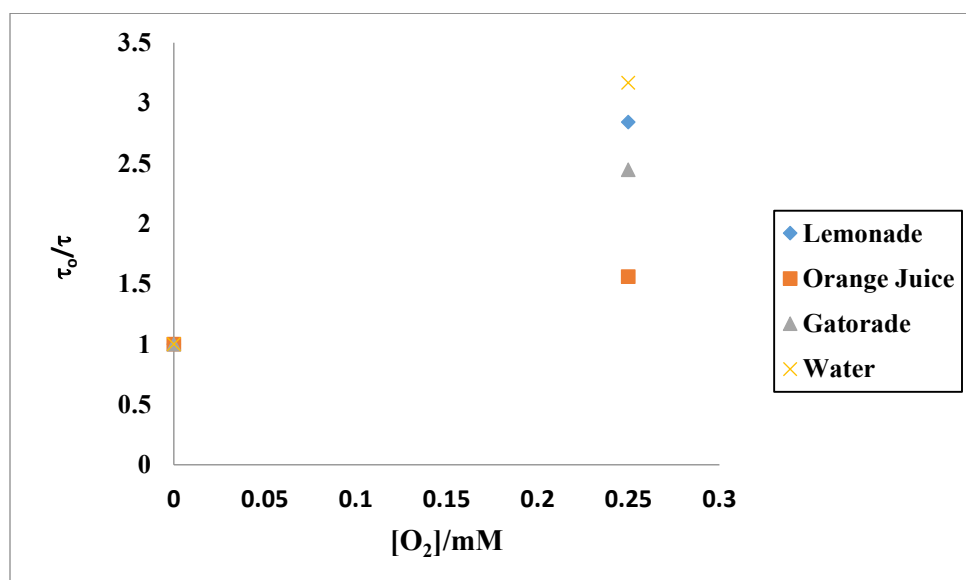
Figure 3-7: Oxygen quenching of erythrosin B labeled gelatin nanoparticles in lemonade, orange juice, Gatorade and water (a) at 3°C and (b) at 10°C.

a
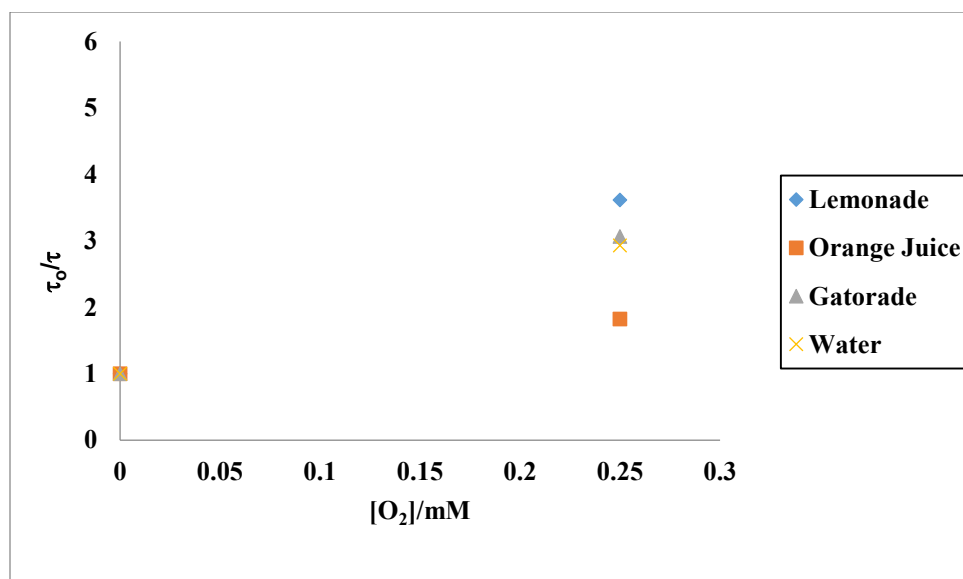
b
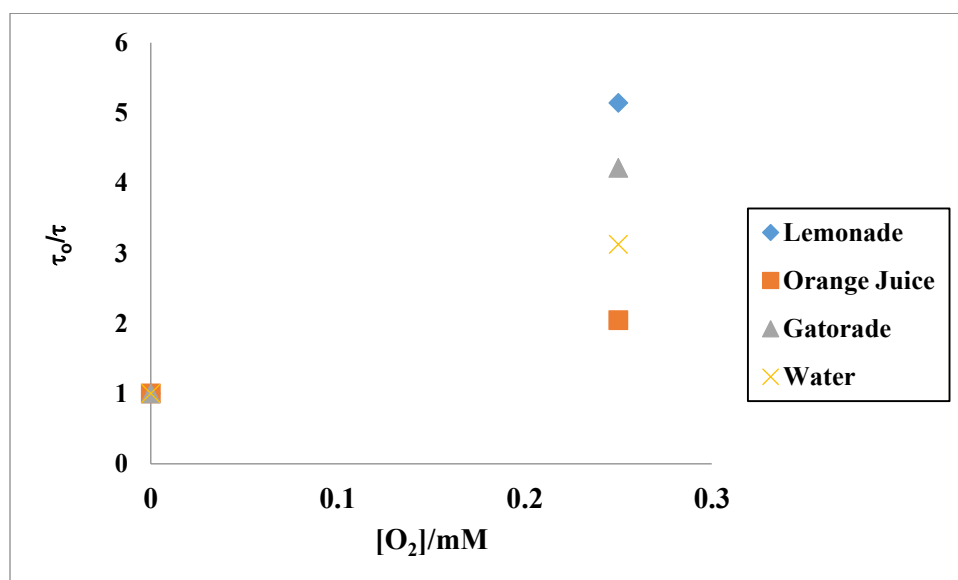
Figure 3-8: Oxygen quenching of erythrosin B labeled gelatin nanoparticles in lemonade, orange juice, Gatorade and water (a) at 20°C and (b) at 30°C.
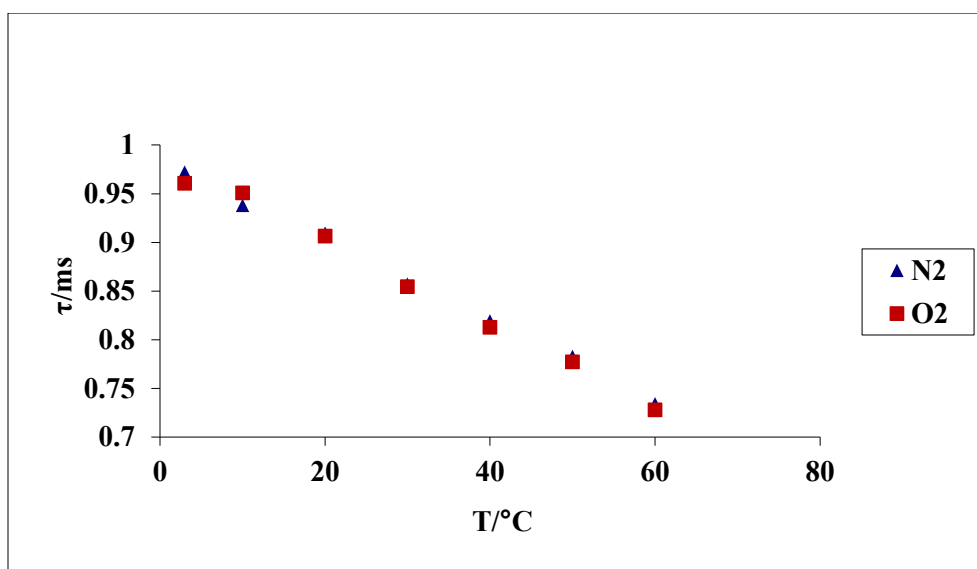
Figure 3-9: Lifetime of erythrosine B labeled gelatin nanoparticles on cheese nacho in absence and presence of oxygen (air) over the temperature range from 3 to 30°C.
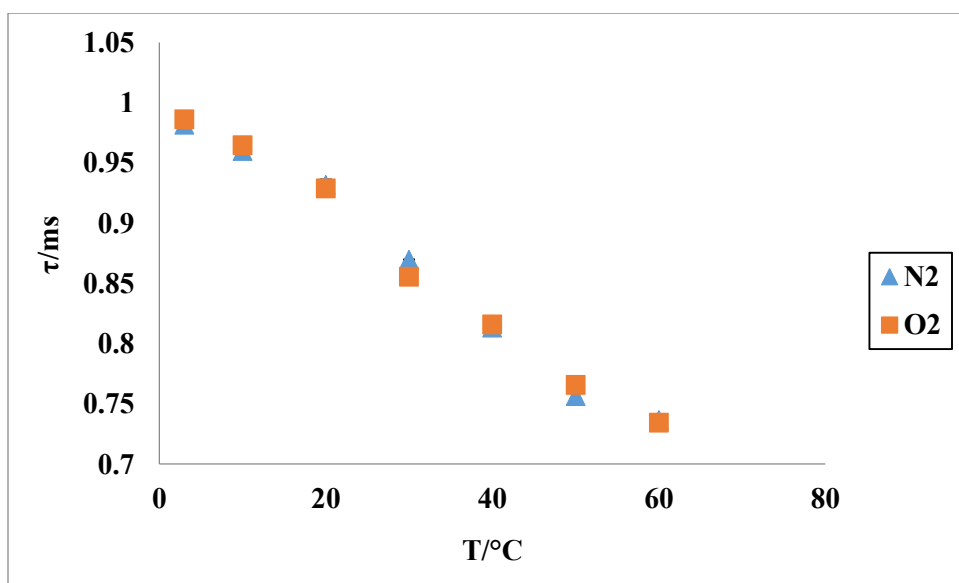
Figure 3-10: Lifetime of erythrosine B labeled gelatin nanoparticles on nacho in absence and presence of oxygen (air) over the temperature range from 3 to 30°C.
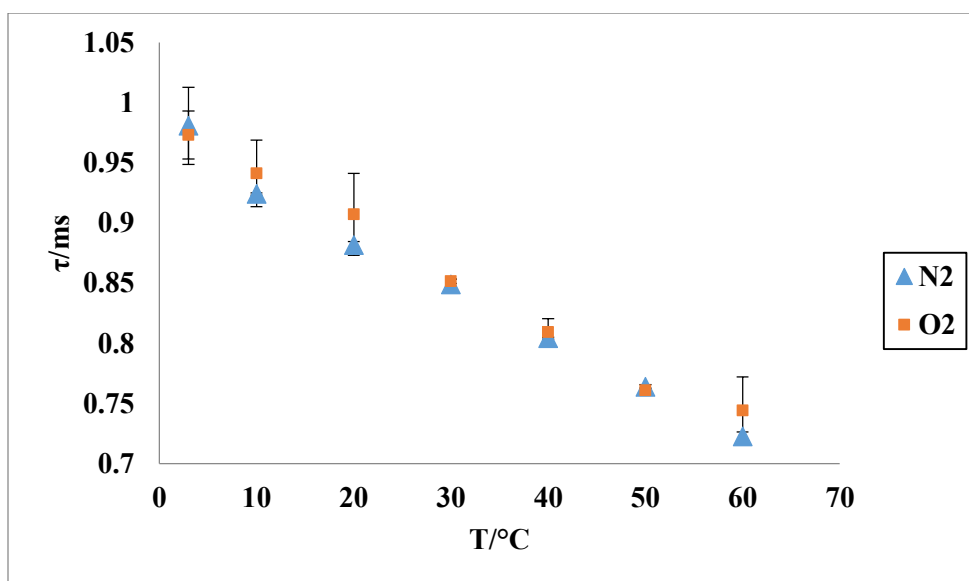
Figure 3-11: Lifetime of erythrosine B labeled gelatin nanoparticles on banana chips in absence and presence of oxygen (air) over the temperature range from 3 to 30°C.
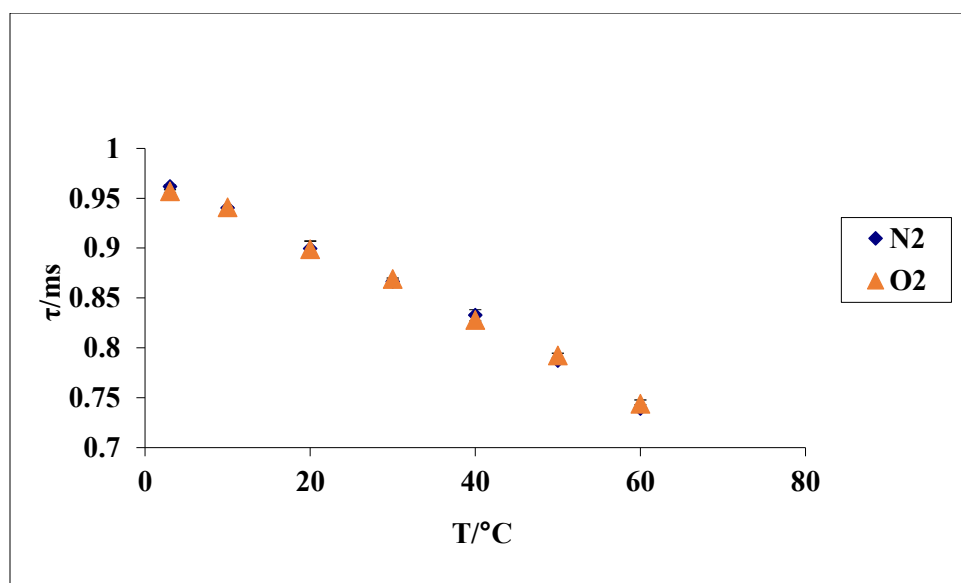
Figure 3-12: Lifetime of erythrosine B labeled gelatin nanoparticles on potato chips in absence and presence of oxygen (air) over the temperature range from 3 to 30°C.

a
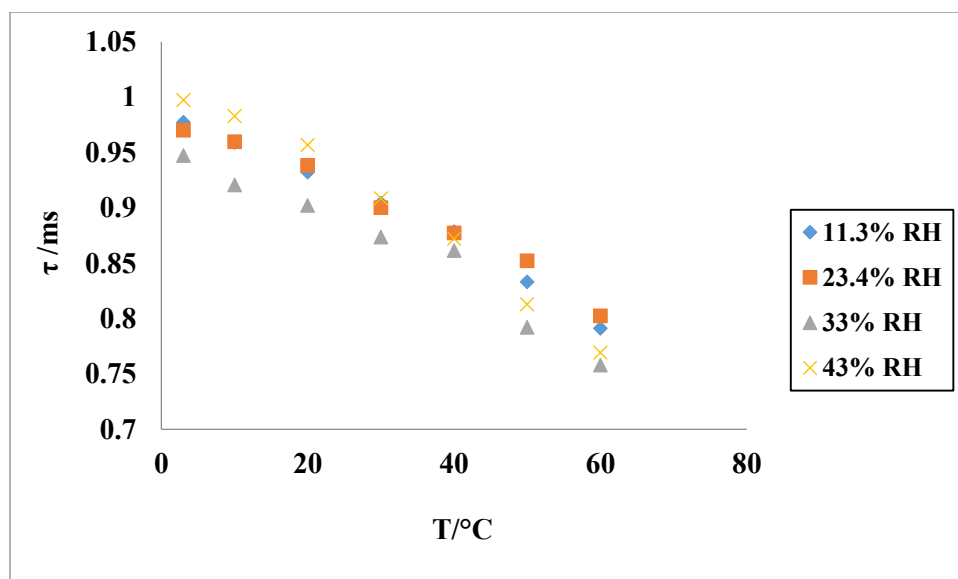
b
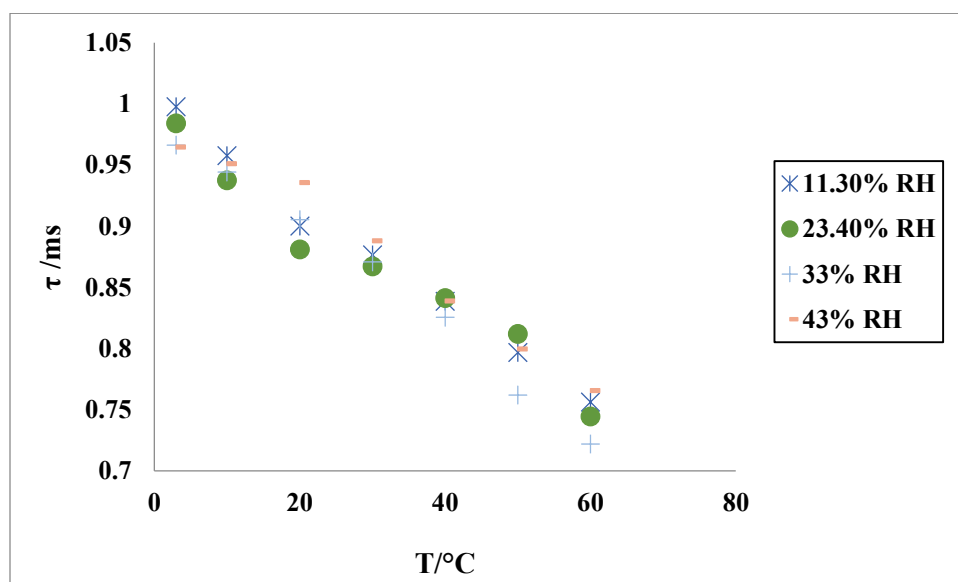
Figure 3-13: Phosphorescent lifetime of erythrosine B labeled gelatin nanoparticles on cheese nacho under anoxic conditions (a) and air (b) with RH=11.3%, RH=23.4%, RH=33.5% and RH =43%.

a
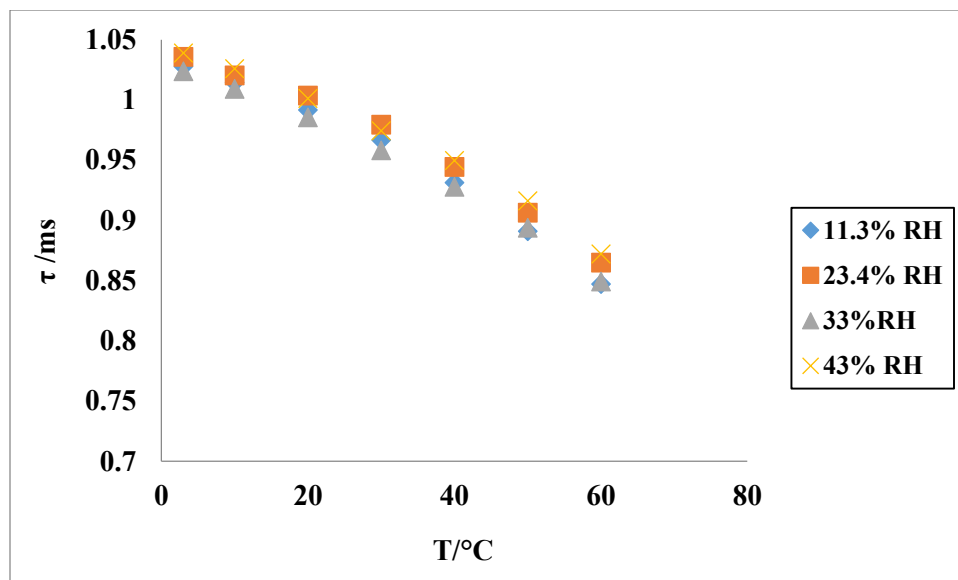
b
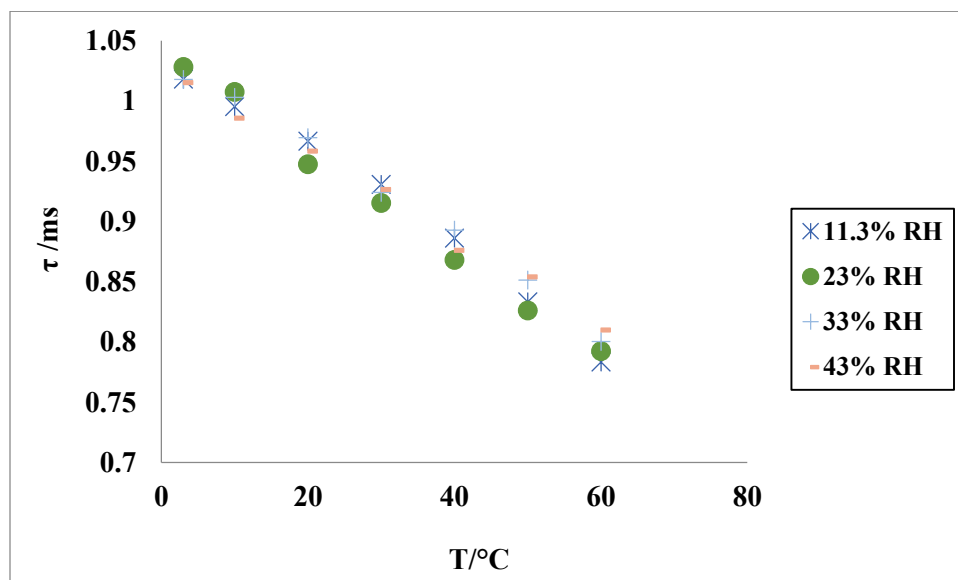
Figure 3-14: Phosphorescent lifetime of erythrosine B labeled gelatin nanoparticles on nacho under anoxic conditions (a) and air (b) with RH=11.3%, RH=23.4%, RH=33.5% and RH =43%.

a
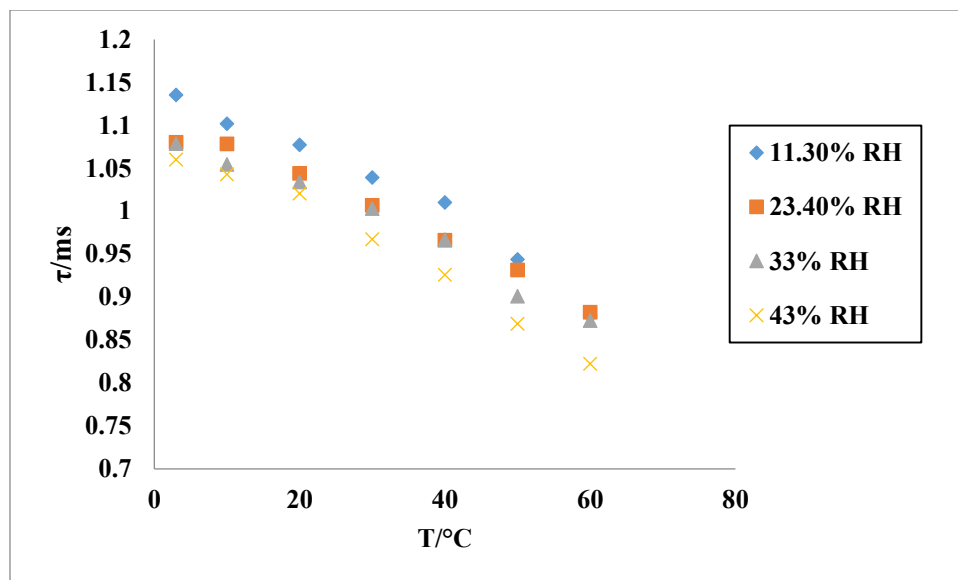
b
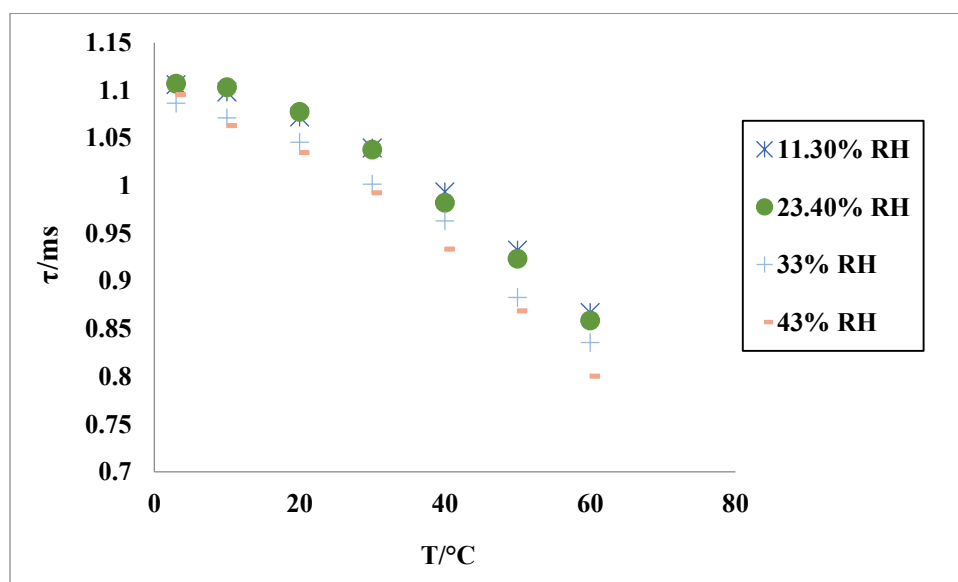
Figure 3-15: Phosphorescent lifetime of erythrosine B labeled gelatin nanoparticles on banana chips under anoxic conditions (a) and air (b) with RH=11.3%, RH=23.4%, RH=33.5% and RH =43%.

a
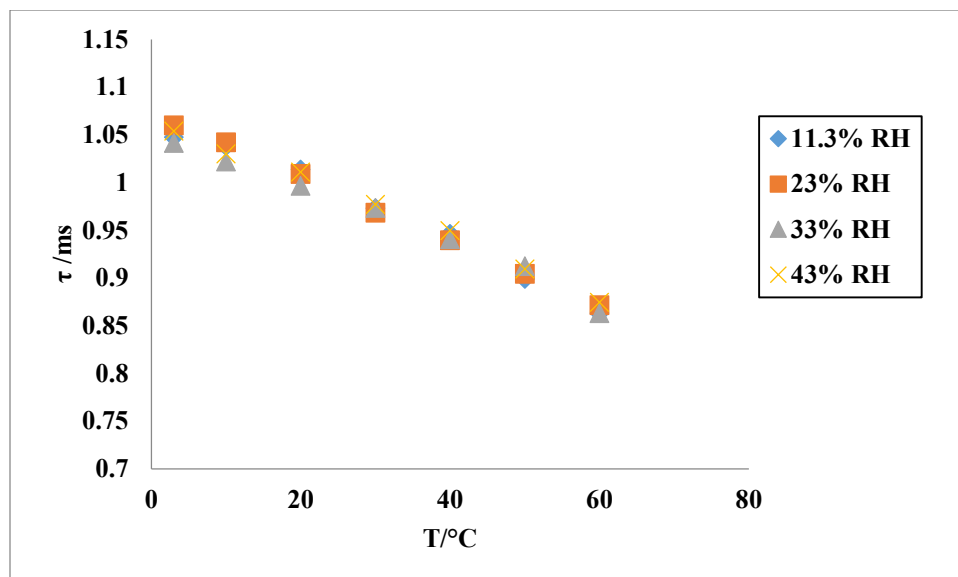
b
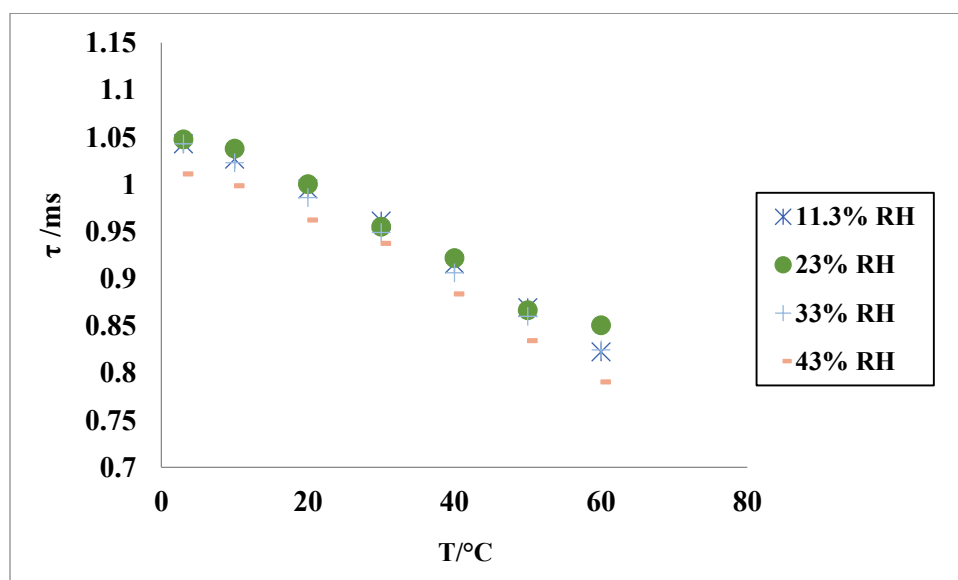
Figure 3-16: Phosphorescent lifetime of erythrosine B labeled gelatin nanoparticles on potato chips under anoxic conditions (a) and air (b) with RH=11.3%, RH=23.4%, RH=33.5% and RH =43%.
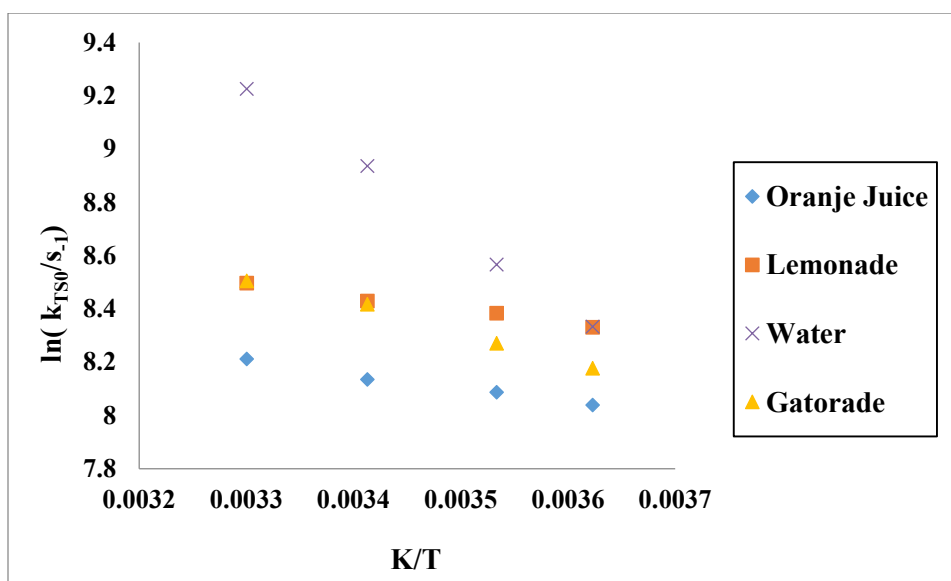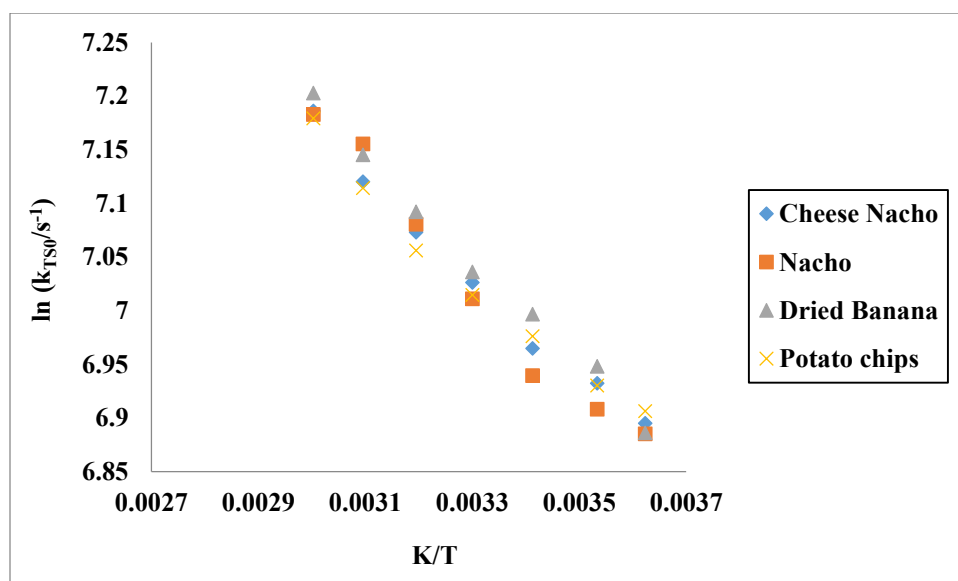
Figure 3-17: Arrhenius plots of the average non-radiative rate ($<k_{TS0}>$) of erythrosine B labeled gelatin nanoparticles on cheese nacho, nacho, banana chips and potato chips.

Liquid Solution	$E_A/(kJ/mol)$	$A/(s^{-1})$
Gatorade	35.1	2.690×10^7
Lemonade	32.2	9.645×10^6
Orange juice	32.2	2.020×10^6
Water	22.6	2.096×10^5

Table 3-1: Activation energy (E_A) and pre exponential (A) for oxygen permeability in liquid solutions.

References

Ahrne L. M., Oliveira F. A. R., Manso M. C., Drumond M. C., Oste R. and Gekas V., Modelling of Dissolved Oxygen Concentration Storage of Packaged Liquid Doods

Durin. Journal of Food Engineering, 34, 213-224, 1997.

Bacon J. R. and Demas J. N., "Determination of oxygen concentrations by luminescence quenching of a polymer-immobilized transition-metal complex," Analytical Chemistry, 59, 2780-2785, 1987.

Bergman I., "Rapid response atmospheric oxygen monitor based on fluorescence quenching," Nature, 218, 396, 1986.

Draganski A.R., Tiwari R.S., Sundaresan K.V., Nack T.J., You Y.M., Ludescher R.D., Photophysical Probes of the Amorphous Solid State of Proteins Food Biophys 5(4), 337–345, 2010.

Duchowicz, R., Ferrer M.L. and Acuna A.U., Kinetic spectroscopy of erythrosin phosphorescence and delayed fluorescence in aqueous solution at room temperature. Photochem. Photobiol, 68, 494-501, 1998.

Fischer, C. J., Gafni, A., Steel, D. G., and Schauerte, J. A., The triplet-state lifetime of indole in aqueous and viscous environments: Significance to the interpretation of room temperature phosphorescence in proteins. Journal of the American Chemical Society, 124, 10359–10366, (2002).

Gruber W.R., Klimant I. and Wolfbeis O. S, "Instrumentation for optical measurement of dissolved oxygen based on solid state technology," Ocean Optics, 12, 448-457, 1993.

Guillet J., Polymer photophysics and photochemistry (Cambridge University Press, Cambridge, 1987.

Hill M., Ogurstov V.I., Papkovsky D.B., Yershov V., Sensor in an accelerated bio remediation process in; proceedings of the 1st senspole workshop, Alcala, Spain, 153-161, 2001.

Jamnongwong M., Loubiere K., Dietrich N. and Hebrard, G., Experimental study of oxygen diffusion coefficients in clean water containing salt, glucose or surfactant: Consequences on the liquid-sidemass transfer coefficients. Chemical Engineering Journal, 165 (3), 758-768, 2010.

Lakowicz, J. R. (1999) Principles of Fluorescence Spectroscopy. Plenum Press, NY.

Lee K.C.B, Siegel J, Webb S.E.D, Leveque-Fort S, Cole M.J, Jones R, Dowling K, Leve M.J, and French P.M.W., Applications of the stretched exponential function to fluorescence lifetime imaging. Biophysical Journal 81, 1265-74, 2001.

Lewis V.M., McKenzie H.A.   Amperometric Determination of Dissolved Oxygen in

Orange Juice. Analytical chemistry , 19(9), 643–646, 1947.

Lübbers D. W. and Opitz N., "The pCO2/pO2 optrode: A new probe for measuring pCO2 and pO2 of gases and liquids," Z. Naturforsch, 30 (C), 532-533, 1975.

Lübbers D. W., "Fluorescence based chemical sensors," Advances in biosensors, 2, 215-260, 1992.

Lukasik K. V. and Ludescher, R. D., "Molecular Mobility in Water and Glycerol Plasticized Cold and Hot-Cast Gelatin Films, 20, 96-105, 2006.

Mills, A., Oxygen indicators and intelligent inks for packaged food. Chemical Society Reviews, 34, 1003-1011, 2005.

Nack, T. J., and Ludescher, R. D., Molecular mobility and oxygen permeability in amorphous bovine serum albumin films. Food Biophysics, 1, 151–162, 2006. In Molecular Luminescence Spectroscopy (S.

Papkovsky, D., O'Riordan, T., Soini, A., Phosphorescent porphyrin probes in biosensor and bioassays. Biochem. Soc. Trans. 28, 74-77. 2000a.

Papkovsky, D., Papkovskaia, N., Smyth, A., Kerry, J., Ogurtsov, V. Phosphorescent sensor approach for non-destructive measurement of oxygen in packaged foods: optimization of disposable oxygen sensors and their characterization over a wide temperature range. Analytical Letters 33, 1755-1777, 2000b.

Papp, S., and Vanderkooi J. M., Tryptophan phosphorescence atroom temperature as a tool to study protein structure and function.Photochem. Photobiol. 49,775–784, 1989.

Parker C.A. Photoluminescence of Solutions. Amsterdam: Elsevier Pub Co., 1968.

Pravinata, L.C., You, Y., & Ludescher, R.D., Erythrosin B phosphorescence monitors molecular mobility and dynamic site heterogeneity in amorphous sucrose. Biophysical Journal, 88, 3551-3561. 2005.

Richert R., Hener A., Macromolecules Rate-Memory and Dynamic Heterogeneity of First-Order Reactions in a Polymer Matrix, 30 (14), 4038, 1997

Sadler G. D, Roberts J. and Cornell J., Determination of Oxygen Solubility in Liquid Foods Using a Dissolved Oxygen Electrode. Journal of Food Science 53(5), 1493–1496, 1988.

Simon-Lukasik, K. V., & Ludescher, R. D., Erythrosin B phosphorescence as a probe of oxygen diffusion in amorphous gelatin films. Food Hydrocolloids, 18, 621–630, 2004.

Strambini GB, Gabellieri E. Intrinsic phosphorescence from proteins in the solid state.Photochem Photobiol. 39(6):725–729, 1984.

Sundaresan, K. and Ludescher, R. D., "Molecular Mobility and Oxygen Permeability in Amorphous β-Lactoglobulin." Food Hydrocolloids 22, 403–413, 2008.

Tan K.K., Thorpe R.B., Gas diffusion into viscous and non-Newtonian liquids. Chemical Engineering Science 47(13-14), 3565–3572, 1992.

Vanderkooi J.M., Maniara G., Green T. and Wilson D., An Optical Method for Measurement of Dioxygen Concentration Based upon Quenching of Phosphorescen. The Journal of Biological Chemistry, 262, 5476-5482, 1987.

Weigl B. H., Holobar A., Trettnak W. et al., "An optical triple sensor for measuring pH, oxygen and carbon dioxide in bioreactors," Journal of biotechnology, 32, 127-138, 1994.

Wolfbeis, O.S., The fluorescence of organic natural products. In Molecular Luminescence Spectroscopy (S. G. Schulman, editor), pp. 167-370, 1985. Wiley, NY

4 NANOPARTICLE SENSOR FOR DETECTING MICROBIAL ACTIVITY IN FOOD

4.1 Introduction

This part of study aims to develop a class of nanoparticle sensors which sense the protease activity of enzymes secreted from food spoilage organisms such as *Bacillus amyloliquifaciens*. Nanoparticle sensor for detection of bacteria in food is developed based on fluorescence resonance energy transfer between two chromophores which are attached to each end of a short oligopeptide, and work as donor and acceptor on the same molecule. To develop the sensor, gelatin nanoparticles were labeled with a pair of fluorophores. Fluorescein isothiocyanate as donor and tetramethylrhodamine isothiocyanate as acceptor are a pair of fluorophores with Förster distance of $R_0=5$ nm making them suitable for this study. Isothiocyanate derivatives were used only to show the feasibility of the approach although they were not food grade dyes. Fluorescein and tetramethylrhodamine have been used as donor and acceptor with $R_0=5$ nm in many scientific studies such as the study of structural features of DNA duplexes containing the photoproduct by fluorescence resonance energy transfer (Mizukoshi, et al. 2001); the study of the formation of DNA tetraplex (Simonson and Sjoback, 1999); and the study of helical geometry of double-stranded DNA in solution by fluorescence resonance energy transfer (Clegg, et al. 1993). Fluorescence resonance energy transfer property of fluorescein and tetramethylrhodamine has been used to monitor the kinetics of both DNA unwinding (Bjornson, et al. 1994) and cleavage (Ghosh et al. 1994). Figure 4-1 shows

that the emission spectrum of fluorescein overlaps the absorption spectrum of tetramethylrhodamine, making them a proper pair of donor and acceptor.

Another fluorophor pair used in this part of the study were tetramethylrhodamine isothiocyanate as donor and Texas red as acceptor with Förster distance of R_0=4 nm. Fluorescence resonance energy transfer (FRET) property of tetramethylrhodamine and Texas red has been used to study mRNA transport in living cells and provides a novel path to monitor DNA-protein interactions. Also, the fluorescence resonance energy transfer property of tetramethylrhodamine-Texas red has been used to study the biological processes and molecular probes which can be integrated into new clinical diagnostics.

4.2 Background

4.2.1 Fluorescence Resonance Energy Transfer

FRET has become popular in biological and biophysical applications to qualitatively and quantitatively measure the distance between donor molecule and acceptor molecule via a long-range dipole–dipole coupling (Kenworthy, 2001; Gordon et al., 1998). The mechanism of fluorescence resonance energy transfer engages a donor fluorophore in an excited electronic state, which can transfer its excitation energy to a close by acceptor chromophore in a non-radiative manner through long-range dipole-dipole interactions (Lakowicz, 2006) (Figure 4-2). This process occurs when the emission spectrum of a donor overlaps with the absorption spectrum of the acceptor (Figure 4-3). In the majority

of cases, the acceptor is a fluorescent dye, although this is not necessary (Berney and Danuser, 2003).The extent of resonance energy transfer is determined by the distance between the donor and acceptor and the extent of spectral overlap. The range over which the energy transfer can take place is limited to approximately 10 nanometers (100 angstroms), and the efficiency of transfer is extremely sensitive to the separation distance between fluorophores, making it a proper technique for exploring a diversity of biological phenomena that make changes in molecular proximity (dos Remedios et al., 1987). This distance is called Förster distance R_0 which is typically < 10 nm. Donor and acceptor molecules can be attached to each end of a short oligopeptide, and energy transfer will effectively quench the donor fluorescence. Any cleavage of a substrate results in separation between the donor and acceptor molecules and termination of the interaction between the chromophores. (Gershkovich, el al, 1996). In this case, the appreciable distance of R_0 < 10 nm is no longer applicable and FRET will not quench the donor florescence and will result in an increase the donor fluorescence spectrum or decrease in acceptor fluorescence spectrum (Berney and Danuser, 2003). The rate of energy transfer $K_T(r)$ is given by (Lakowicz, 1999):

$$k_T(r) = \frac{1}{\tau_D}\left(\frac{R_0}{r}\right)^6 \tag{1}$$

where, r is the distance between donor and the acceptor and τ_D is the lifetime of donor in the absence of energy transfer. R_0 is the Förster radius at which the efficiency of energy transfer is 50%.

The efficiency of the FRET process depends on the inverse sixth power of the distance between the donor and acceptor pair and is given by (Lakowicz, 1999):

$$E = \frac{R_0^6}{R_0^6 + r^6} \qquad (2)$$

This equation demonstrates that the transfer efficiency is highly reliant on distance when donor-acceptor distance is in close proximity to R_0. If the donor-acceptor distance decreases below R_0, the efficiency rapidly increases to 1.0. If r increases above R_0 the transfer efficiency decreases to zero (Lakowicz, 1999). Characteristic distance R_0, is given by equation:

$$R_0 = (8.79 \times 10^{-25} J k^2 n^{-4} q)^{1/6} \text{ (cm)} \qquad (3)$$

where, k_2 is the orientation factor; J the spectral overlap integral; n is the refractive index of the solvent; and q is the donor quantum yield in the absence of transfer (Gershkovich, el al. 1996).

4.2.2 *Bacillus amyloliquifaciens*

Bacillus amyloliquefaciens (B-amyl) is Gram-positive, catalase positive, aerobic, rod-shaped and motile, measuring $0.6 - 0.9$ μm by $1.8 - 4$ μm. Cells are often in chains. This particular organism is found in soil samples in nature. As with other members of the family Bacillaceae, it forms a strong endospore when conditions are not favorable and can be dispersed in this form into dust which then also gets into water supplies for plants and animals. Cylindrical spores are formed centrally or paracentrally in non-swollen

sporangia. The most favorable temperature for growth is 30-40°C. There is no growth below 15°C or above 50°C (Borriss et al. 2010).

Japanese scientist named Fukumoto discovered *B-amyl* in soil in 1943. He gave the bacterium its name because it produced (*faciens*) a liquifying (*lique*) amylase (*amylo*). Resemblance of *B-amyl* with *Bacillus subtilis* has long been recognized, and it has been given subspecies status as *"B. subtilis* subsp. *amyloliquefaciens"* because of similar and massive production of extracellular enzymes (Priest *et al.,* 1987). After long time discussion about *B-amyl* taxonomical position (Welker and Campbell, 1967), finally it became accepted as a species of its own by 1987 (Priest *et al.,* 1987). Fukumoto (1943) described *B-amyl* as a major producer of liquefying amylase and other extracellular enzymes of industrial importance (Borriss et al. 2010).

B-amyl is a food spoilage organism and some of its strain such as *Bacillus amyloliquefaciens* TMW 2.479 which causes food intoxication and spoilage, is considered as the most high-pressure-resistant bacterial spore (Margosch, et al. 2006). *B-amyl* hydrolyses gelatin, casein, elastin, starch, hemoglobin (Priest et al. 1937; Welker and Campbell, 1967; Borriss et al. 2010, Idriss et al. 2002). *Bacillus amyloliquefaciens* DC-4 produces a fibrinolytic enzyme which hydrolyses the fibrin and causes spoilage in a traditional Chinese soybean-fermented food (douche) (Peng et al. 2003). Bacterial α-amylases were derived in large quantities from *Bacillus amyloliquefaciens* by some industries (Bessler et al. 2003). The hydrolyzed products are broadly incorporated in the food, paper, and textile industries (Nigam et al. 1995). Typical applications include starch hydrolysis to transform starch into fructose and glucose syrups in the starch liquefaction

process, partial malt replacement in brewing industry to reduce cost, flour enhancement in baking industry, starch modification for the paper industry, starch removal in textile industry and detergent additives (Gangadharan, et al. 2006).

4.3   Material and Method

4.3.1   Double Labeling Gelatin Nanoparticles

The preparation of gelatin nanoparticles is explained in chapter 2. 10 mg freeze-dried gelatin nanoparticles was dissolved in 10 ml DI water and stirred under constant heating until a clear solution was obtained. Fluorescein isothiocyanate (FITC) from Sigma Aldrich was dissolved in acetone that was purchased from VWR international to make 10mM stock solution. Tetramethylrhodamine isothiocyanate (TMR-ITC) was dissolved in spectrophotometric grade dimethylformamide from sigma Aldrich to prepare a 10 mM stock solution. 10 μL FITC and 10 μL TMR-ITC from stock solutions were added to 10 ml of gelatin nanoparticle solution. The solution was stored over night at room temperature. Then the double labeled gelatin nanoparticles were transferred to a dialysis membrane tube having 1000 Da molecular weight cutoff and dialyzed against distilled water for 72 hr to remove the unreacted, free dyes.

The dialysis during the labeling process aims to remove unlabeled free probes. Detectable fluorescence signals of unreacted probes were observed normally in the first two batches of dialysis water and almost disappeared or became very weak after 24 hr of dialyzing; therefore, 72 hr dialyzing deemed sufficient to eliminate all free dyes from gelatin

nanoparticle solution. FITC and TMR-ITC were attached covalently to gelatin nanoparticles due to having isothiocyanate group which is an amine reactive group. Isothiocyanate is a chemical group –N=C=S, formed by substituting sulfur for oxygen in the isocyanate group. Another double labeled gelatin nanoparticle solution was made with TMR-ITC as a donor and Texas red (TR) from Sigma Aldrich as an acceptor following the same method as explained above.

All double-labeled gelatin nanoparticle (DLGNP) samples were filter sterilized with syringe filter, sterile, 0.2 micrometer pore (Nalgene, Rochester, NY) under sterilized condition in the laminar flow hood and were stored in the refrigerator for further use.

4.3.2   Preparing the microbial sensor

All microbial experiments were performed in Dr Chikindas' microbiology laboratory in food science building at Rutgers University.

Preparation of MRS broth: Lactobacilli MRS Broth is based on the formulations of deMan, Rogosa and Sharpe (MRS) (DeMan et al. 1960). This medium supports luxuriant growth of lactobacilli from oral, fecal, dairy, and other sources. 52.25 gr of the medium was dissolved in one liter of distilled water and was mixed well under constant heating with frequent agitation. The solution was then boiled for one minute until completely dissolved. The clear solution was transferred into appropriate container and sterilized in autoclave at 121°C for 12 minutes. The prepared medium was stored at room temperature. The dehydrated medium should be homogeneous, free-flowing and beige in

color. Prepared medium should be clear to slightly hazy and dark amber to red-amber in color.

A vial of frozen *Bacillus amyloliquefaciens* KATMIRA1933 (*B-amyl*) was added to 100 ml of MRS (Difco) broth and was left in 37 ℃ incubator in shaking position overnight in order to activate the cells. Then *B-amyl* was cultured on solid MRS with sterilized inoculation loop by streak method. The plate was left in 37 ℃ incubator overnight. Then this plate which contained grown *B-amyl* cells was stored in the refrigerator for further use. The initial cultures were subcultured multiple times before use in experimental testing and incubated at 37℃ for 24 hr to get fresh cells with maximum activity. After incubation, cells were removed from the growth medium by centrifugation (6,000×g for 10 min, 4℃) in Beckman- Allegra ^{TM} 21R Centrifuge. Supernatant was discarded. In order to wash cells and remove all the MRS, 15 ml of phosphate buffered saline (PBS) was added to the cells and vortexed for 3 minutes then centrifuged (6,000×g for 10min, 4℃). Supernatant was discarded and cells were washed 2 more times with PBS to make sure that no more MRS is left in the test tube. Then 15 ml PBS was added to the washed cells and vortexed for few minutes and these cells were used for further experiments. MRS had the same emission spectrum as fluorescein isothiocayanate and could interfere with the results of experiment. All experiments described in this chapter were done under the sterilized condition in the laminar flow hood.

4.3.3   Growth of B-amyl in DLGNP With no Other Source of Nutrient

This experiment was performed to study if *B-amyl* can grow in the DLGNP with no other source of nutrient in the solution. DLGNP was diluted with DI water with the relative ratio of 1-10 respectively and filter sterilized with syringe filter, sterile, 0.2 micrometer pore under sterilized condition in the laminar flow hood. The sample contained filter sterilized diluted DLGNP and 150 µl of *B-amyl* suspended in PBS with a total volume of 15 ml. Control sample contained 15 ml filter sterilized diluted DLGNP. The samples were incubated in the 37 ºC incubator in shaking position for 72 hr.

4.3.4   Growth of B-amyl in DLGNP with Other Sources of Nutrient

4.3.4.1   First set of experiments

 DLGNP with FITC & TMR-ITC (F&T) or TMR-ITC & TR (T&T) were diluted with PBS with relative ratio of 1-10 respectively and filter sterilized with sterile syringe filter of0.2 micrometer pore diameter under sterilized condition in the laminar flow hood. 15 ml of total solution was made which contained 1% casamino acid (bacto), 1% glucose solution (1gr/100ml) (Glucose was purchased from Sigma Aldrich), 150 µl of *B-amyl* suspended in PBS and diluted DLGNP - F&T. Next sample contained 1% casamino acid, 1% glucose solution (1gr/100ml), 150 µl of *B-amyl* suspended in PBS and diluted DLGNP - T&T in a total volume of 15 ml. Another sample prepared for this set of experiment contained 1% casamino acid, 1% glucose solution (1gr/100ml) and 150 µl of *B-amyl* suspended in PBS with a total volume of 15 ml. The last sample contained 150 µl

of *B-amyl* which was added to PBS with the total volume of 15 ml. The controls for this set of experiment were: 1% casamino acid, 1% glucose solution (1gr/100ml) and PBS with the total volume of 15 ml; diluted DLGNP – F&T in PBS, 1% casamino acid and 1% glucose solution (1gr/100ml) in a total volume of 15 ml; another sample was diluted DLGNP –T&T, 1% casamino acid and 1% glucose solution (1gr/100ml) in a total volume of 15 ml and the last one just 15 ml PBS. The samples were incubated in the 37 ℃ incubator in shaking position overnight. *B-amyl* needed to have some nutrient in the solution; therefore, some casamino acid as source of amino acids and some glucose as a source of sugar were added to the solution, since MRS could not be used due to having similar emission spectrum as FITC. Casamino acid is usually used in microbial growth media and is a mixture of amino acids and some very small peptides as a result of acid hydrolysis of casein (Mueller el al, 1941). Typical amino acids content in casamino acid by percent (%) is as follows: Alanine 2.9±0.1, Arginine 3.4±0.2, Asparagine 0, Aspartic Acid 6±0.6, Cystine 0.5±0.1, Glutamic Acid 18.5±1.7, Glycine 2.5±0.1, Histidine 2.5±0.2, Isoleucine 3.9±0.6, Leucine 8.3±0.5, Lysine 6.8±0.7, Methionine 2.4±0.2, Phenylalanine 4.4±0.5, Proline 18.9±2.4, Serine 6±0.4, Threonine 4.5±0.5, Tryptophan 0.7±1.1, Tryrosine 3.9±1.1, and Valine 4.7±1.4 (Justo et al. 2004). Amino acids are soluble and are good source of nutrient for different microorganism.

Summary of the first set of experiments:

PBS+*B-amyl*=15 ml

PBS + *B-amyl* + Casamino acid + Glucose solution (1gr/100ml) = 15 ml

Diluted DLGNP-F&T + *B-amyl* + Casamino acid + Glucose solution (1gr/100ml) =15ml

Diluted DLGNP-T&T+ *B-amyl* + Casamino acid + Glucose solution (1gr/100ml) =15ml

Controls:

PBS=15 ml

PBS + Casamino acid + Glucose solution (1gr/100ml) =15 ml

Diluted DLGNP-F&T + Casamino acid + Glucose solution (1gr/100ml) =15 ml

Diluted DLGNP-T&T + Casamino acid + Glucose solution (1gr/100ml) =15 ml

4.3.4.2   Second set of experiments

This set of experiments were conducted to study of effect of *B-amyl* on different concentrations of DLGNP-T&T. 15 ml of total solution was made which contained 10% DLGNP-T&T, 1% casamino acid, 1% glucose solution (1gr/100ml) and 150 µl of *B-amyl* suspended in PBS. The second sample contained 20% DLGNP-T&T, 1% casamino acid, 1% glucose solution (1gr/100ml) and 150 µl of *B-amyl* suspended in PBS with a total volume of 15 ml. The third sample was 40% DLGNP-T&T, 1% casamino acid, 1% glucose solution (1gr/100ml), 150 µl of *B-amyl* suspended in PBS with a total volume of 15 ml. The forth sample was 1% casamino acid, 1% glucose solution (1gr/100ml), 150µl of *B-amyl* suspended in PBS with a total volume of 15 ml and the last sample was 150µl of *B-amyl* which was added to PBS with a total volume of 15 ml. The controls were 10% DLGNP-T&T, 1% casamino acid, 1% glucose solution (1gr/100ml) with a total volume of 15 ml. The second sample was 20% DLGNP-T&T, 1% casamino acid and 1% glucose

solution (1gr/100ml) with a total volume of 15 ml. The third sample was 40% DLGNP-T&T, 1% casamino acid and 1% glucose solution (1gr/100ml) with a total volume of 15 ml. The forth sample contained 1% casamino acid and 1% glucose solution (1gr/100ml) which were added to PBS with a total volume of 15 ml and the last sample was 15 ml of PBS. The samples were incubated in the 37 ºC incubator in shaking position overnight.

Summary of the second set of experiments:

PBS+*B-amyl*=15 ml

PBS + *B-amyl* + Casamino acid + Glucose solution (1gr/100ml) = 15 ml

DLGNP-T&T (10%) + *B-amyl* + Casamino acid + Glucose solution (1gr/100ml) =15 ml

DLGNP-T&T (20%) + *B-amyl* + Casamino acid + Glucose solution (1gr/100ml) =15 ml

DLGNP-T&T (30%) + *B-amyl* + Casamino acid + Glucose solution (1gr/100ml) =15 ml

Controls:

PBS=15 ml

PBS + Casamino acid + Glucose solution (1gr/100ml) =15 ml

DLGNP-T&T (10%) + Casamino acid + Glucose solution (1gr/100ml) =15 ml

DLGNP-T&T (20%) + Casamino acid + Glucose solution (1gr/100ml) =15 ml

DLGNP-T&T (40%) + Casamino acid + Glucose solution (1gr/100ml) =15 ml

4.3.5   *Optical density (OD) Test*

In order to observe the growth of *B-amyl* optical density (OD) test was performed on all samples. Optical density (OD) at 600 nm was measured using the BIQ-RAD Smartspec 3000 spectrophotometer. 5 measurements were obtained during the first 48 hr (0 hr – 48 hr). 1.5 ml of each sample in the sterilized condition was transferred into a clean cuvette. To quantify the OD_{600} of the growth media, measurements were obtained before the inoculation of the bacterial culture, to provide blank values of each sample. To measure the growth properties, the values of blanks for each sample were subtracted. In order to pursue the OD_{600} test and study the growth of *B-amyl* one sample which contained MRS and 150 µl of *B-amyl* with the total volume of 15 ml was made to compare the growth of *B-amyl* in MRS with defined media.

4.4   **Fluorescent measurements**

Luminescence measurements were made using Cary Eclipse (Varian Instruments, Walnut Creek, CA) fluorescence spectrophotometer equipped with a temperature controller and multi-cell holder. After each OD_{600} test, samples were immediately transferred to the Cary Eclipse fluorescence spectrophotometer and fluorescence spectrum of each sample was measured.

Fluorescence emission spectra were measured at room temperature and were collected over the range of 500-800 nm with an excitation wavelength of 490 nm for DLGNP-F&T, over the range of 540-800 nm with an excitation wavelength of 530 nm for DLGNP-T&T and over the range of 500-800 nm with an excitation wavelength of 490

nm for DLGNP-F. The excitation and emission monochromators were both set at 5 nm band pass. Each data point was collected at 1 nm intervals with a 0.1 s averaging time.

4.5   Results and Discussion

4.5.1   Growth of B-amyl in DLGNP with presence of casamino acid and glucose solution

The purpose of this set of experiments was mainly to detect the effect of *B-amyl* on DLGNP-F&T and DLGNP-T&T and their fluorescence emission spectra. The solution sample contained diluted DLGNP-F&T, *B-amyl*, casamino acid and glucose turned into turbid solution after overnight incubation which was the sign of cell growth. Figure 4-4 shows the control sample solution (DLGNP-F&T, casamino acid and glucose) on the right before inoculation of *B-amyl* which is a clear pale pink solution. The sample on the left is the experimental solution of DLGNP-F&T, *B-amyl*, casamino acid and glucose after 24 hr incubation in 37 ºC incubator which turned into a turbid orange solution which is the sign of cell growth..

Figure 4-5 shows the control sample solution (DLGNP-T&T, casamino acid and glucose) on the right before inoculation of *B-amyl* which was a clear pale purplish solution. The sample on the left is the solution of DLGNP-T&T, *B-amyl*, casamino acid and glucose after 24 hr incubation in 37 ºC incubators which turned into a turbid orange solution. Figure 4-6 shows the normalized fluorescence emission spectra of DLGNP-F&T in the presence and absence of *B-amyl* in the solution over a 48 hr time period.

There was not any significant change in fluorescence spectra of DLGNP-F&T either with or without presence of B-amyl in the solution during the 48hr time period of experiment. All fluorescence spectra almost overlapped and did not show any remarkable deviation to indicate that B-amyl hydrolyzed the DLGNP-F&T which was present in the solution as nutrient.

Figure 4-7 demonstrates the normalized fluorescence emission spectra of DLGNP-T&T in the presence and absence of B-amyl in the solution over the 48hr time period. There was not any significant change in fluorescence emission spectra of DLGNP-T&T either with or without presence of B-amyl in the solution during the 48hr time period of experiment. All the fluorescence spectra overlapped and did not show any remarkable deviation to conclude that B-amyl consumed the DLGNP-T&T which was present in the solution as nutrient. The emission spectra of controls and original samples followed the same pattern and there was not any change either in the emission intensity of donor TMR-ITC or acceptor TR.

The second set of experiments was performed to determine whether different concentrations of DLGNP can affect the result of this study. In this part, the total concentration of DLGNP-T&T was different in the experimental solutions as it was explained in the Materials and Methods section for the second set. The concentrations of DLGNP-T&T were 10%, 20% and 40% of total solution of 15 ml. Figure 4-8 through Figure 4-10 illustrate the fluorescence emission spectra of DLGNP-T&T with different concentrations in the presence and absence of *B-amyl* in the solution over a 48hr time period. The normalized fluorescence emission spectra of all samples with different

concentrations of DLGNP-T&T in presence of B-amyl and control samples overlapped. There was not any change either in the emission intensity spectra of donor TMR-ITC or acceptor TR in this case.

4.5.2 Optical density (OD_{600}) test

Optical density (OD_{600}) test was used to obtain growth curves using optical density as the indicator of growth. The test was performed on all samples to study the growth pattern of *B-amyl*.

Figure *4-11* shows the growth pattern of *B-amyl* in DLGNP-F&T; DLGNP-T&T; 10%, 20% and 40% DLGNP-T&T solutions; *B-amyl* with MRS and *B-amyl* in PBS. This figure demonstrates that there was not any growth in PBS but there was growth in other samples. OD_{600} test showed that *B-amyl* cells reached their maximum growth and started entering the stationary phase after 24 hours. As a result, it can be concluded that although there was growth of *B-amyl* in the samples, there was not any change in the fluorescence intensity of emission spectra of the samples. Therefore, it is concluded that *B-amyl* did not consume gelatin nanoparticles as a source of nutrient and did not hydrolyze DLGNP and consequently did not affect the resonance energy transferred between the donor and acceptor in DLGNP in 48 hr.

The samples remained in 37 ºC incubator for 7 days and the fluorescence spectra of all samples were checked and there was not any change in emission intensity of donors and acceptors.

The result of these experiments showed that *B-amyl* did not have any effect on FRET between different donors and acceptors which were covalently attached to gelatin nanoparticles. This can be due to the abundance of other nutrients such as glucose and amino acids from casamino acid in the sample. *B-amyl* cells preferred to consume those nutrients first and therefore, they did not hydrolyze gelatin as a source of nutrient and ultimately did not affect the FRET property between donor and acceptor. On the other hand, *B-amyl* did not show any growth in the sample containing only DLGNP over a 48 hr time period which means that *B-amyl* cells need some other source of nutrient in the solution to grow.

Console and Rahn (1937) showed that gelatin decomposition by *Bacillus subtilis* is partially due to an extracellular enzyme. This study showed that gelatin decomposition was almost 0 during the first 72 hours of incubation and began to rapidly increase after day 7, although the cells reached their maximum growth on the 5th day. Thus, no specific relation exists between the number of cells and the amount of decomposed gelatin. They also showed that the addition of 0.5% glucose at the start of experiment prohibited the formation of the proteolytic enzyme completely. They observed that adding 0.5% glucose to a culture in which multiplication of cells had stopped did not prevent the formation of more enzymes while the rate of enzyme action was decreased by the acid formed from glucose. They suggested that the glucose might affect its action inside the cell, and particularly the formation and secretion of more proteolytic enzyme since it cannot affect the action of partly extracellular enzyme. Therefore, another explanation for this experiment can be the presence of glucose as a source of nutrient in the solution samples

which inhibited the production of the proteolytic enzyme since this strain of *B-amyl* and *bacillus subtilis* act in a similar way (Karlyshev et al. 2014). Abrusci et al. (2004) studied the biodegradation of photographic grade gelatin (Bloom 225 & 75) by a strain of *B-amyl* (*B3BA*) and a strain of *bacillus subtilis* (*B3BS*) by viscometry in aqueous solution. *B-amyl* (*B3BA*) showed a very slow growth at 4 ºC and a faster growth at 37 ºC. There has not been any data in literature particularly with regard to the effect of *Bacillus amyloliquefaciens* KATMIRA1933 on gelatin or gelatin nanoparticles. There is a possibility that this strain of *B-amyl* cannot hydrolyze gelatin at all or can only hydrolyze gelatin under certain conditions; therefore, a more detail study can be conducted on this subject in future. Since this study aims to show the sensitivity of DLGNP with the FRET property as a sensor, it was not meaningful to continue the experiment more than 48 hours because the purpose of this microbial sensor is to detect any microbial contamination in food at the onset of the growth not after the completion of the growth.
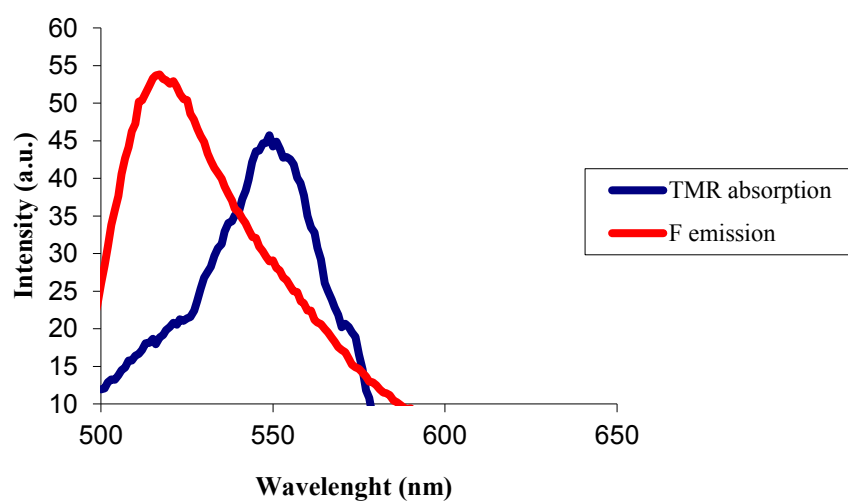
Figure 4-1: Emission spectrum of fluorescein overlapping the absorption spectrum of tetramethylrhodamine.
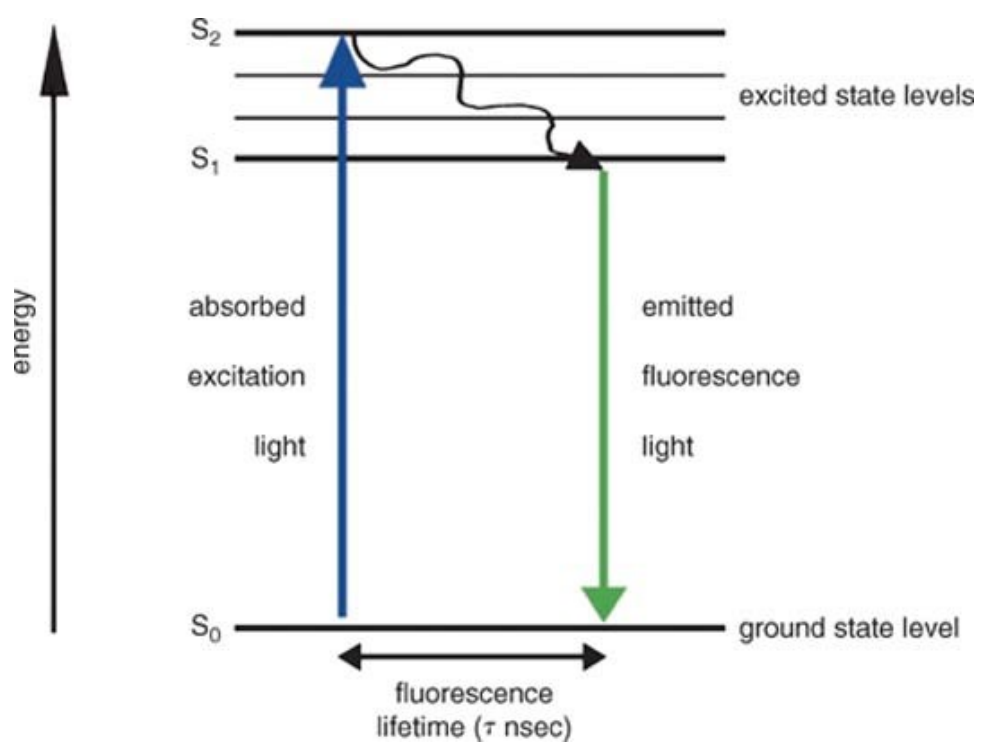
Figure 4-2: A Jablonski diagram representing Förster resonance energy transfer (FRET) (Llères, et al. 2007).
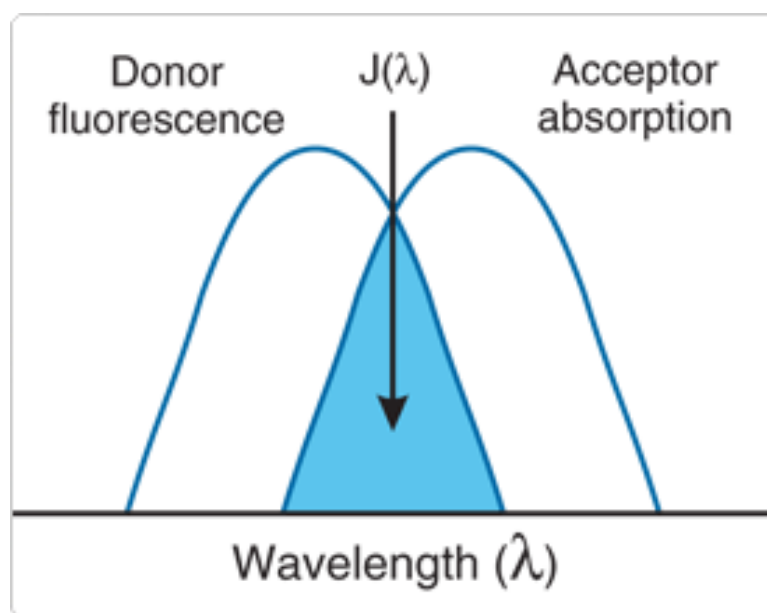
Figure 4-3: Schematic representation of the FRET spectral overlap (http://www.invitrogen.com).
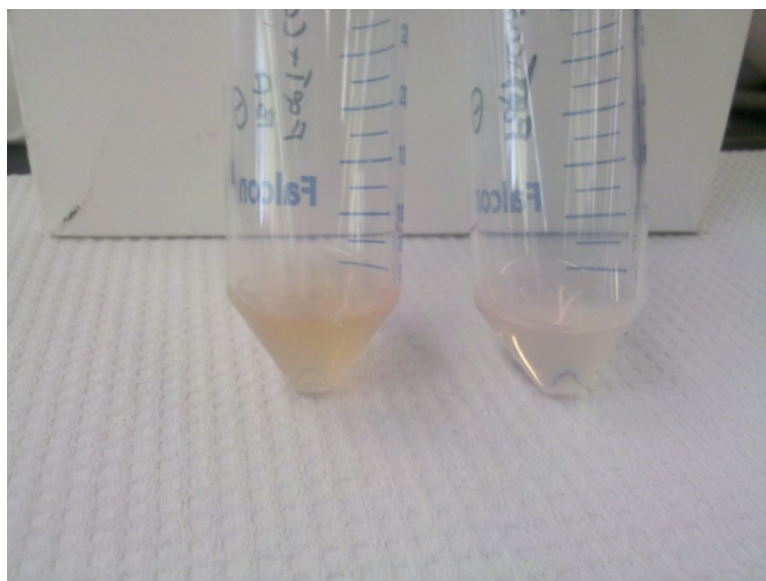
Figure 4-4: Clear pale pink solution on the right is DLGNP-F&T before inoculation of B-amyl and turbid orange solution on the left is DLGNP-F&T after 24hr incubation in 37 ºC incubator in the presence of B-Amyl.

Figure 4-5: Clear pale purplish solution on the right is DLGNP-T&T before inoculation of B-amyl and turbid orange solution on the left is DLGNP-T&T after 24hr incubation in 37 ºC incubator in the presence of B-Amyl.
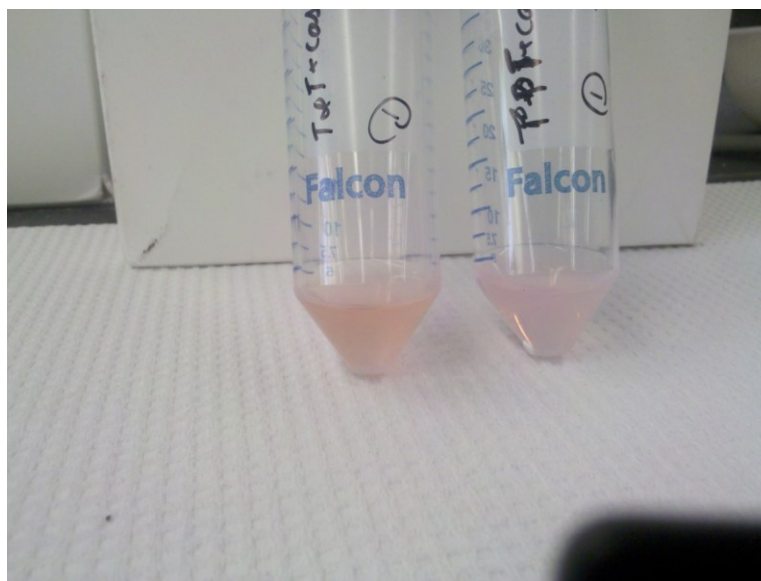
Figure 4-6: Normalized fluorescence emission spectra of DLGNP-F&T in the presence and absence of B-amyl in the solution over a 48hr time period. Where Cont=control sample, BA=B-amyl and Orig= Original sample.
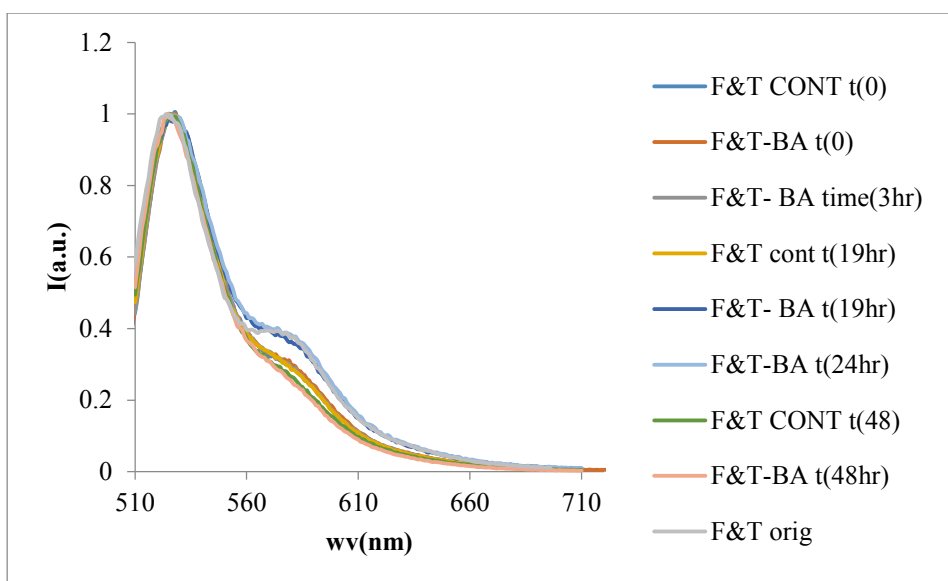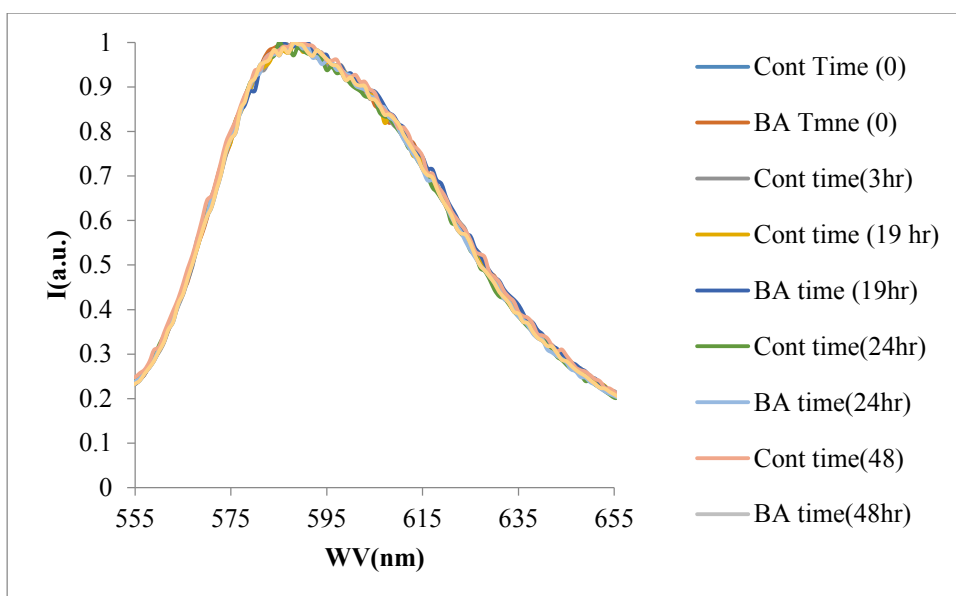
Figure 4-7; Normalized fluorescence emission spectra of DLGNP-T&T in the presence and absence of B-amyl in the solution over a 48hr time period. Where Cont = control sample and BA=B-Amyl.
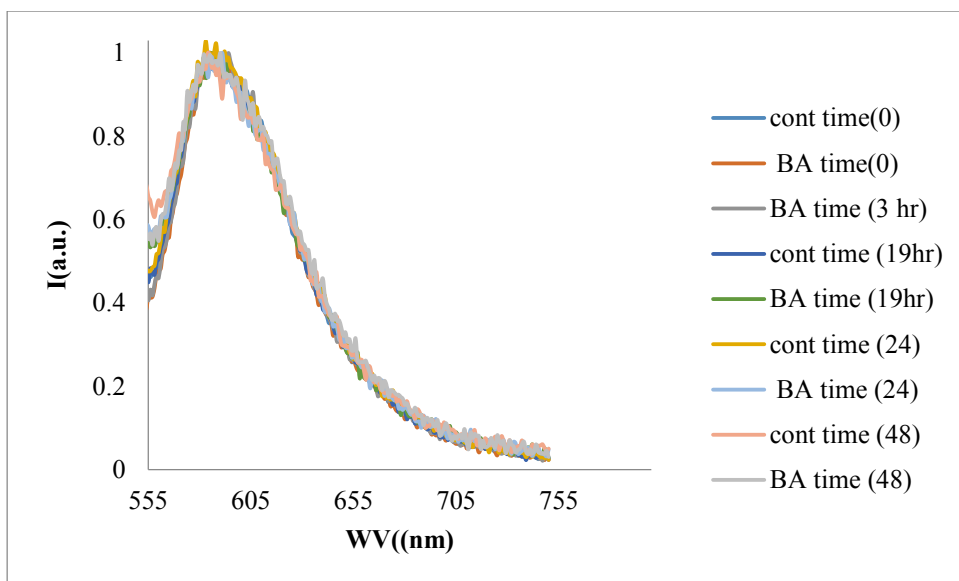
Figure 4-8:Fluorescence emission spectra of DLGNP-T&T with 10% concentration in the presence and absence of B-amyl in the solution over a 48hr time period. Where Cont = control sample and BA=B-Amyl

Figure 4-9: Fluorescence emission spectra of DLGNP-T&T with 20% concentration in the presence and absence of B-amyl in the solution over a 48hr time period. Where Cont = control sample and BA=B-Amyl.

Figure 4-10: Fluorescence emission spectra of DLGNP-T&T with 40% concentration in the presence and absence of B-amyl in the solution over a 48hr time period. Where Cont = control sample and BA=B-Amyl.
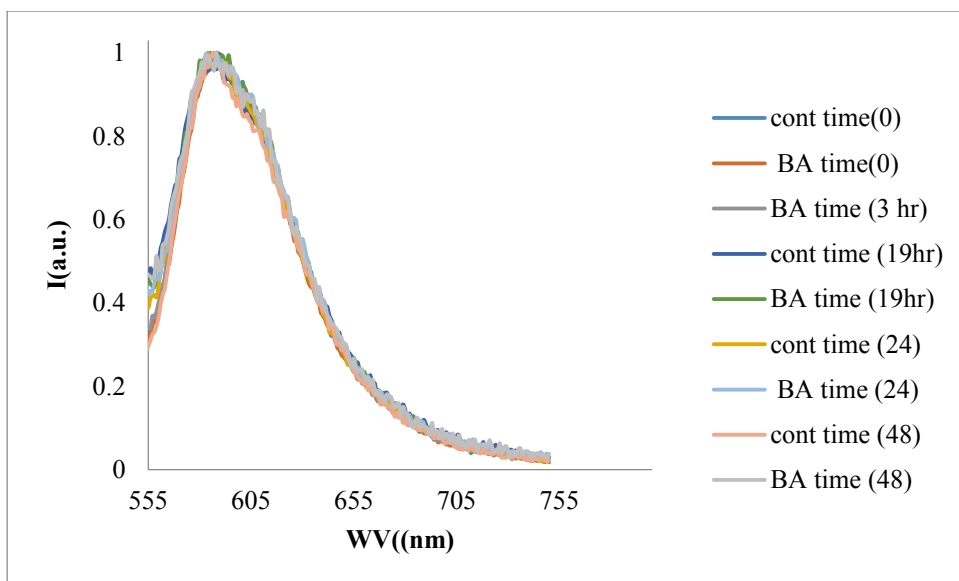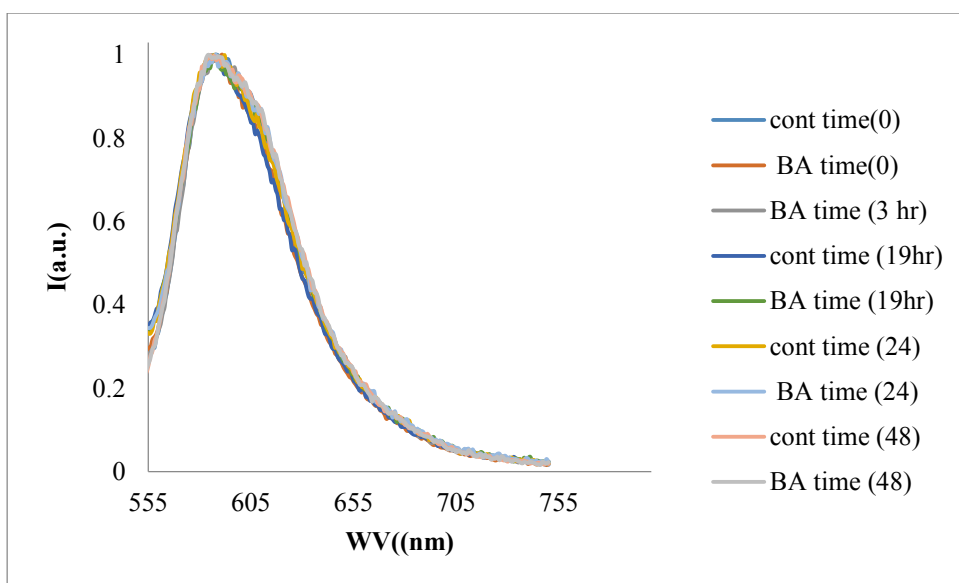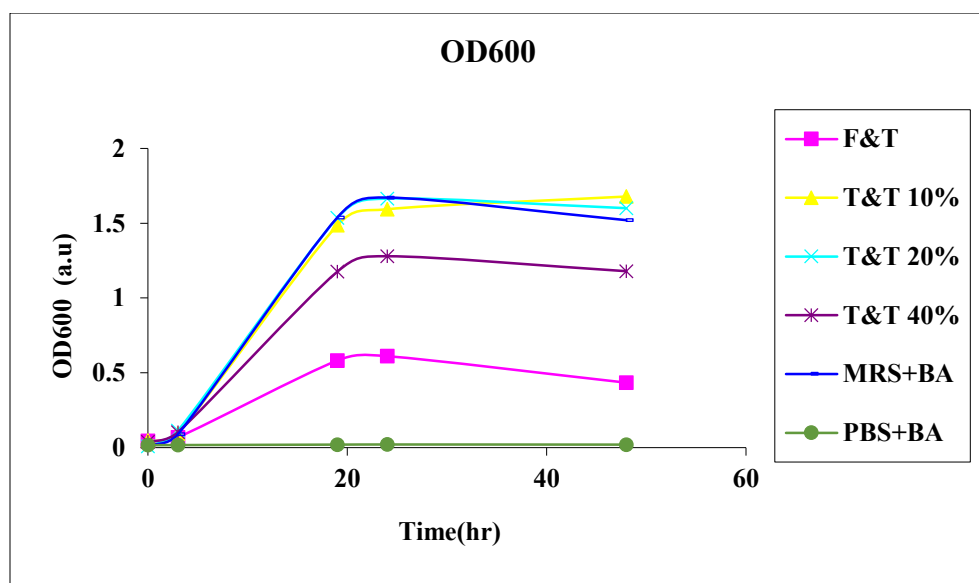
Figure 4-11: Growth pattern of B-amyl in DLGNP-F&T; DLGNP-T&T; 10%, 20% and 40% DLGNP-T&T solutions; B-amyl with MRS and B-amyl in PBS.

References

Babia T, Ledesma M.D., Saffrich R, Kok J.W, Dotti C.G., Egea G.. Endocytosis of NBD-Sphingolipids in Neurons: Exclusion from Degradative Compartments and Transport to the Golgi Complex, Traffic, 2, 395-405, 2001.

Berney C.and Danuser D., FRET or No FRET: A Quantitative Comparison, Biophysical Journal, 84, 3992–4010, 2003.

Bessler C., Schmitt J., Maurer K., Schmid D.R., Directed evolution of a bacterial amylase: Toward enhanced pH-performance and higher specific activity, *Protein Sci*. *12*, 2141–2149,2003.

Bjornson KP, Amaratunga M, Moore KJ, Lohman TM. Single-turnover kinetics of helicase-catalyzed DNA unwinding monitored continuously by fluorescence energy transfer. Biochemistry, 29, 33(47), 14306-16, Nov1994.

Borriss R., Chen X-H., Rueckert C., Blom J., Becker A., Baumgarth B., Fan B. , Pukall R., Schumann P., Spröer C., Junge H., Vater J., Pühler A. and Klenk HP. Relationship of *Bacillus amyloliquefaciens* clades associated 1 with strains DSM 7^T andFZB42: a proposal for *Bacillus amyloliquefaciens* subsp. *amyloliquefaciens* subsp. nov. and *Bacillus amyloliquefaciens* subsp. *plantarum* subsp. nov. based on their discriminating complete genome sequences IJSEM Papers in Press. Published September 3, 2010 as doi:10.1099/ijs.0.023267-0.

Chao S.H., Cheng TH., Shaw CY., Lee MH., Hsu YH. and Ying-Chieh Tsai YC., Characterization of a Novel PepF-Like Oligopeptidase Secreted by *Bacillus amyloliquefaciens* 23-7A. Applied and environmental microbiology, , 72(1), 968–971 Jan. 2006.

Clegg. R. M., Murchie A. I. H., Zechel A. and. Lilley D. M. J**.** Observing the helical geometry of double-stranded DNA in solution by fluorescence resonance energy transfer Proc. Natl. Acad. Sci. USA, 90, 2994-2998, April 1993.

Console A.D. and Rahn O. A Study of Gelatin Digestion by **Bacillus subtilis**. J Bacteriol., 36, 1, 47–52, July1938

de Man, J.D., Rogosa, M., Sharpe, M.E. A Medium for the Cultivation of *Lactobacilli*. *J* Appl Bact 23,130–135, 1960.

dos Remedios, C.G., Miki M. and Barden J.A. Fluorescence resonance energy transfer measurements of distances in actin and myosin: A critical evaluation. J. Muscle Res. Cell Motil. 8: 97–117. 1987.

Förster, T. 1965. Delocalized excitation and excitation transfer. *In* Modern Quantum Chemistry. Vol. 3. O. Sinanoglu, editor. Academic Press Inc., New York. 93–137.

Gangadharan D., Sivaramakrishnan S., Nampoothiri K.M. and Pandey A, Solid Culturing of *Bacillus amyloliquefaciens* for Alpha Amylase Production, a-Amylase Production by *B. amyloliquefaciens,* Food Technol. Biotechnol. 44, 2, 269–274, 2006.

Gershkovich A.A., Kholodovych V.V., Fluorogenic substrates for proteases based on intramolecular fluorescence energy transfer (IFETS), J. Biochem. Biophys. Methods, 33, 135-162, 1996.

Ghosh S. S., Eis P. S., Blumeyer K., Fearon K. and Millarl D. P., Real time kinetics of restriction endonuclease cleavage monitored by fluorescence resonance energy transfer. Nucleic Acids Research. 22, 15, 3155-3159, 1994.

Gordon, G. W., Berry G., Liang X. H., Levine B. and Herman B.. Quantitative fluorescence resonance energy transfer measurements using fluorescence microscopy. Biophys. J., 74, 2702–2713, 1998.

Herz E., Burns A, Lee S., Sengupta P., Bonner D., Ow H., Liddell C., Baird B. A. and Wiesner U., Colloidal Quantum Dots for Biomedical Applications, Proc. SPIE, 6096, 1–12, 2006.

http://www.invitrogen.com

http://www.sigmaaldrich.com

Hussain S.A., An Introduction to Fluorescence Resonance Energy Transfer (FRET), Aug 2009, http://arxiv.org/abs/0908.1815

Idriss E.E., Makarewicz O., Farouk A., Rosner K, Greiner R., Bochow H., Thomas Richter T. and Borriss R., Extracellular phytase activity of *Bacillus amyloliquefaciens* FZB45 contributes to its plant-growth-promoting effect, *Microbiology*, 148, 2097–2109, (2002).

Justo Pedroche, María M Yust, Hassane Lqari, Julio Girón-Calle, Javier Vioque, Manuel Alaiz, Francisco Millán. Production and characterization of casein hydrolysates with a high amino acid Fischer's ratio using immobilized proteases. International Dairy Journal 14, 6, 527–533, 2004

Karlyshev A. V., Melnikov V. G., Chikindas M. L., Draft Genome Sequence of *Bacillus subtilis* strain KATMIRA1933., 2, 3, e00619-14 Genome Announcements (genomea.asm.org)

Kenworthy, A. K. Imaging protein-protein interactions using fluorescence resonance energy transfer microscopy. Methods. 24, 289–296, 2001.

Kohl T., Heinze K.G., Kuhlemann R., Koltermann A. and Schwille P., A protease assay for two-photon crosscorrelation and FRET analysis based solely on fluorescent proteins. PNAS, 99(19), 12161–12166, 2002

Lakowicz, J. R. Principles of Fluorescence Spectroscopy.Plenum Press, NY., 2006

Lakowicz, J.R. 1999. Principles of Fluorescence Spectroscopy. 2nd ed. Plenum Publishing Corp., New York. pp 692.

Lanier, L. L., and Loken, M.R., Human lymphocyte subpopulations identified by using three-color immunofluorescence and flow cytometry analysis: correlation of Leu-2, Leu-3, Leu-7, Leu-8, and Leu-11 cell surface antigen expression. J. Immunol., 132,1, 151-156,1984.

Lefevre C., Kang H.C., Haugland R. P., Malekzadeh N., Arttamangkul S. and Haugland R.P. Texas Red-X and Rhodamine Red-X, New Derivatives of Sulforhodamine 101 and Lissamine Rhodamine B with Improved Labeling and Fluorescence Properties. Bioconjugate Chem. 7, 482-489, 1996

Llères D, Swift S, Lamond AI. Detecting protein-protein interactions in vivo with FRET using multiphoton fluorescence lifetime imaging microscopy (FLIM). Curr Protoc Cytom. 2007 Oct;Chapter 12:Unit12.10.

Loken, M. R., and Lanier, L. L., Three-color immunofluorescence analysis of Leu antigens on human peripheral blood using two lasers on a fluorescence-activated cell sorter. Cytometry, 5, 2, 151-158, 1984.

Margosch D. , Ehrmann M. A., Buckow R., Heinz V., Vogel R. F. and Ganzle M. G. High-Pressure-Mediated Survival of *Clostridium botulinum* and *Bacillus amyloliquefaciens* Endospores at High Temperature. Applied and Environmental Microbiology, , 3476–3481, May 2006.

Marras SA, Kramer FR, Tyagi S, Efficiencies of fluorescence resonance energy transfer and contact-mediated quenching in oligonucleotide probes, Nucleic Acids Res, 30, 122, 2002.

Mchedlov-Petrossyan N.O, Kukhtik V.I, Bezugliy V.D., Dissociation, tautomerism and electroreduction of xanthene and sulfonephthalein dyes in *N,N*-dimethylformamide and other solvents. Journal of Physical Organic Chemistry, **16(7), 380–397, 2003.**

Mizukoshi T. , Kodama T. S. , Fujiwara Y. , Furuno T. , Nakanishi M., and Iwai S., Structural study of DNA duplexes containing the (4-6) photoproduct by fluorescence resonance energy transfer. Nucleic Acids Reserch, 29, 24, 4948-4954, 2001.

Mueller J. H., Johnson, E. R. Acid Hydrolysates of Casein to Replace Peptone in the Preparation of Bacteriological Media. The Journal of Immunology, 40, 1, 33–38, 1 Jan 1941.

Neckers D.C., Valdes-Aguilera OM. Photochemistry of the xanthene dyes, Adv. Photochem. **18**, 315–394, 1993.

Nigam P., Singh D., Enzyme and microbial system involved in starch processing. Enzyme Microb. Technol. 17, 770–778, 1995.

Ow H., Larson D. Srivastava R., Baird M., B. A., Webb W. W. and Wiesner U., Self-Assembly of Metallic Nanowires from Aqueous Solution**,** Nano Lett. 5, 113–117, 2005.

Peng Y., Huang Q., Zhang R-h., Zhang Y-Z. Purification and characterization of a fibrinolytic enzyme produced by *Bacillusamyloliquefaciens* DC-4 screened from *douchi*, a traditional Chinese soybean food. Comparative Biochemistry and Physiology Part B: Biochemistry and Molecular Biology. 134, 1, 45–52, January 2003.

Priest F. G., Goodfellow M.,Shute, L. A. & Berkeley W. *Bacillus amyloliquefaciens* sp. nov., nom. rev. Int J Syst Bact. 37, 1, 69-71, 1987.

Proudnikov D., Yuferov V., Zhou Y., LaForge KS., Ho A., Kreek MJ. Optimizing primer--probe design for fluorescent PCR, J Neurosci Methods 123,31-45, 2003.

Simonsson T. and Sjoback R. DNA Tetraplex Formation Studied with Fluorescence Resonance Energy Transfer. The journal of biological chemistry 274, 24, June 11, 17379–17383, 1999.

Szejda, P., Parce JW., Seeds MS., Bass DA., Flow cytometric quantitation of oxidative product formation by polymorphonuclear leukocytes during phagocytosis. J. Immunol., 133,6, 3303-3307,1984.

Titus   J. A., Haugland R, Sharrow S. O, Segal D. M, Texas Red, a hydrophilic, red-emitting fluorophore for use with fluorescein in dual parameter flow microfluorometric and fluorescence microscopic studies. J. Immunol. Methods, 50, 2, 193-204, 1982.

Wang L., Gaigalas A.K., Blasic J., Holden M.J., Spectroscopic characterization of fluorescein- and tetramethylrhodamine-labeled oligonucleotides and their complexes with a DNA template. Spectrochimica Acta Part A 60, 2741–2750, 2004.

Weichel, W., Weichel W, Liesegang B, Gehrke K, Göttlinger C, Holtkamp B, Radbruch A, Stackhouse TK, Rajewsky K., Inexpensive upgrading of a FACS I and isolation of rare somatic variants by double-fluorescence sorting. Cytometry, 6, 2, 116-123, 1985.

Welker, N. E. & Campbell L.L. Unrelatedness of *Bacillus amyloliquefaciens* and *Bacillus subtilis*. J Bacteriol, 94, 1124-1130, 1967.